Chem Soc Rev

Inverted Organic Photovoltaic Cells

Journal:	*Chemical Society Reviews*
Manuscript ID	CS-SYN-11-2015-000831.R2
Article Type:	Review Article
Date Submitted by the Author:	09-Mar-2016
Complete List of Authors:	Wang, Kai; polymer engineering, university of akron; The University of Akron, LIU, CHANG; The University of Akron, polymer engineering meng, tianyu; The University of Akron, Polymer Eng Yi, Chao; University of Akron, Gong, Xiong; The University of Akron, Polymer Eng

SCHOLARONE™
Manuscripts

Inverted Organic Photovoltaic Cells

Kai Wang,[#] Chang Liu,[#] Tianyu Meng, Chao Yi, Xiong Gong*

Department of Polymer Engineering, College of Polymer Science and Polymer Engineering, University of Akron, Akron, Ohio 44325, USA

Abstract

The advance in humanizations, modern industrialization and future technological revolution are always at high expense of energy consumption. Unfortunately, there exist serious issues such as limited storage, high cost and toxic contamination in conventional fossil fuel energy sources. Instead, solar energy represents as a renewable, economic and green alternative in the future energy market. Among all the photovoltaic technologies, the organic photovoltaics (OPVs) demonstrate a cheap, flexible, clean and easy-processing way to convert solar energy into electricity. However, OPVs with a conventional device structure are still far away from industrialization mainly because of the short lifetime and the energy-intensive deposition of top metal electrode. To address the stability and cost issue simultaneously, an inverted device structure has been introduced into OPVs, bridging the laboratory research with the practical application. In this review, recent progresses in device structures, working mechanisms, functions and advances of each layer as well their correlations with the efficiency and stability of the inverted OPVs are reviewed and illustrated.

*Corresponding author, E-mail: xgong@uakron.edu; Fax: (330) 972 3406

[#]These authors are equally contributed to this work.

1. Introduction

1.1 Energy Source

Driven by economic acceleration, demographic explosion and technical evolution, the available energy supplies have been placed on a huge strain.[1-2] And modern humanizations, industrialization and future technological revolution require at least 56% increase in the world energy consumption in the next 30 years.[1] However, the currently being used fossil fuel energy are of limited storage, high cost and low environmental harmony.[3] In addition, the environmental pollutions and climate issues raising from the combustion of fossil, would inevitably cause irreversible damage to biological diversity, climate and world economies.[3,4] Therefore, to find novel renewable, cheap and clean energy sources is one of the most comprehensive insurance for long-term development of human beings in the future.[5]

1.2 Solar Energy and Photovoltaics

Solar energy shows great potential in the future energy market due to its huge reserves and renewable, cheap and clean nature.[5] The solar power received upon earth is approximately 6.12×10^{20} J/h,[6] which could cover the world's total energy consumption in a whole year ($\sim 5.6 \times 10^{20}$ J in the year of 2010).[7] The solar cells with an efficiency of 10% covering 0.16% of land area would produce 20 Terawatts energy with extremely low economic and environmental cost, which is approximatively twice of the energy produced by fossil fuel and numerous times of that from nuclear fission reactors.[8] However, the application of solar energy today is still not widespread, mainly due to the compromise between the costs and the power conversion efficiency (PCE). The commercial available silicon-based photovoltaic cells (85% market share) are relatively expensive because of their critical manufacture processing.[9] Alternatively, organic photovoltaics (OPVs) have shown their outstanding potentials in the cost-effective

manufacturing thanks to their unique properties such as wide material availability, low-temperature solution-processibility, and roll-to-roll manufacturing processibility.[10,11] However, there still exist critical requirements for the commercialization of OPVs. **Scheme 1** demonstrates a critical pentagram summarizing the requirements in five technology driving aspects that the OPVs need to reach. In addition to the conventional three primary factors, "efficiency", "lifetime" and "cost" (per watt-peak),[12] new requirements such as "clean" and "prospect" have been also added. The "clean" is defined to be the environmental impact of the OPVs and the "prospect" is how far the OPVs will go in the market.[13] Successful commercialization can be achieved only if all the technology driving aspects are fulfilled at the same time.

2. Device Structures

2.1 Conventional Device Structure

A single-junction OPVs is a sandwich structure, where bulk heterojunction (BHJ) composite is sandwiched between the low work-function (WF) metal cathode (aluminum (Al), calcium (Ca) or barium (Ba)) and the high WF transparent conducting metal oxide anode, e.g., indium-tin oxide (ITO) or fluorine doped tin oxide (FTO).[14-17] The device architecture of a conventional device structure is shown in **Scheme 2a**. Typically, poly(3,4-ethylenedioxythiophene):poly-(styrenesulfonate) (PEDOT:PSS) as an anode buffer layer is used to smooth the surface of the ITO electrode or the FTO electrode.[14] However, the ITO can be etched over time upon directly exposure to the acidic PEDOT:PSS buffer layer, especially at an elevated temperature and humidity.[18-21] Moreover, the casted PEDOT:PSS layer always exhibits large microstructural and electrical inhomogeneity including order-of-magnitude variations in film morphological and electrical conductive gradient from the near surface region

to bulk, which inevitably deteriorates charge transport and results in inferior device performance.[22] Furthermore, the high-cost vacuum evaporation for the top metal electrode makes the fabrication incompatible with the large-scale roll-to-roll process. The microspores can be formed within the top metal electrode during the vacuum evaporation process, allowing both oxygen and moisture to be diffused into polymer layer, degrading the underlying polymers.[16] As a result, poor device efficiency and low device stability would be inevitable in the conventional structured OPVs.[17]

2.2 Inverted Device Structure

In order to circumvent above problems, the inverted device structure, as shown in **Scheme 2b**, has been developed.[23,24] The ITO or the FTO acts as the cathode and the high WF metals act as the anode, respectively. And the polarity of charge collection is reversed in inverted OPVs, which allows the utilization of more ambient stable and high WF metals such as gold (Au), silver (Ag) and copper (Cu) as the top anode,[24,25] making it possible for printing technologies to deposit the metal anode instead of the conventional energy consuming thermal deposition technologies.[26] Meanwhile the acidic PEDOT:PSS buffer layer is also eliminated to avoid the proton etching ITO or the cation derogating the organics. At this point of view, the inverted OPVs possess huge commercialization potentials in comparison to the conventional OPVs.

2.3 Top-illuminated Device Structure

The device structures of conventional and inverted OPVs are shown in **Schemes 2a & 2b**, both of which are illuminated from the transparent substrate in the bottom because light cannot pass through the opaque metal electrode on the top. In comparison, a top-illuminated device structure, as shown in **Scheme 2c**, has also been developed by applying either ultra-thin metal films (e.g., ultra-thin Au), or structured materials (e.g., metal/metal grid, metal nano-wires, metal

foil substrates or plastic foils with translucent metal coatings), or novel highly conductive materials (e.g., highly conducting polymers, carbon nanotubes (CNTs), graphene) as the transparent top electrode to avoid utilization of traditional expensive electrode materials. Moreover, solution-processible top electrode would allow OPVs being fabricated on either rigid or flexible subtracts by printing technologies.[28,29]

The top-illuminated device structure was firstly introduced by M. Glatthaar et al by constructing the OPVs with a device structure of glass/Al (80 nm)/titanium (Ti) (20 nm)/photo active layer (150 nm)/PEDOT:PSS (250 nm)/Au-grid (50 nm),[30] where the top electrode (in the combination of highly transparent and conductive PEDOT:PSS with thin Au-grid) allowed sufficient photons passing through and reaching the active layer. Moreover, an ohmic contact was formed between the highest occupied molecular orbital (HOMO) energy level of p-type materials and the WF of the top electrode, so that the holes can be effectively extracted to the electrodes. The thin titanium layer was inserted to prevent the formation of the highly insulating Al_2O_3 at the surface of Al. A PCE of 1.4% under AM 1.5 solar illumination was achieved by using such semi-transparent top electrode configuration with a BHJ composite of poly(3-hexylthiophene) (P3HT) blended with phenyl-C_{61}-butyric acid methyl ester ($PC_{61}BM$) in the year of 2005. In 2007, Takahito et al demonstrated a similar bi-layer OPVs using the concept of "top light-harvesting" based on the structure of Si/SiO_2 layer/cathode/organic layer/semitransparent metal anode. A PCE of 1.05% was achieved, which was comparable to that of the conventional OPVs at that time.[31] In addition, such top-illuminated inverted OPVs was further rejuvenated to a superior mechanically flexible device with a higher PCE of ~3%, which was reported by Chen *et al.* in 2009. By applying a device structure of stainless-steel foil/photoresist/SiO_x/Ag/ITO/Cs_2CO_3/P3HT:$PC_{61}BM$/MoO_x/Al   counter   electrode   grid

(10%)/ITO, flexible OPVs with excellent mechanical flexibility and high air stability was reported.[31] Moreover, device engineering for highly efficient top-illuminated OPVs has been further developed recently.[31-33] Particularly, optical microresonant cavity system consisting of a photoactive layer sandwiched between two metallic electrodes has received featured attention not only due to its low photon loss rate, but also its functions of confining and storing optical energy in small volumes allowing more photons being captured. By coating a functional layer on the Ag electrode, both the electrode transmittance and the electric field intensity in the photoactive layers can be enhanced, which is attributed to an induced microresonant cavity arising from fine-tuning-thickness of the capping layer.[32-35] As a result, PCE of 4.5% was achieved by Hee-Tae Jung's group using a device architecture of PET/Al/PCDTBT:PC$_{61}$BM/MoO$_x$-Ag-MoO$_x$ (nanopatterned 3D microresonant cavity layer), where PET is polyethylene terephthalate, PCPDTBT is poly[4,4-bis(2-ethylhexyl)-4Hcyclopenta[2,1-b;3,4-b']dithiophene-2,6-diyl-alt-2,1,3-benzothiadi azole-4,7-diyl], respectively. The idea of confining photons by microcavity structures was also reported by Lin et al.[36] They applied such structures into top-illuminated small-molecule OPVs and obtained the over 5% PCEs.[36] Jen's group further pushed the PCEs to 9.4% on flexible substrates by integrating the plasmonic effect into the ITO-free microcavity architecture. Due to the synergetic resonant coherence, a broadband and high absorption response of photoactive layer could be accomplished, which contributed to a substantially increased photocurrent.[37] By tailoring the absorption response, tandem OPVs with solution-processed silver paste as the reflective bottom electrode and silver nanowires as the transparent top electrode was reported by Brabec's group.[38] Although the PCE of 5.81% (on the glass substrate) and 4.85% (on the flexible substrate) were not sufficiently high, the possibility of printing efficient tandem OPVs

under ambient conditions was well demonstrated. Furthermore, other ITO-free OPVs have also been developed. For example, a top illuminated inverted organic photosensors with single layer graphene electrodes were demonstrated by Chabinyc's group.[39] Ag nanomesh transparent conducting electrode was demonstrated by Dong-Ho Kim and Dae-Geun Choi et al.[40] Highly electrical conductive polymer as the anode was demonstrated by Dong-Yu Kim's group.[41] Detailed explanations on materials and mechanisms of the top electrodes will be discussed in the **Section 6**.

The innovation of functional transparent electrode, particularly the methodology of layered light-trapping or microresonant cavity, would boost the PCEs. And the top-illuminated OPVs, (semi-)transparent OPVs and all-solution-processed OPVs would further push forward the commercial application prospects of the inverted OPVs.[42]

3. Electrode Buffer Layer

Although the polarity of charge collection is completely opposite in the inverted OPVs compared to their conventional counterparts (as shown in **Schemes 2a & 2b**, respectively), the photovoltaic processes are almost the same for both. The photons are firstly absorbed by the active layer and the electrons from the HOMO level of active layer (e.g., P3HT and $PC_{61}BM$) can be excited to the corresponding lowest unoccupied molecular orbital (LUMO) level, forming the excitons there (the majority of excitons are formed in the electron-donor materials, e.g., P3HT; and the minority excitons can also be formed in the electron-acceptor materials, e.g., $PC_{61}BM$). The difference of chemical potentials at the interface of the electron donor (P3HT) and the electron acceptor ($PC_{61}BM$) can act as an additional "field" to separate the excitons, where a charge-transfer state model is extensively employed to understand the processes in many reports.[42,43] The separated charge carriers can be selectively transported to the corresponding

electrodes due to the different energy levels of the charge extraction layer (CEL) between the active layer and the electrodes, for example, MoO_x and ZnO as shown in **Scheme 2b**. Therefore, both CEL and the electrodes function as the "selector" that can select a certain kind of charge carriers (the holes or the electrons) to be collected and thus the polarity of charge collection in the device is tuned. Apart from *charge selection*, the interfacial layers should possess the following functions as well:[43] *photon transmission* (allow photons to pass though and reach the active layer), *efficient charge transport* (allow charge carriers to be transported from active layer to the corresponding electrode with less charge loss), *energy level offset* (reduce charge carrier extraction barrier to increase photocurrent extraction from the active layer), and *surface modification* (modify the surface of the electrodes or the active layer). By inserting such functional interfacial layers between active layer and the electrodes, the PCEs of OPVs can be increased in various scales.[43] In addition, the material stability should also be considered to maintain the lifetime of OPVs.

3.1 Electron Extraction Layer

The electron extraction layer (EEL) was firstly introduced in organic light emitting diodes (OLEDs) to balance the charge carrier injection. By applying such layer into organic thin film transistors[44] and OPVs, device performance were dramatically improved as well. In general, the function of the EEL can be classified as suppressing surface states of active layer, protecting the active layer from being damaged by the metallic cathode, and changing the energy level alignment by forming dipole moments at the active layer/cathode interface.[45] Transition metal oxides (TMOs), alkali-metal compounds and ultrathin layer are the major three types of EELs and will be demonstrated below.

3.1.1 Transition Metal Oxides

ZnO

The most representative TMOs EEL is ZnO, which possesses several favorable physical properties including good transparency, high electron mobility, non-toxicity and low production cost.[46,47] ZnO is a n-type metal oxide with a LUMO and a HOMO energy level around -4.3 eV and -7.6 eV, respectively. The LUMO energy level of the commonly used electron acceptors (e.g., $PC_{61}BM$ and $PC_{71}BM$) is about -4.3 eV, and the HOMO energy level of the electron donors is around -5.0 eV, indicating that ZnO is a good EEL and hole blocking layer in BHJ OPVs.

In 2004, Tomoki Shirakawa and Katsumi Yoshino et al reported a sputter-deposited ZnO thin film (50-100 nm) as the EEL in the bi-layer structured OPVs with a device structure of $ITO/ZnO/C_{60}/P3HT/Au$. A monochromic external quantum efficiency (EQE) of over 70% at the peak wavelength and a PCE of 1.0% were obtained. Late on, White et al demonstrated a solution-processed ZnO thin film via using a precursor solution of zinc acetate in 2-methoxy ethanol and ethanolamine.[48] The OPVs with a device structure of $ITO/ZnO/P3HT:PC_{61}BM/Ag$ showed a comparable PCE with an enhanced short-circuit current (J_{SC}), which was attribute to the effective hole blocking effect from the inherently n-type characteristics of the solution-processed ZnO EEL. The Kelvin probe measurements demonstrated that the WF of sol-gel processed ZnO layer is -4.3 eV, which is close to its conduction band (-4.1 eV). Four-probe Hall effect technique illustrated the low carrier concentration of 10^{16}-10^{17} cm^{-3}, and high electron mobility of solution-processed ZnO thin film. Nevertheless, it was the small grains in ZnO thin film visualized in x-ray diffraction (XRD) spectra and atomic force microscopy (AFM) images that probably decreased the charge carrier mobility and deteriorated the charge transport. Taking these issues into account, our group improved the sol-gel method by using

optimized precursor solution and ameliorated thermal annealing process to make the higher

quality ZnO EEL.[49] Morphological characterizations by AFM and scanning electron microscope

(SEM) demonstrated that the ZnO thin film was quite uniform with nanoscale fibrils of ~10 nm

diameters. The ripple pattern on the ZnO surface was further proved to give light absorption

enhancement by light scattering effect. Moreover, the electron mobility of ZnO was measured to

be 4.46×10^{-4} $cm^2V^{-1}s^{-1}$, which was comparable to the electron mobility from most of organic

materials used as the EEL in organic electronics. By employing such high quality ZnO as the

EEL in the inverted OPVs, high PCE of 3.8% was observed with a device structure of

ITO/ZnO/PSiF-DBT:PC_{61}BM/MoO_x/Au, which is more than twice larger than that of OPVs

without ZnO layer, where PSiF-DBT is

poly[(2,7-dioctylsilafluorene)-2,7-diylalt-(4,7-bis(2-thienyl)-2,1,3-benzothiadiazole)-5,50-diyl]).

Moreover, other methods such as manipulating the concentration of solution, fine-tuning the

solvent and changing the processing conditions (e.g. temperature or spin-casting kinetic

parameters) have also been developed to achieve a conformal and pinhole-free film.[50-54] **Table 1**

compares the device performances of OPVs with similar architecture of ITO (or

FTO)/ZnO/organic active layer/HEL/metal cathode, where the ZnO EEL was processed by

different processing methods. Specifically, Shane O'Brien et al used single step sol-gel thin film

deposition, as shown in **Scheme 3a**, by changing the precursor concentrations, ZnO thickness

could be tuned from 80 nm to 350 nm with highest optical transmittance over 90% at wavelength

ranging from 400 to 800 nm.[50] Kyaw et al modified the sol-gel methods by changing solvents,

precursor concentrations and processing temperatures, as shown in **Scheme 3b**, to get higher

quality ZnO thin films.[51] It was found that lower concentrations ranging from 0.3 M to 0.5 M

with optimized solvent and temperature would result in a higher quality ZnO thin film with

smaller grain sizes and more uniform film morphology. By employing such ZnO thin film in OPVs with a device structure of FTO/ZnO/P3HT:PC$_{61}$BM/Au, a PCE of 2.01% was obtained from the OPVs with 120 nm thickness of the ZnO EEL. In addition, by changing the precursor concentration to tune the transparence of ZnO thin film, Kyaw et al obtained a high transparence of 95% in the visible region and a 43% enhancement in J$_{SC}$ thereby.[52] Hau et al further boosted the PCE to 3.78% and developed OPVs on the flexible plastic substrate by adopting the low-temperature solution-processed ZnO EEL.[53] The revolutionary application of solution-processed ZnO in roll-to-roll manufacture of the inverted OPVs was reported by Krebs et al.[54] A PCE of 2.67% was achieved from OPVs with a device area of 1 cm^2. Very recently, Basudev Pradhan et al reported an efficient inverted OPVs by using low-temperature (~100 °C) solution-processed diethylzinc precursor solution to form ZnO EEL.[55] The enhanced transparency and elevated electrical properties resulted in a highest PCE of 4.03% from P3HT:PC$_{61}$BM based OPVs.[55] In spite of different precursor concentrations, or temperatures or solvents, the overall sol-gel methods for preparing the ZnO EEL were almost identical, which can be classified into the typical process flow for the preparation of thin metal-oxide layers from solution, as shown in **Scheme 3c**.[56]

On the other hand, conformal and pinhole-free film can also be achieved via using atomic layer deposition (ALD) by controllably introducing reactant gas into the reaction zone at low temperatures.[57,58] In addition, the large-scale mass-production and low-temperature (<100 °C) processiblity of ALD makes it more preferable for industrialization. The device performance of OPVs using ALD processed ZnO EEL and the corresponding device structures are summarized in **Table 1**. Jen-Chun Wang et al reported an ALD prepared ZnO EEL in OPVs and observed a PCE of 4.18% from P3HT:PC$_{61}$BM based OPVs. The high PCE was resulted from the enhanced

hole blocking effect and enhanced electron collecting efficiency due to the fine-controlled high quality ZnO EEL.[58] And Hyeunseok Cheun et al found that the WF, surface roughness, and thin film morphology of ZnO EEL were independent on the thickness of the ZnO EEL, but the device performance was strongly dependent on the thickness of ZnO EEL. Thinner ZnO EEL would lead to a dramatically decreased electrical conductivity because of the oxygen trap effect.[59] Higher PCE of 4.1% was realized by using a 60 nm ALD ZnO film deposited at 90 °C. It was also found that low carrier concentration (2.1×10^{17} cm^{-3}) and high electron mobility (9.6 cm^2 V^{-1} s^{-1}) of the ALD film led to a high J_{SC} and FF.[60] Robert L.Z. Hoye et al reported an atmospheric ALD processed ZnO EEL, with an extremely high transparency (~100%) in visible region.[61] The processing procedure is simplified in **Scheme 3d**. Using similar strategies, more and more studies focusing on ALD ZnO EEL have been reported recently. Mi-jin Jin et al tuned the structural and optical properties of ZnO EEL by sequentially injecting ZnO precursor solution and using O_2 plasma treatment during the ALD process. By changing the processing conditions, tunable nanocrystal of ZnO was realized, rendering a high PCE for the final device.[62] Mohamed Eita et al applied ALD to fabricate the layer-by-layer structured multilayers of polyacrylic acid and ZnO nanoparticles as the EEL in OPVs.[63] Zhe Lu et al applied Au/LiF-modified ZnO interlayer to enhance the charge collection efficiency and obtained a 40% enhancement in PCE.[64] It was found that the major enhancement was originated from J_{SC}, which was due to the enhanced electrical transport properties of modified ZnO EEL. Similar study was also conducted in dye-sensitized solar cells (DSSCs), where Li^+ being inserted into ZnO nanocrystalline particles were used as the EEL. The incorporation of Li^+ was found to improve the charge transport and suppress the recombination and consequently to enhance J_{SC} dramatically.[65] The open-circuit voltage (V_{OC}) can be enlarged by modifying the energy state of ZnO layer. Hongli

Gao and Xin Liu et al obtained a V_{OC} of 0.67 V from P3HT:PC$_{61}$BM system by applying

H-plasma treatment to tune the WF of ZnO.[66]

TiO$_2$

Similar to ZnO, TiO$_2$ is another TMO as an efficient EEL. TiO$_2$ possesses the features of

good transparency, high electron mobility, non-toxicity and low-production cost. Due to the well

matched conduction band (-4.4 eV) with the LUMO energy level of PC$_{61}$BM (-4.3 eV) and the

low-lying valence band (-7.5 eV) for effectively blocking the holes, TiO$_2$ stood out as a

promising EEL in the inverted OPVs. The investigation on fundamental physics of TiO$_2$,[67,68] the

application of TiO$_2$ in photocatalysis[69] and in DSSCs have been well reviewed previously.[70-72]

Here, a brief introduction will be given on the processing methods and the corresponding device

performance of the inverted OPVs using the TiO$_2$ EEL.

Various methods have been reported to prepare TiO$_2$ thin films. These include micelle and

inverse micelle methods, sol-gel method, solvothermal method, hydrothermal method, direct

oxidation method, physical vapor deposition, chemical vapor deposition, electrodeposition,

sonochemical method, and microwave method.[67-69] Among them, the sol-gel method using

hydrolysis of a titanium precursor was most widely used for preparation of TiO$_2$ in OPVs.[73,74]

The general preparing procedures outlined by Pasquarelli et al, was similar to those used for

preparation of other TMOs as schematically described in **Scheme 3d**. By changing the

processing conditions such as deposition methods and precursor solvents to tune the TiO$_2$ crystal

forming environment, TiO$_2$ with various crystal types and film morphologies can be achieved.

Schemes 4a & 4b display different deposition methods and the reaction schemes for the

formation of phase-pure TiO$_2$.[67,75]

The early application of TiO$_2$ in DSSCs was reported by Grätzel's group in 1990's.[76-78] The

titanium isopropoxide precursor was treated at a high temperature of 450 °C to give a very thick film, which impede its application in thin-film OPVs. Instead, Heeger's group introduced a low-temperature sol-gel process based on a precursor solution of titanium isopropoxide mixed with 2-methoxyethanol and ethanolamine.[79,80] High transparency (Eg ~ -3.7 eV) with small surface roughness was obtained. **Table 2** summarizes the device performance of OPVs using TiO_2 or TiO_x EEL.[81-83] Specifically, Kim et al reported the gel-deposited ultrathin TiO_x layer (30 nm) in the conventional OPVs, which induced a 50% enhancement in J_{SC}.[84] The spatial redistribution of the light intensity led to an increased photogeneration of charge carriers and a 100% internal quantum efficiency was realized thereby.[85] Xichang Bao et al[86] applied the trabutyl titanate as the Ti precursor to obtain TiO_x EEL by the traditional sol-gel method, and a highest PCE of 4.65% was observed from $P3HT:PC_{61}BM$ system. The low temperature (90°C) processed TiO_x shows a good electrical conductivity of 7.4×10^{-6} S cm^{-1}.[87] Apart from tuning temperature in the thermal treatment, ultraviolet (UV) irradiation is another way to optimize the TiO_x layer by reducing the electron traps in the titanium oxide.[88]

Nanostructured TMOs

In addition to planar TMOs layer, nanostructured TMOs have also been introduced in OPVs. By using certain nanostructures such as well-ordered, mesoporous and nano-wire TiO_x and ZnO, the interfacial area between the TMOs layer and active layer can be further enlarged. Such OPVs was also referred as the "double-heterojunction" devices (here the "double-heterojunction" was different from that in the tandem OPVs), where one heterojunction was the disordered BHJ at the electron donor/electron acceptor (D/A) interface and the other one was an ordered heterojunction at the electron donor/n-type metal oxide (D/EEL) interface, as shown in **Scheme 5a**. The enlarged D/A interfaces in BHJ composite can offer an additional "field" to separate the excitons.

The enlarged D/EEL interface from the ordered heterojunction can also offer an additional "field" to separate the photo-generated excitons due to the difference in chemical potentials between D and EEL (n-type materials). On the other hand, an ordered heterojunction at the A/HEL interface can also be realized by using nano-structured HEL materials knowing that excitons can also be formed in A. In this way, enhanced charge extraction efficiency can be realized and more charge carriers are expected to be extracted, transported and collected. Since TiO_x can be patterned into a continuous network for electron transport,[89-90] the excitons can be dissociated effectively at the interface between TiO_x and polymer if polymer and TiO_x can be structured in an ordered style with a pore size of 20-30 nm, which is comparable to the exciton diffusion length. **Scheme 5b** shows a TiO_x nanotube infilled by P3HT:PC_{61}BM BHJ composite. The vertical channel confinement can also improve the charge transfer property. It was reported that the charge carrier mobility of polymer was enhanced about 20-fold due to the vertical "channel confinement effect" in the pores of TiO_x nanotube along the direction perpendicular to the substrates.[91-93] As a result, the concept of "double-heterojunction", including the disordered BHJ at D/A interfaces and ordered heterojunction at D/EEL interfaces, would not only facilitate the exciton dissociation due to the enlarged large-surface area, but also optimize the ordered network morphology and improve charge transport properties. This idea can be revealed by filling the BHJ composite into the pores of sintered TiO_x nanocrystals.[94,95] Gopal K. Mor et.al, realized the "double-BHJ" via utilizing a vertically oriented TiO_x nanotube arrays as the EEL, and infiltrating with P3HT:PC_{61}BM (**Scheme 5b**). The length of TiO_x nanotube was 270 nm and the size of pores was chosen to be 50 nm, which was large enough to infiltrate the nanotubes from the subsequent polymeric layer, allowing the polymer chains to coil, aggregate and have a more film-like environment.[95] The well patterned P3HT originated from the TiO_x nanotube was demonstrated

to have the coiled chains pattern with a shorter conjugation length. Thus, the vertically oriented TiO_x nanotube led to enhanced charge-carrier mobility due to the ordered nano-structure. Combined with the additional excitons dissociation sites at the TiO_x/P3HT interfaces, an enlarged J_{SC} of 12.4 mA/cm^2, elevated EQE (maximum 80% at 538 nm) and enhanced PCE of 4.1% were observed from P3HT:PC$_{61}$BM system. Bang-Ying Yu et al reported a similar work from OPVs with a device structure of ITO/TiO_x/P3HT:PC$_{61}$BM/V$_2$O$_5$/Al.[96] The self-organized TiO_x nanotubes arrays were grown by anodizing Ti metal in glycerol electrolyte containing 0.5 wt% NH$_4$F and 1.0 wt% H$_2$O with 20 V potential, after annealing at 500°C for 1 hour, the TiO_x film with an anatase phase and a diameter of 15-25 nm was formed. The enhanced electrical conductivity of TiO_x thin film gave rise to an enlarged J_{SC} due to reduced charge carrier loss during the transport process.[96]

As shown in **Scheme 5d**, the nanofiber structured ZnO film has also been studied.[97] Dana C. Olson et al fabricated the vertically aligned ZnO nanofibers, and filled the ZnO nanopores with polymer and the polymer:fullerene composite. The hybrid solar cells with BHJ composite of ZnO nanofibers:P3HT exhibited a V_{OC} of 0.44 V, a J_{SC} of 2.2 mA/cm^2, a fill factor (FF) of 0.56, and a PCE of 0.53%. In contrast, the double heterojunction OPVs based on P3HT:PC$_{61}$BM system using ZnO nanofibers exhibited a V_{OC} of 0.44 V, a J_{SC} of 10.0 mA/cm^2, a FF of 0.43, and a PCE of 2.03%. The dramatically increased J_{SC} confirmed the function of the double heterojunction. Although the hypothesis of mid-gap states and cascading electron transfer from PC$_{61}$BM to the ZnO nanorods have been provided, the reason for the erratically small V_{OC} and the mechanism for the electron transport need to be further addressed. In this point of view, Kazuko Takanezawa et al studied P3HT:PC$_{61}$BM/ZnO nanorod OPVs with a thicker hybrid layer of 450 nm.[98,99] By increasing the length of the ZnO nanorods, the FF was increased from 38%

to 50%, which was due to the enhanced electron collecting and transporting property of ZnO nanorod arrayed in P3HT:PC_{61}BM/ZnO nanorod system. Moreover, the presence of the highly electrical conductive ZnO nanorod (high electron mobility of ~ 1-5 $cm^2 s^{-1} v^{-1}$) shortened the average distance from the generation point of the charge carriers to the ZnO surface.

Apart from "double heterojunction" structures, TMOs/TMOs and TMOs/organic nano-composites have also been used as the efficient EEL. Jian Liu et al applied a TiO_x modified ZnO nanocrystal layer as the EEL in the inverted OPVs. The improved contact with the metals electrode effectively reduced the interfacial charge recombination loss, resulting in a PCE of 6.53% from the PCDTBT:PC_{61}BM BHJ system.[100] Furthermore, Liu sensitized the ZnO nanocrystals with a blue fluorescent conjugated polymer, poly(9, 9-bis-(6′-diethoxylphosphorylhexyl) fluorene) to obtain a more uniformly dispersive and high electrical conductive EEL. A PCE of 7.56% was achieved for P(IID-DTC):PC_{61}BM BHJ system,[101] where P(IID-DTC) is poly[N-dedocyldithieno[3,2-b;6,7-b]carbazole-alt-N,N'-di(2-octyldodecanyl)-isoindigo]. Ting Hu and Yiwang Chen et al reported a ZnO/graphene oxide composite modified by amphiphilic fullerene-end-capped poly(ethylene glycol) as the EEL to reduce charge carrier recombination and to enhance the electron extraction efficiency. A PCE of 8.1% was realized by using the polythieno[3,4-b]thiophene/benzodithiophene (PTB7):PC_{71}BM system.[102] Other studies on TMOs/self-assemble monolayer and TMOs/polyelectrolyte will be overviewed in the **Section 4**.

3.1.2 Alkali-Metal Compound

Similar to the functions in OLEDs, insulating alkali-metal compounds such as LiF, CsF, Li_2O and Na_2O were also utilized to establish the desired interfacial chemistry and desired trapped interface charge density for balancing the injection between the electrons and the holes. Among them, LiF was the most commonly used EEL modification layer in OPVs.[103] Alkali

metals, alkaline earth metals incorporated with organic molecules and alkali metal (Li^+, Na^+, K^+, Rb^+, and Cs^+) acetates and fluorides were also reported as the EEL in both OLEDs and OPVs.[104]

The representative alkali-metal compound Cs_2CO_3 as an interfacial layer was firstly reported by Canon group.[105] In 2006, Gang Li et al reported its applications in OPVs with a device structure of ITO/Cs_2CO_3(1 nm)/P3HT:$PC_{61}BM$/V_2O_5/metal.[107] A PCE of 2.25% was demonstrated with a J_{SC} of 8.42 mA/cm^2, V_{OC} of 0.56 V. The relatively low PCE was mainly due to the thin active layer. Still in Yang's group, low temperature annealed Cs_2CO_3 interfacial buffer layer was reported in 2008, an improved PCE with J_{SC} of 11.17 mA/cm^2, V_{OC} of 0.59 V, and FF of 63% was observed from the inverted OPVs.[107] In general the decomposition temperature of Cs_2CO_3 is 550-600 °C,[108] while during low temperature annealing, the Cs_2CO_3 may decompose into cesium oxide, indicating the formation of a n-type doped Cs_2CO_3 thin film after the annealing process. The surface energy of the Cs_2CO_3 thin film was also demonstrated to be changed by thermal annealing, with surface property shifting from hydrophilic to hydrophobic, and consequently favoring the polymer film growth.[109] A. Barbot also reported a C_{60} doped Cs_2CO_3 thin film as the EEL, reaching a PCE of 3.79%, with 26% improvement compared to the control devices.[110] Very recently, thermal-annealing-free inverted OPVs using ZnO nanoparticles (NPs)/Cs_2CO_3 bilayer as the electron-selective layer was reported by G. Cheng et al.[111]

Apart from Cs_2CO_3, a number of other salts, including alkali carbonate such as Li_2CO_3, and cesium-containing salts such as CsF, cesium acetylacetonate, were also utilized as the EEL in OPVs. The processes are as following: the salts were firstly dissolved in water or polar organic solvent such as 2-ethoxyethanol to form dilute (0.2 wt %) solutions,[112] followed by spin-coating

process to form a 0.6-3 nm thick film. The function of the thin layer was to lower the WF of the ITO or FTO electrode. With the addition of only a few monolayers of molecules, it was believed that strong dipole layer was formed at the interface. As shown in **Scheme 6**, a thin layer of oxygen-metal species was formed at the surface of ITO or FTO electrode. The dipole here pointing from the ITO electrode to the vacuum level reduced the ITO surface WF. Moreover, the interfacial charge transfer rate at the cathode was enhanced, leading to a decreased series resistance. As a result, both J_{SC} and V_{OC} were increased.

3.1.3 Ultrathin Layer

Low-Work function Metals

In the conventional OPVs, the charge collection and the built-in potential can be increased by introducing a thin layer of low WF metal (Ca and Mg).[113] The low WF metals can be served as an interfacial layer to collect the electrons efficiently when they are sandwiched between the ITO electrode and the active layer in the inverted OPVs. D. W. Zhao et al reported an inverted OPVs using an ultrathin Ca layer (1 nm) as the EEL.[113] With an optimal MoO_x (3 nm) as the anode buffer layer, the inverted OPVs using P3HT:PC_{61}BM possessed a PCE of 3.55%. The WF of Ca is -2.9 eV, which lowered the WF of ITO through the Fermi level pinning between Ca and PC_{61}BM, thereby increasing the V_{OC} of OPVs.

Conjugated Polymers

Similar to the alkali-metal compounds, the mechanism for using conjugated polymers as the interfacial layer was originated from the formation of an interface dipole layer that leads to a substantial reduction of the WF of the electrodes. Organic interfacial modifiers such as polythylene oxide,[114] polyethyleneimine based structures[115,116] and polyvinylpyrrolidone[117] have been reported recently. **Scheme 7** presents a few conjugated polymers used as the EEL for

the inverted OPVs. Tang et al utilized a thin (<10 nm) cathode interlayers of conjugated polymer, poly(3,3'-([(9',9'-dioctyl-9H,9'H-[2,2'-bifluorene]-9,9-diyl)bis(1,4-phenylene)]bis(oxy))bis(N,N -dimethylpropan-1-amine)) to improve the device performance.[118] As a result, an approximatively 20% enhancement was demonstrated in J_{SC} and FF. Moreover, Cao's group also reported OPVs with enhanced PCEs by using an interlayer of poly[(9,9-bis(3'-(N,N-dimethylamino)propyl)-2,7-fluorene)-alt-2,7-(9,9–dioctylfluorene)] (PFN).[119] In addition, ethanol-soluble poly (9,9-bis(60-diethoxylphosphorylhexyl)fluorene) (PF-EP), quinoxaline-containing poly(4,5-ethylene-2,7-carbazole) (PECz-DTQx) have also been used as the interfacial layers.[120] The conjugated polyelectrolytes (CPEs), which consist of a conjugated backbone with side groups that carry ionic functionality have been identified as very promising materials for lowering the WF of the cathode.[120-122] Scanning Kelvin probe microscopy revealed that the enlarged V_{OC} was attributed to the introduction of paralleled dipole moment due to the ultra-thin interfacial layer. Furthermore, the electric field from the interfacial dipole layer is estimated to be 6×10^5 V cm^{-1}, which is orders of magnitude higher than that of average built-in field in the control device under the short-circuit condition.

On the other hand, the interfacial layer without forming a dipole moment to enhance device performance have also been reported.[122,123] The enhanced electrical conductivity of the interfacial layer resulted in enhanced J_{SC}, where the V_{OC} did not change because no dipole moments were induced. The representative work in this direction was demonstrated by our group.[122,123] The details will be described in the **Section 4**.

3.2 Hole Extraction Layer

In comparison to the EEL, to effectively facilitate hole extraction, transportation and collection, the hole extraction layer has also been introduced in OPVs. The HEL materials

including PEDOT:PSS,[123] graphene oxides (GOs),[124] novel composites[125] and semiconducting TMOs (MoO_3, WO_3, NiO and V_2O_5, etc.)[126,127] have been introduced to modify the surface of the anode. However, the most applications of solution-processed PEDOT:PSS, GOs and some novel composites were reported in OPVs with a conventional device structure. These materials were directly solution-deposited on the ITO/glass substrates followed with thermal annealing at various elevated temperatures.[128-131] While directly applying these materials on the top of BHJ composite in the inverted OPVs may cause some serious issues. For example, the aqueous acidic PEDOT:PSS would cause degradation of conjugated polymers and give a poor contact with the hydrophobic photoactive layer. In addition, high temperature annealing would also damage the film morphology of BHJ active layer.[132,133] In contrast, these issues can be avoid by using the thermal-evaporated TMOs, which therefore, are the most widely used HEL materials in the inverted OPVs.

The TMOs including V_2O_5, MoO_3 and RuO_2 were firstly introduced as the anode electrode modification interlayers to increase the hole-injection in OLEDs by Tokito et al in 1990's.[134] The motivation for investigating these materials was mainly stemmed from their high WF, good semiconducting properties and high optical transparency, which are the critical characteristics for efficient charge carrier extraction and collection.[135] By applying these TMOs in the inverted OPVs, device efficiency can be dramatically boosted because of their abilities of tuning the effective WF of the electrode[136] and keeping the excitons away from the electrodes to prevent undesired surface charge recombination.[137,138] To efficiently select charge carriers, the WFs of the TMOs HEL need to be large enough to form the ohmic contact with BHJ composite, lowering the energy barrier for hole extraction and preventing the electrons "back-transfer" from the metals electrode to BHJ composite.[139] The WF of commonly used TMOs, the HOMO and

LUMO energy levels of both D and A are summarized in **Scheme 8**. Proper selection of these materials can make an ohmic contact between BHJ active layer and the HEL, which could minimize the energy loss during the charge extraction processes. Similar to the EEL, the HEL should also have other properties such as good electrical conductivity, robust chemical stability and easy-processibility. Based on different mechanisms for the hole extraction, both n-type and p-type semiconductor TMOs can be used as the efficient HEL to modify the anode in the inverted OPVs.

3.2.1 n-type Transition Metal Oxides

n-type semiconducting transition metal oxides (TMOs) such as MoO_x, WO_3 and V_2O_5 have been widely used as the HEL in the inverted OPVs. It is noted that MoO_x was previously reported as p-type semiconducting materials, with the LUMO (or electron affinity (EA)) and the HOMO (or ionization energy (IE)) located at -2.3 eV and -5.3~ -5.4 eV, respectively.[140-144] However, they were recently unambiguously demonstrated to be n-type materials with very deep lying electronic states.[145-148] The combined ultraviolet photoelectron spectroscopy (UPS) and inverse photoemission spectroscopy (IPES) spectra taken from MoO_x, WO_3 and V_2O_5 layers showed the similar deep-lying electronic states, with the valance band (VB) edge located at -2.5 ~ -3 eV, which is below the Fermi level and the conduction band (CB) edge, as shown in **Scheme 8**. The n-type conducting properties was mainly originated from the slightly non-stoichiometric composition, with some oxygen deficiency proved by x-ray photoelectron spectroscopy (XPS).[149]

The applications of these TMOs as the HEL in OPVs have been widely studied despite of their n-type features. The WFs of these TMOs films are close to the HOMO (IE) energy levels of organic materials (**Scheme 8**), which allows the electrons to be transferred from organic layer to

the TMOs layer until a thermodynamic equilibrium established across the interface, resulting in the Fermi level pinning. Such band bending occurrences are described in **Scheme 9a**, which shows the energy level alignment and the band bending at the MoO_x/ 4,4'-bis(carbazol-9-yl)biphenyl (CBP) interface.[150] The low HOMO energy level (or large IE) of MoO_x (-9.7 eV) precludes the holes being transported via the VB. While the energy level difference between the LUMO energy level of MoO_x and the HOMO energy level of CBP is small enough to ensure efficient electrons being transported among these two materials. Under the positive bias, the hole-injection into the organic film can take place due to the electron being transferred from the HOMO of CBP to the LUMO (CB) of MoO_x. In OPVs, as shown in **Scheme 9b**, at the interface between the MoO_x HEL and organic layer, the photo-generated holes in the electron donor polymers recombines with the electrons from the MoO_x HEL, leaving the holes in the MoO_x, which was equivalent to the "hole-extraction". Such "hole-extraction" model was also demonstrated with $ITO/MoO_3/NPD$ devices, as shown in **Scheme 9c**,[151] where NPD is N,N'-diphenyl-N,N'-bis(1-naphthyl)-1,1'-biphenyl-4,4'-diamine. The hole-extraction via using above n-type TMOs layers is widely employed in the inverted OPVs, although the "hole-extraction model" was of less awareness in most reports. Here the detailed application of MoO_x, WO_x and V_2O_5 in the inverted OPVs will be summarized.

MoO_x

Among all the TMOs, MoO_x shows premium device performance with easy processing such as thermal evaporation deposition and solution deposition. Thermal evaporated MoO_x (e-MoO_x) allows film thickness to be controlled at a nanometer scale and gives a denser and uniform film. For e-MoO_x, the oxygen deficiency cause the Fermi level close to the CB of MoO_x.[152,153] The WF of e-MoO_3 is strongly dependent on the stoichiometry and highly sensitive to the surface

contamination. Particularly, in oxygen or air, the WF decreases from 6.7 eV to -5.3 ~ -5.7 eV[154,155], but still sufficient to yield good ohmic contacts with organic hole transporting materials, giving that the optimum HOMO level of polymers generally resides between -5.2 ~ -5.6 eV.

Cephas E. Small et al showed that compared with the conventional bottom MoO_x p-contact, enhanced ohmic contacts can be made in the inverted OPVs via using e-MoO_x and silver as a top p-contact.[156] By using MoO_x as the anode buffer layer in the inverted OPVs, our group demonstrated high PCE of ~8.6% from the inverted OPVs. Cao's group further demonstrated a PCE of over 9%. Nevertheless, the processing of thermal evaporation still limits its application in large-scale production. To overcome this issue, solution-processed MoO_x (s-MoO_x) was introduced by Galatsis et al via using sol-gel technology.[157-160] While most solution-processed MoO_x layer possess large surface roughness with trap states and of complicated processing procedures and high annealing temperature over 350 °C.[161,162] A rather simple way to prepare the high quality MoO_x film without any thermal annealing processing has been developed in our group. The precursor solution was firstly prepared by drop-wisely adding H_2O_2 (30%) into molybdenum powder in the ice-water bath followed by further purification and then dried by heating, and then using methanol to dissolve the solid to get a precursor solution with a concentration of 10 mg/mL.[163] The s-MoO_x thin film was then spin-coated from the above precursor solution without further thermal annealing. By using an ultra-thin s-MoO_x in OPVs, enhanced PCE of 4.55% for OPVs based on poly(thienothiophene-co-benzodithiophenes)7-F20 (PTB7-F20):$PC_{71}BM$ BHJ system and increased detectivity of 1.02×10^{13} Jones (detectivity at λ= 800 nm) for polymer photodetector based on poly(5,7-bis(4-decanyl-2-thienyl)thieno[3,4-b]diathiazole-thiophene-2,5) (PDDTT):$PC_{71}BM$

BHJ system, respectively, were observed.[164,165] In comparison, Liu et al also prepared the precursor solution by dissolving ammonium molybdate into a mixture of hydrochloric acid and de-ionized water.[166,167] Girotto et al[168] prepared the precursors by directly dissolving MoO_x powder into H_2O_2. Zilberberg et al[169] reported a precursor based on bis(2,4-pentanedionato) molybdenum (VI) dioxide isopropanol solution. Due to the rough manipulation in solution process in comparison with thermal evaporation, the film quality of s-MoO_x was inferior to that of the e-MoO_x. To obtain a high-quality s-MoO_x film, following requirements need to be considered: (1) the film roughness should be low enough to avoid the pin-hole induced leakage current; (2) the processing should be simple to lower down the manufacturing cost; (3) the WF of s-MoO_x should not be sacrificed.[170] Although the s-MoO_x possesses the priority over e-MoO_x in respect to manufacturing simplicity, the OPVs performance was inevitably restricted due to the direct deposition processing of s-MoO_x on the surface of photoactive layer. This is because that highly reactive precursors of s-MoO_x may damage the organic materials.[171] Moreover, the critical post-processing such as UV-plasma and high temperature annealing may also damage the BHJ thin film morphology, which is precisely the prerequisite to high device performance.

In contrast, the e-MoO_x was widely employed in the inverted OPVs alternatively. **Table 3** summarizes the major applications of e-MoO_x in the inverted OPVs. It is noted that in H. Choi's studies, high FF of 70% was achieved in the inverted OPVs with a device structure of ITO/TiO_x/FPQ-Br/P3HT:$PC_{61}BM$/MoO_x/Au, which was 60% larger than that without the FPQ-Br interfacial modification layer. These results indicated that the contact between photoactive layer and the MoO_x layer is critical for approaching high PCE. Utilization of s-MoO_x to realize full printing OPVs is another ongoing direction. Weiming Qiu et al reported solution-processed nafion-modified MoO_x layer for the inverted OPVs with a comparable

PCEs.[171] However, the current bottle-necks are the poor contact between photovoltaic layer and s-MoO_x and the low film quality of s-MoO_x layer.

WO_3

WO_3 is another n-type semiconductor with very deep lying electronic states,[173] which are strongly dependent on its stoichiometry, crystalline structure and processing conditions.[173] Similar to MoO_x, thermally evaporated WO_3 (e-WO_3) are highly n-doped due to oxygen vacancies, which tunes the Fermi level close to the CB of WO_3. Further oxygen deficiency would lead to metallic properties of WO_2. Thus the surface contamination, particularly in air and oxygen, can strongly affect the final device performance of OPVs incorporated with WO_3.

The application of WO_3 in the inverted OPVs was firstly reported by Chen Tao et al.[174,175] They claimed that the high WF of WO_3 (-4.8 eV) would enhance the hole collection at the photoactive layer/Ag interface. The OPVs with a device structure of ITO/TiO_x/P3HT:PC_{61}BM/WO_3/Ag exhibited a V_{OC} of 0.60 V and a FF of over 60%. The thickness of WO_3 layer was controlled to be ~10 nm, where a thicker film would introduce extra series resistance within itself and a thinner layer cannot effectively form a good contact between photoactive layer and the top electrode. Seungchan Han et al also reported an e-WO_3 thin film with a notably small root-mean-square (RMS) roughness of 0.88 nm, which is favorable to make a good contact between active layer and the HEL, thereby resulting in an over 70% FF.[176] On the other hand, solution-processed WO_3 (s-WO_3) has also been demonstrated.[177,178] Weiming Qiu et al reported a PCE of 3.49% from OPVs based on P3HT:PC_{61}BM system with the s-WO_3 HEL, which was processed from bis(2,4-pentanedionato) molybdenum (VI) dioxide precursor solution. These results indicated s-WO_3 is a promising candidate for large-scale solution-processed OPVs.[179]

V$_2$O$_5$

The third widely used n-type metal oxide as the anode buffer layer is V$_2$O$_5$, which possesses a band gap of 2.8 eV.[180] Noted that the WF of V$_2$O$_5$ (using thermal deposition processing in ultra-high-vacuum conditions <10^{-10} Tor) is -7.0 eV, which offers an excellent ohmic contact between organic materials and the V$_2$O$_5$ HEL.

Early studies of vacuum-evaporated V$_2$O$_5$ (e-V$_2$O$_5$) layer as the anode buffer layer in OPVs with a conventional device structure of ITO/V$_2$O$_5$/BHJ composite/Al and an inverted device structure of ITO/Cs$_2$CO$_3$/BHJ composite/V$_2$O$_5$/Al were reported by Shrotriya et al.[181-184] Comparable device performance from OPVs with both conventional and inverted device structures indicated that V$_2$O$_5$ can be an efficient HEL in OPVs.

Similar to other n-type TMOs, the WF of V$_2$O$_5$ was significantly depended on the processing methods. Especially, the WF of solution-processed V$_2$O$_5$ (s-V$_2$O$_5$) layers prepared by sol-gel method was relatively lower than that of e-V$_2$O$_5$.[185] V$_2$O$_5$ layer processed from nano-particles dispersions was also reported.[185-187] However, the RMS of the s-V$_2$O$_5$ thin film was generally larger than that of the e-V$_2$O$_5$, which indicated the contact between the s-V$_2$O$_5$ HEL and BHJ active layer would cause energy loss, resulting in an inferior PCE. For the s-V$_2$O$_5$ prepared by sol-gel deposition, high-temperature processing (>300 °C) is need to achieve a certain microstructure or the pure crystalline phase, which, however, will cause the decomposition of the active layer materials in the inverted OPVs. Instead, low-temperature solution-processed s-V$_2$O$_5$ has been reported in recent years. Kirill Zilberberg et al reported sol-gel processed s-V$_2$O$_5$ HEL in the inverted OPVs. A high work function of -5.3 eV was realized for s-V$_2$O$_5$ prepared in ambient air using vanadium (V)-oxitriisopropoxide as a precursor without any post-annealing or plasma treatment.[188] Furthermore, Chih-Ping Chen et al employed a precursor solution of the vanadium (V) triisopropoxy oxide in the mixture of isopropyl alcohol and deionized water to

fabricate the s-V_2O_5 layer. Enhanced PCE was achieved by using s-V_2O_5 as the HEL in the inverted OPVs, which was originated from the minimized interface defects, and reduced charge recombination and decreased leakage current thereby.[189] In addition, Terho Kololuoma et al developed a stable and flexoprintable ink by modifying the vanadium alkoxide precursor with a right type of coordinating ligands to print out the HEL for the inverted OPVs.[190] Although the PCE ranging from 3.5 % to 4.5 % was slightly lower than the reference cells using the vacuum-deposited V_2O_5 as the HEL, it still implied a bright vista for full-printable cheaper OPVs in the near future.

3.2.2 p-type Transition Metal Oxides

Different from n-type TMOs, p-type characteristics of NiO is originated from positive charge compensation at the thermodynamically favored Ni^{2+} vacancies.[191-193] The WF of NiO is strongly depended on the surface chemistry, crystal orientation and processing conditions. The surface of NiO film may adsorb surface contaminants (nitric oxide, carbonaceous and hydroxyl species) upon exposing in ambient air, leading to a decreased WF.[194-196] Interestingly, Ratcliff et al reported that O_2 plasma treatment may increase the WF of NiO from -4.7eV to -5.3 eV due to the dipolar nickel oxyhydroxide formed on the NiO surface.[197] The NiO used in OPVs was firstly introduced by Irwin et al.[198] An optimized ~10 nm NiO layer was inserted between BHJ active layer and the ITO anode by using pulsed laser deposition. Over 5% PCE was obtained from OPV based on P3HT:$PC_{61}BM$ system. Recently, solution-processed NiO was also reported for OPVs.[198-200]

Since the pure stoichiometric NiO is an excellent insulator, with the electrical conductivity in the order of 10^{-13} S cm^{-1} at room temperature,[201] while after stoichiometric changes, the NiO_x becomes a wide bandgap p-type semiconductor. For the inverted OPVs, the NiO acts as both

HEL and electron blocking layer on the top of BHJ active layer. Proper methods for preparing

premium NiO layer in the inverted OPVs are still need to be studied.

4. Interfacial Modification Layer

As aforementioned, TMOs such as ZnO, MoO$_x$ were widely used as the EEL and the HEL in

the inverted OPVs, respectively. However, poor electrical coherence at the organic/inorganic

interface,[202-205] would result in an inferior device performance. Such poor contact was

originated from the hydroxyl groups on the surface of the metal oxide, which would cause charge

trapping and high charge carrier recombination at the interface,[206] leading to limited FFs in the

inverted OPVs. Therefore, the electrical properties of these TMOs need to be appropriately

manipulated to minimize the resistance throughout the interfaces and maximize the charge

carrier collection efficiency at the electrodes. On this concern, several modification materials are

thereby introduced to improve the electrical properties of TMOs and thus boosting PCEs.

4.1 Non-Cross-Linkable Self-Assembled Monolayers

One of the factors that restrict the performance of the inverted OPVs is the film morphology

of BHJ composite layer. Since non-appropriate phase separation will generate geminate and

non-geminate charge recombination, causing energy losses within OPVs.[207-210] Therefore, it is

imperative to decrease the series resistance across the interfaces and to control the phase

distribution in BHJ active layer simultaneously. One approach to solve these two issues

synchronously is to insert an ultra-thin layer of self-assembled monolayers (SAMs) between the

inorganic charge extraction layer (HEL or EEL) and BHJ active layer.[211-216] Through the

chemical reaction between the hydroxyl groups and the anchoring group (usually carboxylic acid

and phospholic acid) on the surface of metal oxides, a corresponding ester linkage can be formed.

Thus, the SAMs can protect the metal oxide layer from organic solvent by the immobilized

function group, and passivate the surface by terminating the hydroxyl groups on the metal oxides as well. Furthermore, the interactions between BHJ active layer and the functional groups on the other side of the SAMs can also provide certain molecular stacking patterns by self-assembling. In this way, stacking pattern of conjugated polymer in BHJ active layer can be tuned from "face-on" to "edge-on" in contacting with the bottom electrodes, which would facilitate charge carriers being transferred from BHJ active layer to the corresponding electrodes.[217]

Scheme 10 lists the chemical structures of several examples of non-cross-linkable SAMs as the interfacial modification layers for OPVs. Hau et al firstly reported to use fullerene derivative SAM (C_{60}-SAM), terthiophene SAM (TT-SAM), benzoic acid SAM (BA-SAM) and lauric acid SAM (LA-SAM) to modify the interface of TiO_x/BHJ composite in the inverted OPVs.[213] The PCE of 2.8% from the control OPVs, to the PCE of 3.0% from LA-SAM modified OPVs, 3.2% from BA-SAM modified OPVs, 3.4% from TT-SAM modified OPVs and 3.8% from C_{60}-SAM modified OPVs, were observed. The overall increased PCEs were originated from the improved interfacial contact by SAMs, which was proved by the contact angle measurement. Among these SAMs, the greatest PCE improvement was obtained from the inverted OPVs with C_{60}-SAM modification. Such enhancement can be understood by an easier electron extraction process, where good electron-withdrawing property of C_{60} molecules makes it much easier for photoinduced charge carriers to be transferred from BHJ composite to the C_{60}-SAM modification layer.[218,219] Thin film morphology of BHJ active layer tuned by underneath C_{60}-SAM layer also dedicated to the improved PCEs. Stacking patterns (face-on or edge-on), ordering (crystallinity) of conjugated polymers, and the film morphology of BHJ active layer can also be influenced by the SAMs underneath in certain degrees. Hau also found that nano-structures of P3HT and accumulation of $PC_{61}BM$ to the bottom of the EEL interface have been increased by using

C_{60}-SAM modification layer,[213] which provided a better percolation conduction pathway for $PC_{61}BM$, consequently improved the overall phase distribution and BHJ film morphology, resulting in enhanced PCEs.

Different anchoring groups in fullerene-based SAMs can also be used to tune the device performance via decreasing the trap-states, tuning the energy level offset and improving the film morphology of upper BHJ composite. Various C_{60}-based SAMs with different anchoring groups (catechol, carboxylic acid, and phosphonic acid), as shown in **Scheme 10** (SAM[1-5]), have been used to improve OPVs performance.[220] PCEs improved from 3.47% (without SAM modification) to ~4.4% (with the carboxylic acid C_{60}-SAMs), 4.19% (with the catechol C_{60}-SAM), and 3.96% (with the phosphonic acid C_{60}-SAM) were observed from the inverted OPVs based on P3HT:$PC_{61}BM$ system. It was found that improvement in PCEs was mainly attributed to the enhancement in J_{SC} and FF. Since C_{60}-SAM interlayer acted as an electron selective and hole blocking layer, charge recombination at the interface was minimized thanks to the improved charge transfer from the active layer to the ZnO layer. Other phosphonic acid-anchored C_{60}-SAM, as shown in **Scheme 10**, were also reported by Brabec et al.[221] Due to the reduced series resistance and enhanced parallel resistance, improved PCEs (3.46%) was observed from OPVs using the phosphonic acid anchored C_{60}-SAM (SAM-C_6-C_{60} and SAM-C_{18}-C_{60}) interlayers and using P3HT:$PC_{61}BM$ active layer. To reduce the potential etching of ZnO, the utilization of less acidic bind terminal units or other anchoring groups have also been investigated. Therefore, C_{60}-SAM with phosphoric ester groups,[222] polyethylene glycol groups,[223,224] amine groups[225] have been developed to modify the interface of inorganic EEL and BHJ organic active layer or even to directly modify the electrode. Our group also reported an amine dendron modified C_{60}-SAM (PCBM-G2 (**Scheme. 10**)) as the interfacial layer in the

inverted OPVs and obtained a dramatically enhanced J_{SC} and FF and an over 30% augment in PCE. The neutral property (ion-free) of PCBM-G2 used in OPVs indicated that no dipole moment was introduced at the EEL/active layer interface, which was further verified by the negligible change in V_{OC}. The enlarged J_{SC} and FF were originated from the greatly enhanced surface electrical conductivity of the EEL, which was evident by the peak force tunneling AFM (PFTUNA) measurement.[226]

Beyond C_{60}-SAM, non-fullerene based SAMs have also been developed to either enlarge the surface electrical conductivity of the EEL or to introduce a dipole to tune the energy level of the electrodes.[227-238] Yueqin Shi et al reported a highly electrical conductive phenylthiophene-appended DPP, 3,6-bis-(5-benzoicacid-thiophen-2-yl)-2,5-bis-(2-ethylhexyl)-2,5-dihydro-pyrrolo[3,4-c]pyrrole-1 ,4-dione (DPP-COOH) conjugated small molecule and a dye molecule di-tetrabutylammonium cisbis(isothiocyanato)bis(2,20-bipyridyl-4,40-dicarboxylato)ruthenium(II) (N719, **Scheme 10**) as the interfacial modification layer between the ZnO EEL and BHJ active layer. The high charge carrier mobility of the interfacial SAMs minimized the energy barrier for charge transportation and extraction, improved the interface quality between the electrode and BHJ active layer, and reduced the interfacial defect of the ZnO EEL, rendering an enhanced PCE of 8.2%.[239,240] Kim et al employed benzoid acid-derivatives with different dipole orientations and magnitudes (4-fluorobenzoic acid (FBA), 4-tert-butylbenzoic (BBA) and 4-methoxybenzoic acid (MBA) in **Scheme 10**) to modify the surfaces of the ZnO EELs.[240] It was found that the dipole moment directed towards the ZnO EEL deteriorated the PCE while SAMs with the opposite dipole moment direction dramatically enhanced the PCE due to the enlarged V_{OC}. In addition, by proper substitution, film morphology of BHJ composite can also be influenced by the SAMs beneath in

certain degrees, which gives rise to the change in J_{SC} and FF.

4.2 Cross-Linkable Self-Assembled Monolayer

The styrene group was initially employed as the cross-linkable SAMs interfacial layer because it could undergo rapid polymerization in the solid state to form polystyrene without the use of any initiators.[241-243] Based on the favorable thermal curable property of styrene group, a fullerene derivative material [6,6]-phenyl-C61-butyric styryl dendron ester (PCBSD, **Scheme 11**), functionalized with small dendrons, has been reported by Yen-Ju Cheng et al.[241] The cross-linked PCBSD (C-PCBSD) network was formed by solution-processing on the top of the ZnO surface, followed by thermal curing at 160 °C for 30 minutes, which served as a robust and adhesive thin film with sufficient solvent resistance. By employing it in the inverted OPVs with a device structure of ITO/ZnO/C-PCBSD/P3HT:PC$_{61}$BM/PEDOT:PSS/Ag,[241] simultaneously enhanced V_{OC}, J_{SC} and FF have been realized. The enlarged J_{SC} and FF were originated from the reduced energy barrier in the cascade pathway for the electrons and the P3HT/C-PCBSD interface for the exciton dissociation.[244,245] The V_{OC} was originated from a well-modified energy level of the ZnO EEL by C-PCBSD.[246] By applying the C-PCBSD into P3HT:indene-C$_{60}$ bisadduct (ICBA) system, the inverted OPVs also showed the PCEs from 4.6% to 6.22%, indicating the general applicability of C-PCBSD.[247] Furthermore, nanostructured C-PCBSD (vertically aligned, as shown in **Scheme 12**) was also introduced to provide a direct pathway for charge transport.[248-252] Such vertically oriented C-PCBSD nanorods was constructed by using anodic aluminum oxide template-assisted approach.[253-256] The inverted OPVs with a device structure of ITO/PEDOT:PSS/C-PCBSD nanorods/P3HT:ICBA/PEDOT:PSS/Ag (**Scheme 12**) showed a decent PCE of 7.3%, with a large FF of 72.3%, V_{OC} of 0.84 V, J_{SC} of 12.07 mA/cm^2. The tremendous enhancement in PCE can be ascribed to the enlarged P3HT/C-PCBSD

interfacial areas and enhanced electron mobility of C-PCBSD nanorods (2.6×10^{-3} $cm^2 V^{-1} S^{-1}$).[257-259]

Oxtane group has also been utilized as an effective cross-linker in organic electronics.[260-264] The ring-opening polymerization process of oxtane features low volume shrinkage of surface layer and excellent adhesion on the substrates, the thin film can thereby be formed homogeneously without microcracks or defects. The non-acidic oxetane based SAMs also gained higher stability and eliminated the acidic etching issues on ZnO layer in contrast to SAMs with carboxylic acid, phosphonic acid, or chlorosilane anchoring groups.[265] On this concern, oxetane based SAMs, [6,6]-phenylc61-butyric oxetane dendron ester (PCBOD) was synthesized by Chain-Shu Hsu et al, with a small dendron containing two oxetane groups as the crosslinkers, as shown in **Scheme 11**.[265] The cationic oxetane ring-opening polymerization was incurred with a catalytic amount of photoacid generator under UV irradiation. By nucleophilic attack of hydroxyl groups on the TiO_x EEL surface, the protonated oxetane rings could be opened, which would be anchored through the etherification condensation by the possible bidentate anchoring reaction.[266] Thus a vertically multimolecular interlayer can be formed through the ring-opening polymerization between oxetane groups, as shown in **Scheme 11**. The inverted OPVs with a device structure of $ITO/TiO_x/C\text{-}PCBOD/P3HT:PC_{61}BM/MoO_x/Ag$ exhibited a decent PCE of 4.5%, with simultaneously improved V_{OC} of 0.61 V, a J_{SC} of 12.25 mA cm^{-2}, and an FF of 61.26%.

Another group for cross-linkable-SAMs is the trichlorosilane functionalities which can readily undergo facile hydrolysis to produce polysiloxane in ambient air and without complicated trigger conditions.[267-273] Liang et al presented a bis(2-(trichlorosilyl)propyl)malonate C_{60} (TSMC) (**Scheme 11**),[274] which can spontaneously form self-assembled and cross-linked

monolayer (SA-C-TSMC) on the TiO_x surface, without external thermal annealing or UV illumination. The operational mechanism is summarized in **Scheme 12**, where the nucleophilic hydroxyl groups on the TiO_x surface would attack the electrophilic silicon atoms of trichlorosilanes to form a self-assembled monolayer via the Ti-O-Si linkages spontaneously, and intermolecular cross-linking between TSMC molecules through the siloxane Si-O-Si linkages also proceeds simultaneously. The inverted OPVs with a device structure of ITO/TiO_x/SA-C-TSMC/P3HT:PC_{61}BM/PEDOT:PSS/Ag exhibited an enhanced PCEs from 3.2% (without interlayer) to 3.9% (with TSMC interlayer), with enhanced V_{OC} from 0.58 V to 0.60 V, J_{SC} from 9.87 mA cm^{-2} to 10.42 mA cm^{-2}, FF from 55% to 61.7%, respectively. Further application of SA-C-TSMC in the inverted OPVs based on Poly [diindenothieno(2,3-b)thiophene-alt-dithienylbenzothiadizole] (PDITTDTBT):PC_{71}BM system exhibited a boosted PCE of 5.8%.[275]

4.3 Water/Alcohol Soluble Conjugated Polymers

The water/alcohol soluble-conjugated polymers (WS-CPs) can be processed from either water or other polar solvents, which is compatible with roll-to-roll fabrication, possess a promising interfacial modification ability for metallic electrodes and show a great potential for applying environmentally friendly processing technologies.[276-278] The polar solvent solubility of WS-CPs interfacial layer, which originates from the hydrophobic polymer back bones and hydrophilic ionic functionalities, ensures the modification layer not being destroyed by upper BHJ active layer and the modified surface would also facilitate charge transport from BHJ active layer to the corresponding electrodes. In addition, the WS-CPs layer may also create a dipole moment at the interface, due to the specific functional groups (such as ethylene oxide, phosphonate, amino or ammonium, etc). This interfacial dipole would give rise to an increased

built-in potential (and hence V_{OC}), and simultaneously, electron transport and collection are facilitated by the lowered WF of the cathode, resulting in a better band alignment and minimized contact resistance. As discussed in the **Section 3**, the WS-CPs can be directly inserted between the ITO electrodes and BHJ active layer to replace the traditional TMOs EEL (e.g., ZnO, TiO$_x$), which even simplifies the processing. The materials design and progress of WS-CPs was specifically reviewed by Yong Cao et al.[82,279] Here, recent applications of WS-CPs in the inverted OPVs and enhancing the surface electrical conductivity of EEL for improving PCEs of OPVs will be emphasized.

In 2010, Na et al demonstrated highly efficient inverted OPVs by interfacial modification via poly[(9,9-bis((6-(-(N,N,N-trimethylammonium)hexyl)-2,7-fluorene)-alt-(9,9-bis(2-(2-(2-methoxy ethoxy)ethoxy)ethyl)-9-fluorene)) dibromide)] (WPF-6-oxy-F)[280,281] (**Scheme 13**). By inserting the WPF-6-oxy-F between the ITO anode and BHJ active layer, V_{OC} was enlarged from 0.35 V to 0.65 V, J_{SC} was enhanced from 8.05 mA/cm^2 to 8.83 mA/cm^2, FF was enlarged from 37% to 59%, correspondingly PCE was enhanced from 1.04% to 3.38% for the inverted OPV with a device structure of ITO/WPF-6-oxy-F/P3HT:PC$_{61}$BM/MoO$_x$/Ag. The enhanced V_{OC} was attributed to the favorable interfacial dipole formed by WPF-6-oxy-F interlayer, which was confirmed by Kelvin probe study. The WF of the ITO anode was raised from -4.66 eV to -4.22 eV after WPF-6-oxy-F modification, which increased the built-in potential for maximizing V_{OC} and minimizing the contact resistance.[282,283]

Triphenylamine based cationic polyelectrolytes are another class of efficient interface modification materials, which have showed excellent applications in OLEDs.[284] Xu et al. firstly employed the triphenylamine based polyelectrolytes, poly[N-(4-(6-diethylphosphorylhexyloxy)phenyl)-4,4'-diphenylamine] (PTPA-EP) (shown in

Scheme 13), in the inverted OPVs.[285] The diethyl phosphonate end groups on side chains resulted in a good solubility in hydrophilic solvents, while the π-conjugated backbones possessed good semi-conducting properties. By employing the PTPA-EP into the inverted OPVs with a device structure of ITO/PTPA-EP/PCDTBT:PC$_{61}$BM/MoO$_x$/Ag, the PCE was significantly enhanced from 2.57% to 4.59%. However, a PCE of 4.59% was still lower than that (5.13%) from the inverted OPVs using ZnO EEL. In 2012, Zhu et al dedicated a breakthrough work by using polycarbazoles interlayer, 2,7-carbazole-1,4-phenylene copolymers poly[(9-(N,N-di(200-hydroxyethyl)-60-aminohexyl)-2,7-carbazole)-alt-(2-hexyloxy-5-(N,N-di(200-hydroxyethyl)-60-aminohexyloxy)-1,4-phenylene)] (PCP-NOH) and poly[(N-(60-diethylphosphoryl)hexyl-2,7-carbazole)-alt-(2-hexyloxy-5-(60-diethylphosphoryl)hexyloxy-1,4-phenylene)] (PCP-EP),[286,287] which comprise surfactant-like diethanolamino and phosphonate end groups on the side chains of the both main chain blocks, respectively, and possess good solubility in alcohol as well, as the ITO surface modifier. The inverted OPVs based on PCDTBT:PC$_{71}$BM system[288] showed an improved PCE from 1.63% to 5.39% for PCP-NOH and 5.48% for PCP-EP, respectively. Later on, 2,7-carbazole based WS-CPs, a homopolymer of 2,7-carbazole with hydrophilic phosphonate side chains (PC-P) as the cathode interfacial modification layer,[289] PCEs from 2.62 % (control devices without incorporated with PC-P) to 6.04% (the OPVs incorporated with the ITO/PC-P as the bilayer cathode) were observed. Such modification on the WF of the ITO electrode eventually enlarged the V$_{OC}$ by 0.38 V. Moreover, the polycarbazole main chain of PC-P created a good contact between organic and inorganic layer, resulting in enhanced J$_{SC}$ and FF.

Various cationic polythiophene derivatives were reported for utilization as the EEL in both conventional and inverted OPVs.[291-294] Zilberberg et al reported

poly(3-[6-(N-methylimidazolium)hexyl]thiophene) bromide (P3ImHT) (shown in **Scheme 13**) as an ultra-thin cathode interlayer to reduce the WF of ITO.[295] By UV illumination, a reduction of the WF of ITO is originated from the formation of the dipole by the conjugated polyelectrolyte, which gives a suitable electron selective cathode, resulting in PCEs of 3.3% and 4.8% from the inverted OPVs based on P3HT:$PC_{61}BM$ and PCDTBT:$PC_{71}BM$ systems, respectively. Similar modification layers have also been applied to boost PCEs of OPVs.[296-298] Worfolk et al developed the poly[3-(6-{4-tert-butylpyridiniumyl}-hexyl)thiophene-2,5-diyl bromide] (P3(TBP)HT$^+$Br$^-$) (shown in **Scheme 13**) and further combined it with anionic PEDOT:PSS, serving as a versatile cathode buffer layer through electrostatic layer-by-layer (e-LBL) assembly.[299] By varying the number of e-LBL layers, the WF of the electrode was precisely tuned from -4.6 eV to -3.8 eV. Using such cathode interfacial buffer layer in the inverted OPVs, an enhanced PCE of 3.8% and 5.8% were observed from OPVs based on P3HT:$PC_{61}BM$ and poly({4,8-di(2-ethylhexyloxyl)benzo[1,2-b:4,5-b′]dithiophene}-2,6-diyl)-alt-({5-octylthieno[3,4-c]pyrrole-4,6-dione}-1,3-diyl) (PBDTTPD):$PC_{71}BM$ BHJ systems, respectively. In addition, it was found that the corresponding inverted OPVs based on P3HT:$PC_{61}BM$ BHJ system maintained 83% of its original PCE after 1 year of storage, which indicated a significantly improved device shelf-stability.[300-304] The detailed stability studies for the inverted OPVs will be addressed in the **Section 7**.

It was reported that PFN can enhance the electron injection from high-WF metals cathode (Al) into organic active layer in PLEDs/OLEDs.[305-307] Based on such favorable property for electron transporting, PFN and its derivatives have been utilized to modify the ITO surface in the inverted OPVs.[308-310] The most excited result was observed from the inverted OPVs with a PCE of 9.2%,[276] where the PFN was used as the EEL.[311] The WF of ITO was lowered from -4.7 eV

to -4.1 eV by inserting a thin PFN layer between the ITO electrode and BHJ active layer. Similar to other WS-CPs aforementioned, the origin of the vacuum level shift was originated from the formation of the interfacial dipole at the ITO surface by PFN.[312,313] The inverted OPVs showed a PCE of 9.15%, with a J_{SC} of 17.2 mA/cm^2, a V_{OC} of 0.74 V and a FF of 72%; whereas the conventional OPVs with a device structure of ITO/PEDOT:PSS/PTB7:PC$_{71}$BM/PFN/Al showed a much lower J_{SC} of 15.4 mA/cm^2. The drastically increased J_{SC} and thus PCE of the inverted OPVs were ascribed to the more efficient charge transport due to the interfacial modification by the PFN layer.

A quantity of metal oxide/conjugated polyelectrolytes bilayers were reported as the ITO surface modifiers.[314-318] In these studies, it was found that the polymer backbones which exhibited hydrophobic property was preferentially orient to the side of BHJ active layer, while the negative counterions with hydrophilic property was orient to metal oxides. Such spontaneous orientations led to the formation of strong interfacial dipoles, lowering the conduction band of metal oxides and correspondingly facilitating the electron being transported from BHJ composite through metal oxides to the cathode. A dramatically enhanced PCE (8.4%) was observed from the inverted OPVs with a device structure of ITO/ZnO/PFN-Br/PBDT-DTNT:PC$_{71}$BM/MoO$_x$/Al, where the PBDT-DTNT is poly{4,8-bis(4,5-didecyl-2-thienyl)-benzo[1,2-b:4,5-b']dithiophene-alt-[4,9-bis(4-hexyl-2-thienyl)-naphtho[1,2-c:5,6-c']bis[1,2,5]thiadiazole-5,5-diyl]}.[315] The LUMO energy levels estimated from UPS were -4.46 eV for ZnO thin film and -4.08 eV for the ZnO/PFB-Br, respectively.[316] The up-shift of the LUMO energy level of ZnO/PFN-Br would eliminate the energy barrier between the LUMO energy level of PC$_{71}$BM and the CB of ZnO, resulting in a large V_{OC}.[317] The OPVs with PFN-Br layer exhibited nearly 10 times smaller dark current than that of the

OPVs without PFN-Br, indicating a larger V_{OC} and suppressed bimolecular charge recombination. In addition, Choi et al found that the insertion of a thin WS-CPs layer could increase the hydrophobicity of TiO_x, originated from the improved wettability by conjugated polyelectrolytes, resulting in enhanced PCEs.[318]

The dipole-induced low WF of the ITO electrode and the modified surface wettability by WS-CPs provided a good contact between the ITO electrode and BHJ active layer, resulting in an efficient pathway for electron extraction and transport. But the neglected low surface electrical conductivity of the buffer layer still limits the PCEs of OPVs, in particular, for the WS-CPs of larger thickness. The dramatically reduced electrical conductivity would introduce the series resistance within the WS-CPs layer and lower the charge transport efficiency. To address such issues, Liu et al designed a novel metallopolymer, Hg-containing derivative of amino-functionalized conjugated polymers (PFEN-Hg) (**Scheme 13**) as the interfacial modification layer.[310] This novel conjugated polymer possesses strong intermolecular and noncovalent Hg-Hg interactions, which would result in increased packing of the PFEN-Hg thin film.[314] The OPVs incorporated with PFEN-Hg showed a small variation of PCEs from 8.64% to 9.11%, even though the thickness of PFEN-Hg was increased to 19 nm. Whereas the inverted OPVs incorporated with poly[(9,9-bis(3'-(N,N-dimethylamino)propyl)-2,7-fluorene)-alt-2,7-(9,9-bis(3-ethyl-(oxetane-3-e thyloxy)-hexyl)-fluorene)] PFN-OX (**Scheme 13**) exhibited PCEs from 9.03% to 1.02% as the thickness of PFN-OX is from 4 nm to 7 nm.

Our group observed a PCE of 8.62% from the inverted OPVs incorporated with the PFN-OX EEL, as shown in **Scheme 14c**.[319] A PCE of 7.24% from the inverted OPVs with BHJ active layer with over 1 μm thickness has been further demonstrated.[319] The inverted OPVs with such

thick BHJ active layer provided a good opportunity for commercializing OPVs products.

In short, WS-CPs is promising candidates to replace or modify metal oxides or metal carbonate EELs. WS-CPs used as the interfacial layer can increase the surface electrical conductivity and the hydrophobicity of the ITO or metal oxide/metal carbonate layer, which facilitates the electron transport. In addition, surface charge carrier recombination can also be suppressed by the introduction of WS-CPs. As a result, both enhanced J_{SC} and FF were observed from the OPVs incorporated with WS-CPs modification layer.

5. Bulk Heterojunction Active Layer

In OPVs, thin film morphology of BHJ active layer plays a critical role in determining the device performance. Due to the relatively low dielectric constant of BHJ composite, large exciton-binding energy gives rise to the strongly localized electron-hole pairs in BHJ active layers, which requires additional driving force to separate the pair of the electrons and the holes. While the energy level offsets between D and A provide an additional electric field with different electrochemical potentials at the molecular interface to separate the excitons into weakly bounded Coulombic pairs, and thereafter separating into free charge carriers.[320] To enlarge the D/A interface, BHJ concept was further introduced to simultaneously enlarge the charge dissociation.[28,321-324] Therefore, the manipulation of the film morphology of BHJ active layer has always been the focus in the field of OPVs.[325,326] For OPVs, almost all the organic active layers are processed from solution, and the difference in surface energy of D and A will leads to an inhomogeneous vertical distribution (or concentration gradient) and phase separation throughout BHJ active layer, causing the "vertical phase separation", which, perceptibly is crucial to the charge transport and device efficiency.[327-333] The model of vertical composition profile of P3HT:PC$_{61}$BM system using variable-angle spectroscopic ellipsometry was reported

by Campoy-Quiles et al. A concentration gradient varying from $PC_{61}BM$-rich domains near the PEDOT:PSS side to P3HT-rich domains adjacent to the free (air) surface was reported in the conventional OPVs, where such composition profile was inefficient for corresponding charge transport and collection. Alternatively, the inverted OPVs with reversed charge transport directions showed advantage over the conventional OPVs because of the vertical phase separation. In the inverted OPVs, the surface energy difference induce D-rich phase more close to the anode on the top and the A-rich phase more close to the cathode beneath, thus shortening charge transport pathways and reducing charge recombination at the electrodes. Besides the surface energy difference induced self-assemble of BHJ active layer, to achieve a more optimized vertical morphology via thermal annealing, processing additives, external electrical field and external magnetic field are reviewed as following.

5.1 Thermal Annealing

Thermal annealing was a common process to tune the thin film morphology of BHJ active layer in OPVs. Xu et al[334] conducted a series of experiments to study the influence of thermal annealing on the compositions at the top and bottom surfaces of BHJ blend films by XPS. $P3HT:PC_{61}BM$ blend film coated on both glass and Cs_2CO_3 were experienced fast-grown, fast-grown with thermal annealing, slow-grown, slow-grown with thermal annealing, respectively. The weight ratios of P3HT and $PC_{61}BM$ were detected by using C/S atomic ratios from the XPS measurement. Both fast-grown and slow-grown film showed similar results, with higher $PC_{61}BM$ concentration at the bottom surface. However, upon thermal annealing, $PC_{61}BM$ concentrations at both sides of the fast-grown films decreased slightly while the slow-grown films remained invariable, predicting more thermodynamically stable for slow-grown films.[335] Moreover, the $PC_{61}BM$ concentration at the Cs_2CO_3/polymer interfaces is higher than that at the

glass/polymer interfaces, illustrating that the vertical separation in BHJ composite is induced by Cs_2CO_3. Similar to the results on the glass substrate, BHJ films on the surface of Cs_2CO_3 also exhibited enhanced inhomogeneous distribution after thermal annealing. The ratio of $PC_{61}BM$ to P3HT at the Cs_2CO_3 side increased over one- and two-fold in the fast and slow-grown films, respectively. While at the top side (top surface of the BHJ film), the ratio of $PC_{61}BM$ to P3HT slightly decrease in both fast and slow-grown films. It was also proposed that not only surface energy contributed to the $PC_{61}BM$ aggregation on the bottom surface, but also charge transfer process played a critical role. Such hypothesis was supported by XPS measurement, which showed a significant binding energy shift (~0.5 eV) to lower binding energy for Cs after spin-coating an ultra-thin $PC_{61}BM$ layer and consequently resulted in a substantial charge transfer. These results are consistent with the previous studies by Ohno et al[336] that the charge transfer process was originated from the dipole formed by Cs_2CO_3 on the ITO substrate, inducing the dipole-dipole interaction between $PC_{61}BM$ and Cs_2CO_3. Later on, Orimo et al[337] demonstrated that pre-annealing of the active layer before thermal deposition of metal electrode and post-annealing after thermal deposition would cause significant differences in the film morphology of BHJ composite. The XPS measurements exhibited that the surface fraction of $PC_{61}BM$ at the interface between BHJ layer and the Al electrode was as low as 31% in the pre-annealing device but was enhanced to 72% in the post-annealing device. The higher $PC_{61}BM$ concentration for post-annealing device was likely attribute to the larger diffusion constant of small molecules ($PC_{61}BM$) than that of polymer chains. This deduction can be further supported by the study from Ma et al,[338] who showed a reduced efficiency for conventional OPVs with pre-annealing of P3HT:$PC_{61}BM$ film but an increased ones with post-annealing. However, Kang et al reported different results.[339] Based on the device structure of

ITO/WPF-oxy-F/P3HT:PC$_{61}$BM/PEDOT:PSS/Ag, where the WPF-oxy-F is poly[(9,9-bis((6'-(N,N,N-trimethylammonium)hexyl)-2,7-fluorene))-alt-(9,9-bis(2-(2-methoxyet hoxy)ethyl)-fluorene)] dibromide, PCEs from 2.13% for the pristine OPVs to 3.86% for the post-annealing ones under 170°C were observed. By studying the annealing sequences for different layers, it was found that the most correlated interface was the active layer/PEDOT:PSS/Ag. V$_{OC}$ was slightly enhanced due to the increased WF of PEDOT:PSS/Ag bi-electrode along with raised temperature from 110°C to 170°C. Consequently, good ohmic contact could be formed between the PEDOT:PSS/Ag bilayer electrode and P3HT, resulting in an increased V$_{OC}$ and reduced series resistance (R$_S$). Moreover, sheet resistance (R$_{sh}$) was increased by two orders of magnitude after annealing at 170°C, due to the smaller leakage current at negative voltage and low positive voltage. The combined reduced R$_S$ and increased R$_{sh}$ resulted in an enhanced FF and thus PCE. Based on these researches, it can be concluded that post-annealing process will not only influence the vertical charge separation between the electron donor and the electron acceptor, but also change the interfacial properties. Therefore, different annealing sequences should be chosen to optimize the OPVs performance.

5.2 Processing Additives

Using different solvents to tune the film morphology of BHJ composite has also been attempted, which, however, do not enhance PCEs dramatically at first.[340] But derived from this idea, Yao et al firstly employed the processing additives, high boiling solvent additive 1,8-octanedithiol (OT or 1,8-ODT) with the combination of low boiling point solvent 1,2-dichlorobenzene (DCB), to optimize the film morphology of BHJ active layer and obtained a difference in PCEs.[341] Thin film morphology studies indicated that a vertical phase separation occurred during the spin-coating process, which was supported by AFM images and XPS

measurement. Highly ordered domains of P3HT were observed within the BHJ composites incorporated with OT additive, facilitating the holes transportation in the inverted OPVs. The underlying device physics can be explained by the model shown in **Scheme 15**. Since P3HT and $PC_{61}BM$ are dissolved in DCB with low concentrations, polymer chains extend freely in the solvent without interaction with $PC_{61}BM$. But during the spin-coating process, $PC_{61}BM$ molecules were dispersed between the P3HT chains because of the evaporation of solvent, breaking the ordering of the P3HT chains. However, with incorporation of processing additive OT, the film shew much ordered phase separation (as shown in **Scheme 15d-f**). During the spin-coating process, DCB evaporates much faster than OT and the concentration of OT is gradually increased in the wet film. Due to the limited solubility of $PC_{61}BM$ in OT, $PC_{61}BM$ will form clusters and be easy to aggregate. On the other hand, the surface energy of $PC_{61}BM$ is higher than that of P3HT, which gives rise to the redistribution that $PC_{61}BM$ rich phase can be accumulated at the bottom of the active layer, leaving the P3HT rich phase in the top of the active layer.[342] Consequently, an electron percolation pathways of $PC_{61}BM$ rich phase at the bottom and a hole percolation pathways of P3HT rich phase in the top would facilitate the charge extraction process, rendering a higher J_{SC}. Later on, Lin et al applied this strategy in the inverted OPVs with the $PCPDTBT:PC_{71}BM$ BHJ system.[343] By adding high boiling solvent additive 1, 8-ODT in DCB, PCE was increased from 2.09% to 3.00%. Great enhancement was observed from J_{SC} (from 9.89 mA/cm^2 to 12.84 mA/cm^2).[344] Similarly, Chen et al employed mixed solvent of chlorobenzene:DCB with diiodooctane (DIO) additive in the inverted OPVs with a device structure of $ITO/ZnO/PBDTTT-C:PC_{71}BM/MoO_x/Ag$.[345] PCE was increased from 0.92% (BHJ composites from pure chlorobenzene) to 4.43% (BHJ composites from 1:1 DCB:CB+2% DIO). It was found that the J_{SC} contributed to the majority part of enhancement in PCEs, rising

from 3.78 mA/cm^2 to 11.82 mA/cm^2. The mixed solvent effect on device performance was also demonstrated by our group. Chao Yi et al investigated the device performance of OPVs fabricated from chlorobenzene solution with different concentrations of solvent processing additive, chloronaphthalene (CN), which has a high boiling point temperature. By adding the CN into chlorobenzene solution, it was found that the film morphology of BHJ layers was tuned and the crystalline degree of the conjugated polymers is maintained.[346] The optimized BHJ film morphology would facilitate more excitons to be diffused into the D/A interface and then dissociated into free charge carriers. A higher J_{SC} is thus obtained. Chang Liu et al also investigated the influence of binary processing additives on the performance of OPVs and obtained a PCE of 8.55%, which was also originated from the optimized morphology of BHJ active layer.[347] The morphological change induced suppressed charge carrier recombination was also demonstrated, enhanced J_{SC} and FF as well as a corresponding higher PCE was realized.

5.3 External Electric Field

It has been reported that the external bias imposed on OPVs can enhance the efficiency of OPVs due to the better arrangement of conjugated polymers in BHJ active layer.[348,349] However, the reason for the improved performance have not been well elucidated, since the extra charges injected by the external field can also fill in the defects in organic layer, rendering less charge carrier recombination.[350] Apart from directly applying external electric field on the electrodes of the OPVs, Ma et al studied the electrical field influence on the P3HT:PC$_{61}$BM active layer during the filming process.[351] The BHJ active layer were placed between two parallel metal plates with bias voltage applied to them, forming an electric field perpendicular to the OPVs, as shown in **Scheme 16a**. A forward electric field was defined as the direction from glass to the active layer, and the opposite was defined as the backward electric field. With the backward electric field

treatment, the efficiency was improved from 3.16% of control device (without external electrical field) to 3.23% (with backward electric field strength of 2.5×10^5 V/m) and 3.51% (with backward electric field strength of 5.0×10^5 V/m) of electric field treated devices, respectively. On the contrary, with the forward electric field treatment, the efficiency decreased to 3.09% (with forward electric field strength of 2.5×10^5 V/m) and 3.04% (with forward electric field strength of 5.0×10^5 V/m). **Scheme 16b** shows the schematic description of different vertical phase separation with different electric field treatments. The authors claimed the electric field can induce the rearrangement of polymer chains by electrical dipolar interaction, giving rise to well-ordered polymer chains and $PC_{61}BM$ side chains. The formation of well-ordered active layer morphology facilitated the charge transportation and therefore resulted in enhanced J_{SC}. And the polarity direction of $PC_{61}BM$ is from side chain to the fullerene, so with the backward electric field, the side chains of $PC_{61}BM$ will be aligned upward to restrain the diffusion of $PC_{61}BM$ to the top, decreasing the tendency of self-assembled $PC_{61}BM$ forming $PC_{61}BM$-rich domains at the top surface. Consequently, the backward electric field helped the formation of P3HT-rich domains at the top surface and $PC_{61}BM$-rich domains at the bottom. The P3HT-rich layer provides more channels for the holes to be transported to the anode and reduced the probability of electron-hole recombination at the anode. Thus, the current leakage was decreased, which led to increased shunt resistance and consequently enhanced FF. On the contrary, the forward electric treatment has the opposite influence on the vertical phase distribution. Despite the interesting idea, further considerations on the polarizing effect within the active materials as well as the direct evidence for the vertical phase change remains to be addressed.

5.4 External Magnetic Field

Our group reported BHJ composite mixed with Fe_3O_4 magnetic nanoparticles (MNPs), and

then employed the external magnetic field to drive the alignment of Fe_3O_4 MNPs during the filming process.[352] Well-developed D-A morphology was induced and the introduced dipole moment from the aligned Fe_3O_4 MNPs offer an additional coercive field to direct the separated charge carrier to be transported to the corresponding electrodes, resulting in a dramatically reduced charge carrier recombination. The aligned Fe_3O_4 MNPs in BHJ composite was confirmed by the grazing incidence small angle x-ray scattering (GISAXS) and transmission electron microscopy (TEM) images, and such aligned "channels" induced enlarged charge mobility was further confirmed by the space charge limited current (SCLC) measurement. **Scheme 17a** shows the processing procedures of the external magnetic field aligned Fe_3O_4 MNPs in BHJ composite. In addition, the idea of using the external magnetic field induced motion of Fe_3O_4 MNPs to tune the morphology of BHJ composite matrix was also employed in HEL. The employment of Fe_3O_4 MNPs and the external magnetic field has also been applied in PEDOT:PSS layer to optimize the film morphology of the HEL, which results in a dramatically enlarged electrical conductivity and consequently an enhanced PCE.[353] **Scheme 17b** shows the processing procedures and differences in the resulting device performances. In addition, it should be noted that pristine Fe_3O_4 MNPs with or without external magnetic field alignment can also applied as the HEL in OPVs and the external magnetic field may also give positive influence on the device performance.[354]

6. Top Anode Electrode

In the previous sections, charge extraction, transport and collection at the interface of the cathode electrode and active layer has been addressed. To realize a balanced charge collection, the charge extraction, transport and collection at the anode side are of importance in determining device performance as well. For simplest metal-insulator-metal photovoltaic devices, V_{OC} is

demonstrated to scale the difference between the WF of the cathode and the anode in condition

of non-ohmic contact, and to exhibit a strong coupling with the reduction potential of the

electron acceptor in condition of ohmic contact.[15,355] Hau et al investigated the influence of

different top electrodes materials on the device performance of the inverted OPVs.[356] Based on

the structure of ITO/ZnO/P3HT:PC$_{61}$BM/top electrode, V$_{OC}$ showed a linear relationship with the

anode WF, with a slope of 0.6. However, after incorporating PEDOT:PSS between the anode

electrode and BHJ active layer, V$_{OC}$ remained almost invariant with different anodes. This

observation was consistent with the results reported by Brabec,[357] indicating the utilization of an

efficient HEL would allow inexpensive materials as the anode electrodes.

6.1 Silver Nanowires

Currently, flexible transparent conducting electrodes have garnered close attention due to the

advances in technologies for flexible optoelectronics, which requires highly transparent

conducting materials for both top and bottom electrodes.[358-360] Moreover, the transparent top

electrode enables the substitution of ITO with much cheaper opaque substrate, such as insulated

steel or metal covered glass. As introduced as the top electrodes in the **Section 2**, nanostructured

conducting materials such as silver nanowires (Ag-NWs),[362-365] CNTs,[366] graphenes[367] and

highly conductive polymers,[368-370] which are fabricated from the latest state-of-the-art

technologies, have been developed as the flexible transparent electrodes to conquer the

disadvantages of the conventional electrodes, such as brittleness, opacity and low electrical

conductivity.[371-373] Among them, Ag-NWs stood out as the one of the most promising

candidates due to their much higher electrical conductivity and transmittances (10-20 Ω/sq with

85% transmissivity over the wavelength from 400 to 800 nm).[371] In the following context, the

topic will be focused on the development of Ag-NWs as the top electrode in the inverted OPVs.

In 2008, Ag-NWs was firstly investigated by Peumanns et al, as a substitution for the ITO electrod.[371] They observed a low shunt resistance of less than 1 kΩ cm^2, with a PCE of only 0.38%. The lower efficiency was solely due to the leakage current, which was the result of the extremely rough Ag-NWs electrode.[374] To mitigate the large roughness induced harmful influence, the Ag-NWs films were further pressed with a clean glass substrate to flatten the nanowire mesh prior to lamination. A significantly improved PCE of 2.5% was obtained.[375,376] However, a low FF of 46% was observed, which was ascribed to the inherent large roughness of Ag-NWs layer. To address such morphological issue, a inorganic-organic composite consisting of Ag-NWs and PEDOT:PSS was developed.[377] The conductive PEDOT:PSS could fill the gaps among Ag-NWs, which would not only smooth the film surface, but also increase the electrical conductivity of Ag-NWs. Similar efforts to improve the properties of Ag-NWs were also paid by other groups in recent years, and the applications of such technology were pervasive in the conventional OPVs and OLEDs.[378,379] Later on, such structure was further employed in the visible transparent inverted OPVs by Yang's group.[380] They demonstrated high performance, visible transparent OPVs fabricated from all-solution process. It is noteworthy that Ag-NWs fused with TiO$_x$ NPs and PEDOT:PSS was used as the top electrode, where the Ag-NWs was treated by TiO$_x$ and PEDOT:PSS solution sequentially.[381] Tighter contact among the crossed Ag-NWs and improved film electrical conductivity was achieved due to the TiO$_x$ solution volume shrinkage and solvent evaporation. While the PEDOT:PSS coating act as a protecting layer for strong adhesion. Consequently, such treatment resulted in a highly conductive Ag-NW composite films possessing excellent optical transparency (over 80% in visible region) and mechanical properties. A decent PCE over 4% was obtained for the inverted OPVs using poly(2,6'-4,8-bis(5-ethylhexylthienyl)benzo-[1,2-b;3,4-b]dithiophene-alt-5-dibutyloctyl-3,6-bis(

5-bromothiophen-2-yl)pyrrolo[3,4-c]pyrrole-1,4-dione) (PBDTT-DPP):$PC_{61}BM$ BHJ system.[382] Later in 2013, Rein et al also demonstrated the semi-transparent OPVs,[365] where PEDOT:PSS and V_2O_5 were separately used as the HEL for solution processed Ag-NWs top electrode. It is noted that using higher electrical conductive material connecting to Ag-NWs electrodes resulted in a more efficient charge collection process and led to a high PCE of 2.37% for the semi-transparent OPVs.

6.2 PEDOT:PSS

Another efficient and attractive candidate for the top electrode in the inverted OPVs is PEDOT:PSS, which has been widely utilized as the top electrode. In 2008, Zhou et al[383] firstly reported the high electrical conductivity PEDOT (PH500) as the anode electrode in all-solution-processed transparent inverted OPVs. However, a relatively low PCE of 0.7% was observed, which was attributed to the less efficient absorption and a bad contact with the cathode. Afterwards, Hau et al demonstrated the OPVs using PEDOT:PSS as both bottom and top electrodes, respectively.[384,385] In this work, dimethyl sulfoxide (DMSO) was added to increase the electrical conductivity of PEDOT:PSS. When DMSO doped PEDOT:PSS was used as the bottom electrode to replace ITO electrode, as the thickness of DMSO doped PEDOT:PSS layer was increased, the optical transparency and sheet resistance were reduced, which lowered the photocurrent but increased the FF. By tuning the thickness of DMSO doped PEDOT:PSS cathode electrode, and applying Ag as the anode electrode, PCE of ~3% was observed. In addition, the DMSO doped PEDOT:PSS electrode showed higher compatibility with flexible substrate regarding to its superior mechanical properties than that of the ITO electrode, exhibiting improved PCE retention (92%) over that of the ITO (50%) electrode after cyclic bending test for corresponding OPVs. Later on, similar structures and processing methods of PEDOT:PSS were

reported by other groups.[386-388] But, using PEDOT:PSS as the transparent top electrode was severely hampered by poor wettability of this hydrophilic material dispersions on hydrophobic organic active layer surfaces. To solve this problem, Zhou et al used a combination of a modified PEDOT:PSS (Clevios CPP 105D) and PH1000 to increase the hydrophobicity of PEDOT:PSS and enabled it being spin-coated on organic active layer surface.[388] Alternative technique to overcome this incompatible surface potential was to use stamp transfer lamination of dry PEDOT:PSS film, which was conducted by Gupta et al.[389] They demonstrated a high conducting (900 S/cm) PEDOT:PSS (PH1000) layer, deposited by a stamp-transfer lamination technique using a poly(dimethylsiloxane) (PDMS) stamp. To further minimize the resistive losses in the large area devices, PEDOT:PSS was incorporated with an Ag grid electrode, providing a proficient and versatile transparent top contact.[389,390] The processing procedure is shown in **Scheme 18**. The resulting PCE was 2.35%, with a J_{SC} of 9.39 mA/cm^2, V_{OC} of 0.54V and FF of 48%. Even though a relatively lower value of FF was obtained, which was originated from the leakage pathways from the non-optimized interfacial contact, it still provided a possible way to gear up the utilization of PEDOT:PSS as an more efficient and compatible electrode in the inverted OPVs.

6.3 Dielectric/Metal/Dielectric Structure

Since the transparent top cathode composed by thin-film of metal layers such as Ag/Al and Ag/Au have low transmittance (<60%), indicating that more than 40% of the incident light was reflected at the surface of the top electrode, resulting in low PCE of OPVs.[391-393] Therefore, in order to circumvent these problems, a series of top electrodes utilizing dielectric/metal/dielectric (DMD) structure to enhance the transmittance have been developed.

In 2009, Tao et al firstly demonstrated dielectric/metal/dielectric (DMD) structure with a

52

high optical transmittance (>75%) in visible region by thermal evaporation, where Ag is sandwiched between two layers of MoO_x with different thicknesses.[394] The inner MoO_x layer was utilized as the HEL and the outer MoO_x layer is used not only as the top-capping layer to enhance light coupling, but also lower the series resistance of photovoltaic devices. This is because the MoO_x/Ag anode would cause a large amount of internal reflection at the metal/air interface due to the large refractive index mismatches.[395] The top MoO_x layer could serve as a transparent conducting index matching layer to enhance the total transmission due to the higher refractive index of MoO_x (~2.1).[396] Therefore, by tuning the thickness of the outside MoO_x layer to the optimum condition (MoO_x/Ag/MoO_x, 1/10/20 nm), transmittance is increased in the visible region compared to MoO_x/Ag anode electrode. As a consequence, OPVs with a device structure of ITO/TiO_x/P3HT:$PC_{61}BM$/MoO_x/Ag/MoO_x showed an enhanced PCE of 1.40% compared to that (1.04%) using MoO_x/Ag anode electrode. Slightly reduced J_{SC} (from 4.04 mA/cm^2 to 3.85 mA/cm^2) was due to the lower reflectivity of MoO_x/Ag/MoO_x in the wavelength ranging from 400 nm to 650 nm.

Even though the PCE from the multilayer anode electrode was not inspiring, it still provided a promising alternative for the transparent top electrode for the inverted OPVs. Three critical requirements can be summarized for effective transparent top electrode: (1) the thin dielectric layer adjacent to the organic active layer serves to transport the holes and block the electrons, which should form an ohmic contact with the photoactive layer;[397,398] (2) tuning the thickness of Ag is very important for balancing the sheet resistance and optical transmittance; (3) the outer dielectric layer incorporated as a light coupling layer is of great importance to tune the optical properties of the anode electrode and particularly mitigate deleterious reflections caused by the large mismatch of refractive indices at the Ag/air interface.[399-401]

Based on these principles, Jin et al demonstrated the application of the DMD top electrode in 25.0 cm^2 large area OPVs monolithic sub-modules.[402] The optimized MoO$_x$/Ag/MoO$_x$ showed an optical transmission of 80% at 520 nm, a sheet resistance of ~5 Ω/sq. The inverted OPVs with a device structure of glass/Al/PCDTBT:PC$_{71}$BM/MoO$_x$/Ag/MoO$_x$ showed a PCE of 3.17% in large scale, which outperformed the equivalent conventional OPVs. FF from large area devices with the DMD electrode maintained almost unchanged with the laboratory-scale cells, while the conventional OPVs show a dramatic loss in FF to <30% when it was fabricated on large-scale. This indicated that at large scale, the power loss in OPVs was derived from the anode whose sheet resistance becomes the only area-scaling parameter. Consequently, this study opened new opportunities to create modules and sub-modules with high geometric FFs and more efficient use of substrate area.

The DMD structures were also utilized in the inverted OPVs as the bottom electrode for the ITO-free cells or in the conventional-semi-transparent-OPVs, which also exhibited promising results.[403-405] Further studies of multilayer transparent electrode are necessary for the realization of large scale and transparent OPVs.

7. Device Stability

Generally, in most conventional OPVs, BHJ active layer is sandwiched between the PEDOT:PSS coated ITO/glass and the low-WF metal, where both PEDOT:PSS and low-WF metal will cause stability issues. The stability of OPVs can be divided into air stability and thermal stability in terms of the materials stability. For air stability, the degradation of OPVs mainly results from the diffusion of oxygen and moisture, leading to the oxidation of aluminum cathode and active layer. In addition, the moisture would facilitate the acidic PEDOT:PSS to etch the ITO/glass. For thermal stability, the phase-separated morphology of BHJ blends is

thermodynamically meta-stable and the materials still have a certain degree of freedom to diffuse slowly or recrystallize over time. Furthermore, the facilitated interaction between active layer and PEDOT:PSS or low-WF metal would inevitably deteriorate the device performance. To solve these problems, inverted OPVs were introduced. As mentioned above, in this structure, stable EEL, HEL and high-WF metal were introduced to replace the unstable PEDOT:PSS and low-WF metals.

7.1 Shelf stability

The commonly used electrode in the conventional OPVs is the metal of low WF, including Al and Ca, which is highly reactive to oxygen and moisture. Among them, the dominant degradation is the diffusion of oxygen and water through pores in the metal and the chemical reaction to form metal oxide, such as Al_2O_3, which is an insulator and may create barrier for charge carrier transport. Frederik C. Krebs and Kion Norrman[406-408] did a systematic work on the oxygen induced degradation by using time of flying-secondary ion mass spectrometry (TOF-SIMS) methodologies for over 13,000 hours. They found that there were two main pathways for oxygen diffusion into OPVs: pin-poles within the metal electrode and edges between the electrodes and active layer. Moreover, the electrodes such as Al, was believed to be gradually dissolved in the constituents of active layer and formed kinds of organoaluminum species at the Al/C_{60} interface, which was confirmed by using isotope ^{18}O marking method. Therefore, to achieve long-term stable OPVs, chemical robust metal electrode such as Ag needs to be used as the electrode instead of the unstable Al. Steven K. Hau, Hin-Lap Yip et al[409] compared the device stability between the conventional OPVs and the inverted OPVs by using the P3HT:PC$_{61}$BM BHJ system. All of the four basic parameters (V_{OC}, J_{SC}, FF and PCE) of the conventional OPVs have a dramatic decline showing the degradation in the first 5 days, while the

inverted OPVs still maintain over 90% performance, as shown in **Figure 1**.

On the other hand, the acidic nature of PEDOT:PSS (pH=1) makes it corrosive to the low WF electrode metal and the ITO electrode.[410] Kawano et al studied the effect of the PEDOT:PSS layer on the degradation of poly[2-methoxy-5-(3',7'-dimethyloctyloxy)-1,4-phenylenevinylene] (MDMO-PPV) based OPVs and found a large dependence of stability on the environmental humidity.[411-412] The humid condition led to a rapid degradation in PCE of OPVs incorporated with PEDOT:PSS either in air or in nitrogen. While for OPVs without PEDOT:PSS, the degradation became much slower. The authors concluded that the hygroscopic PEDOT:PSS layer took up water from the atmosphere, increasing the sheet resistance. Another research done by Voroshazi et al showed that PEDOT:PSS will also enhance the oxidation of the cathode due to hygroscopic nature of PEDOT:PSS.[413,414] In the inverted OPVs, TMOs such as MoO_x was deposited as the HEL instead of the acidic PEDOT:PSS layer to improve the stability. The chemical susceptibility to moisture and oxygen of TMOs are less sensitive than that of PEDOT:PSS thin films, thus the acidic ions diffusion into active layer and ITO electrodes can be eliminated. Various studies have shown that the life-time of the inverted OPVs using the TMOs HELs can be increased dramatically.[409,415-417] Our group also demonstrated that by using TMOs like Fe_3O_4 MNPs as the HEL in the conventional OPVs to eliminate the PEDOT:PSS, the device stability was significantly enhanced.[14] It should be noted that the degradation in OPVs comprises a complex range of mechanisms that presumably have not been completely identified.[418] Besides the moisture and oxygen diffusion induced device performance degradation, the degradation of interfaces, active materials, interlayer and electrode diffusion, reaction between the electrode and organic materials, as well as film morphological changes including delamination and cracks

formation can also cause device performance degradation.[418] Although for a long time, the moisture and oxygen diffusion are known as the dominant degradation mechanisms, a quantitative understanding in performance degradation of the inverted OPVs still remains a challenging task.

7.2 Operational Stability

Beyond the shelf stability, the operational stability for the inverted OPVs with a device structure of ITO/ZnO/BHJ composite/MoO$_x$/Ag was also investigated by our group.[49] As shown in **Figure 2**, the inverted OPVs with ZnO buffer layer showed no obviously degradations in J$_{SC}$, V$_{OC}$ and FF after continuously illuminating OPVs for 4 hours. However, for the inverted OPVs without ZnO buffer layer, significant degradations in V$_{OC}$, FF and J$_{SC}$ were observed after continuously illuminating OPVs only for 1 hour. All these results indicated that the inverted OPVs by using ZnO as the buffer layer had a good operational stability, whereas the inverted OPVs without ZnO buffer layer were unstable under the illumination condition. By studying the absorption of ZnO, it is concluded that a good operational stability of the inverted OPVs with ZnO buffer layer was probably originated from blocking effect of ZnO layer against the UV light, which resulted in a negligible UV light induced photodegradation of organic materials.

During the solar cell operation, another inevitable issue is the heat effect from the continuously exposure in the solar irradiation. The accumulated heat may accelerate the molecular diffusion between layers and in the BHJ nano-composite. Although the diffusion of the acidic ions in PEDOT:PSS to adjacent layers to degrade the ITO or conjugated polymers can be eliminated in the inverted OPVs, the elevated temperature in BHJ composite may induce the film morphological change within the active layer. In addition, due to the relatively low glass transition temperature (T$_g$) of commonly used conjugated polymers, as well as the thermal

induced polymeric crystallization at higher temperatures, the BHJ D-A phase separation can be driven from nanoscale to a detrimental microscale or even macroscale, which is significantly larger than the exciton diffusion length.[419,420] In addition, the concomitant D/A interfaces reduction are also expected. To address the thermal issues, strategies including introducing the compatibilizers to store the extensive thermal energy within the active layer and reduce the interfacial tension between D-A phases,[421-425] developing cross-linkable active light harvest materials to form a robust BHJ network,[426-430] employing amorphous aggregation inhibitor or fullerene derivatives to substitute PCBM,[431-433] lowering the effective regioregularity of conjugated polymers to suppress the thermal induced crystalline at high temperatures,[434-435] and developing high T_g active layer materials with reduced rotational freedom to maintain the BHJ morphology,[436,437] have been developed. However, it should be noted that although various methods have been developed to maintain the ~10 nm D-A separation, the charge transport properties within the active layer may somewhat be sacrificed due to the introduction of insulating additives or the formation of disordered phases. The trade-off between exciton transport and charge carrier transport still remain unsolved.

8. Conclusions & Outlook

As discussed above, the inverted OPVs have been developed to address the stability issues of conventional OPVs by introducing more air-stable TMOs as the electrode buffer layer and high-WF metals as the electrode. And the application of multi-functional robust electrode buffer layers and interfacial modification layers not only prolong the device lifetime but also improve the device performance in certain degrees. In specific, the strong development efforts for electrode buffer layers and interfacial modification layers enable them to ameliorate the contact

between the organic and inorganic interfaces and to optimize the electrical coherence throughout the devices and boost the charge collection efficiency. Moreover, due to the reversed polarity in the inverted OPVs, surface energy difference would induce self-optimized vertical D-A phase redistribution. And tremendous works have been done to further optimize the D-A morphology by critically tuning processing conditions such as thermal annealing, using processing additives and exerting external fields. By properly selecting materials, over 10% PCEs have been realized since early 2014 in inverted OPVs. Although the highest PCE of $11.0 \pm 0.3\%$ in OPVs released by Toshiba is still lower than that of ~15% in the commercial silicon photovoltaics,[9] the continuing PCE growth in OPVs still shows an optimistic future.

Besides the advances on the PCE, the lifetime has also surged thanks to the state-of-the-art encapsulation technologies. Over 50% lifetime prolongation was observed in inverted OPVs and an extrapolated operation time of ~18,000 h corresponding to a light dose of ~15 years of operation under ambient conditions outdoor was realized, which is closing to the norm lifetime of silicon photovoltaic cells.[302,438,439] The promising robust inverted OPVs also exhibit advantages over the newly emerged perovskite hybrid solar cells knowing the intrinsically unstable organolead trihalide perovskite materials are extremely sensitive to moisture and heat.[440] Moreover, the clean nature of OPVs also eliminates the environmental and pollution apprehensions and ensures a sustainable employment. Longer lifetime OPVs are expected after deeper investigation on both scientific and technological aspects of device stability.

Another motif for commercializing the OPVs is the low processing cost. Although the recent development in silicon photovoltaic cells show a reduced cost, the low-temperature processability of inverted OPVs still reserve their potentials in the future energy market. By using the roll-to-roll filming and electrode printing technologies, the cost may still be lowered in

certain degrees.

By taking consideration of environmental impact and developing prospect, the inverted OPVs exhibit as a promising candidate for future solar market. And to facilitate the industrialization, future research focus may still lie on answering the fundamental questions of the underlying photophysical process to help improving device structures as well as better selection of materials, and lie on technical revolution on addressing challenges in massive production such as scrutinizingly controlling the BHJ morphology, deposing homogeneous nanometer-scale-thick films and developing accessary systems to maintain high device stability. In this way, accompanying with the unique merits of OPVs such as light, green, flexibility, and easy-processing, the commercialization of inverted OPVs would be realized in the near future.

Acknowledgements

Nomenclatures

Full nomination	Abbreviation	Full nomination	Abbreviation
organic photovoltaics	OPVs	power conversion efficiency	PCE
bulk heterojunction	BHJ	work-function	WF
aluminum	Al	calcium	Ca
barium	Ba	indium-tin oxide	ITO
fluorine doped tin oxide	FTO	poly(3,4-ethylenedioxythiophene):poly-(styrenesulfonate)	PEDOT:PSS
gold	Au	silver	Ag
copper	Cu	carbon nanotubes	CNTs
titanium	Ti	highest occupied molecular orbital	HOMO
poly(3-hexylthiophene)	P3HT	phenyl-C_{61}-butyric acid methyl ester	$PC_{61}BM$

polyethylene terephthalate	PET	poly[4,4-bis(2-ethylhexyl)-4Hcyclopenta[2,1-b;3,4-b'] dithiophene-2,6-diyl-alt-2, 1,3-benzothiadiazole-4,7-di yl]	PCPDTBT
lowest unoccupied molecular orbital	LUMO	charge extraction layer	CEL
electron extraction layer	EEL	organic light emitting diodes	OLEDs
transition metal oxides	TMOs	external quantum efficiency	EQE
short-circuit current	J_{SC}	x-ray diffraction	XRD
atomic force microscopy	AFM	scanning electron microscope	SEM
poly[(2,7-dioctylsilafluoren e)-2,7-diylalt-(4,7-bis(2-thi enyl)-2,1,3-benzothiadiazol e)-5,50-diyl])	PSiF-DBT	hole extraction layer	HEL
atomic layer deposition	ALD	dielectric/metal/dielectric	DMD
dye-sensitized solar cells	DSSCs	open-circuit voltage	V_{OC}
ultraviolet	UV	internal quantum efficiency	IQE
amorphous TiO_x	a-TiO_x	electron donor	D
electron acceptor	A	fill factor	FF
poly[N-dedocyldithieno[3,2 -b;6,7-b]carbazole-alt-N,N' -di(2-octyldodecanyl)-isoin digo]	P(IID-DTC)	polythieno[3,4-b]thiophene /benzodithiophene	PTB7
nanoparticles	NPs	polythylene oxide	PEO
poly(3,3'-([(9',9'-dioctyl-9 H,9'H-[2,2'-bifluorene]-9,9 -diyl)bis(1,4-phenylene)]bi s(oxy))bis(N,N-dimethylpr opan-1-amine))	PFPA-1	poly[(9,9-bis(3'-(N,N-dime thylamino)propyl)-2,7-fluo rene)-alt-2,7-(9,9– dioctylfluorene)]	PFN
poly (9,9-bis(60-diethoxylphosp horylhexyl)fluorene)	PF-EP	quinoxaline-containing poly(4,5-ethylene-2,7-carb azole)	PECz-DTQ$_x$
conjugated polyelectrolytes	CPEs	scanning Kelvin probe microscopy	SKPM
graphene oxides	GOs	electron affinity	EA
ionization energy	IE	ultraviolet photoelectron spectroscopy	UPS
inverse photoemission spectroscopy	IPES	valance band	VB
conduction band	CB	x-ray photoelectron spectroscopy	XPS
4,4'-bis(carbazol-9-yl)biphe	CBP	N,N'-diphenyl-N,N'-bis(1-	NPD

nyl		naphthyl)-1,1'-biphenyl-4, 4'-diamine	
evaporated MoO_x	$e-MoO_x$	solution-processed MoO_x	$s-MoO_x$
poly(thienothiophene-co-benzodithiophenes)7-F20	PTB7-F20	poly(5,7–bis(4–decanyl–2–thienyl)thieno[3,4–b]diathiazole–thiophene–2,5)	PDDTT
evaporated WO_3	$e-WO_3$	root-mean-square	RMS
solution-processed WO_3	$s-WO_3$	evaporated V_2O_5	$e-V_2O_5$
solution-processed V_2O_5	$s-V_2O_5$	self-assembled monolayers	SAMs
fullerene derivative SAM	C_{60}-SAM	terthiophene SAM	TT-SAM
benzoic acid SAM	BA-SAM	lauric acid SAM	LA-SAM
peak force tunneling AFM	PFTUNA	3,6-bis-(5-benzoicacid-thiophen-2-yl)-2,5-bis-(2-ethyl hexyl)-2,5-dihydro-pyrrolo [3,4-c]pyrrole-1,4-dione	DPP-COOH
di-tetrabutylammonium cisbis(isothiocyanato)bis(2, 20-bipyridyl-4,40-dicarboxylato)ruthenium(II)	N719	4-fluorobenzoic acid	FBA
4-tert-butylbenzoic	BBA	4-methoxybenzoic acid	MBA
[6,6]-phenyl-C61-butyric styryl dendron ester	PCBSD	cross-linked PCBSD	C-PCBSD
indene-C_{60} bisadduct	ICBA	[6,6]-phenylc61-butyric oxetane dendron ester	PCBOD
bis(2-(trichlorosilyl)propyl) malonate C_{60}	TSMC	self-assembled and cross-linked bis(2-(trichlorosilyl)propyl)malonate C_{60}	SA-C-TSMC
poly [diindenothieno(2,3-b)thiophene-alt-dithienylbenzothiadizole]	PDITTDTBT	water/alcohol soluble-conjugated polymers	WS-CPs
poly[[9,9-bis((6(-(N,N,N-trimethylammonium)hexyl)-2,7-fluorene)-alt-(9,9-bis(2-(2-(2-methoxyethoxy)ethoxy)ethyl)-9-fluorene)) dibromide)]	WPF-6-oxy-F	poly[N-(4-(6-diethylphosphorylhexyloxy)phenyl)-4,4'-diphenylamine]	(PTPA-EP)
poly [N-9''-hepta-decanyl-2,7-carbazole-alt-5,5-(4',7'-di-2-thienyl-2',1',3'-benzothiadiazole)]	PCDTBT	poly[[9-(N,N-di(200-hydroxyethyl)-60 -aminohexyl)-2,7-carbazole)-alt-(2-hexyloxy-5-(N,N-di(200-hydroxyethyl)-60 -aminohexyloxy)-1,4-phenylene)]	PCP-NOH

poly[(N-(60-diethylphosphoryl)hexyl-2,7-carbazole)-alt-(2-hexyloxy-5-(60-diethylphosphoryl)hexyloxy-1,4-phenylene)]	PCP-EP	2,7-carbazole homopolymer	PC-P
poly(3-[6-(N-methylimidazolium)hexyl]thiophene) bromide	P3ImHT	poly[3-(6-{4-tert-butylpyridiniumyl}-hexyl)thiophene-2,5-diyl bromide]	P3(TBP)HT$^+$ Br$^-$
electrostatic layer-by-layer	e-LBL	poly({4,8-di(2-ethylhexyloxyl)benzo[1,2-b:4,5-b′]dithiophene}-2,6-diyl)-alt-({5-octylthieno[3,4-c]pyrrole-4,6-dione}-1,3-diyl)	PBDTTPD
poly{4,8-bis(4,5-didecyl-2-thienyl)-benzo[1,2-b:4,5-b']dithiophene-alt-[4,9-bis(4-hexyl-2-thienyl)-naphtho[1,2-c:5,6-c']bis[1,2,5]thiadiazole-5,5-diyl]}	PBDT-DTNT	Hg-containing derivative of amino-functionalized conjugated polymers	PFEN-Hg
poly[(9,9-bis(3'-(N,N-dimethylamino)propyl)-2,7-fluorene-alt-2,7-(9,9-bis(3-ethyl-(oxetane-3-ethyloxy)-hexyl)-fluorene)]	PFN-OX	poly[(9,9-bis((6'-(N,N,N-trimethylammonium)hexyl)-2,7-fluorene))-alt-(9,9-bis(2-(2-methoxyethoxy)ethyl)-fluorene)] Dibromide	WPF-oxy-F
series resistance	R$_S$	sheet resistance	R$_{sh}$
1,8-octanedithiol	OT or 1,8-ODT	1,2-dichlorobenzene	DCB
diiodooctane	DIO	chloronaphthalene	CN
magnetic nanoparticles	MNPs	grazing incidence small angle x-ray scattering	GISAXS
transmission electron microscopy	TEM	space charge limited current	SCLC
silver nanowires	Ag-NWs	poly(2,6'-4,8-bis(5-ethylhexylthienyl)benzo-[1,2-b;3,4-b]dithiophene-alt-5-dibutyloctyl-3,6-bis(5-bromothiophen-2-yl)pyrrolo[3,4-c]pyrrole-1,4-dione)	PBDTT-DPP
dimethyl sulfoxide	DMSO	poly(dimethylsiloxane)	PDMS
time of flying-secondary ion mass spectrometry	TOF-SIMS	poly[2-methoxy-5-(3',7'-dimethyloctyloxy)-1,4-phenylenevinylene]	MDMO-PPV

References

1. A. Datta and B. K. Mandal, *Energy Technology & Policy*, 2014, **1**, 8-14.

2. D. Pimentel, L. E. Hurd, A. C. Bellotti, M. J. Forster, I. N. Oka, O. D. Sholes and R. J. Whitman, *Science,* 1973, **182**, 443-449.

3. I. Naseem and J. Khan, *Int. j. Afr. Asian stud.,* 2015, **7**, 33-42.

4. A. Alam, I. A. Malik, A. B. Abdullah, A. Hassan, U. Awan, G. Ali, K. Zaman and I. Naseem, *Renew Sust Energ Rev.,* 2015, **41**, 818-829.

5. D. Angmo and F. C. Krebs, *Energy Technol.,* 2015, **3**, 774-783.

6. P. Wurfel, *Physics of Solar Cells,* Weinheim Wiley-VCH, 2005, p2, 8, 34.

7. US Energy Information Administration, *Annual Energy Outlook 2012,* available on the EIA Home Page (www.eia.gov/ieo). U.S. Energy.

8. D. L. Emanuele, *Nature,* 2015, **518**, 310-311.

9. M. A. Green, K. Emery, Y. Hishikawa, W. Warta and E. D. Dunlop, *Prog Photovoltaics Res Appl.*, 2015, **23**, 1-9.

10. I. Etxebarria, J. Ajuria and R. Pacios, *Org. Electron.,* 2015, **19**, 34-60.

11. Y. Sun, W. Zhang, H. Chi, Y. Liu, C. L. Hou and D. Fang, *Renewable and Sustainable Energy Reviews*, 2015, **43**, 973-980.

12. C. J. Brabec, *Sol. Energy Mater. Sol. Cells,* 2004, **83**, 273-292.

13. X. Wang, L. Kurdgelashvili, J. Byrne and A. Barnett, *Renew Sustain Energy Rev.,* 2011, **15**, 4248-4254.

14. K. Wang, H. Ren, C. Yi, C. Liu, H. Wang, L. Huang, H. Zhang, A. Karim and X. Gong, *ACS Appl. Mater. Interfaces,* 2013, **5**, 10325-10330.

15.   G. Yu, J. Gao, J. C. Hummelen, F. Wudl and A. J. Heeger, *Science,* 1995, **270**, 1789-1790.

16.   K. W. Wong, H. L. Yip, Y. Luo, K. Y. Wong, W. M. Lau, K. H. Low, H. F. Chow, Z. Q. Yeung and C. C. Chang, *Appl. Phys. Lett.,* 2002, **80**, 2788-2790.

17.   M. P. De Jong, L. J. Van IJzendoorn and M. J. De Voigt, *Appl. Phys. Lett.,* 2000, **77**, 2255-2257.

18.   H. Yan, P. Lee, N. R. Armstrong, A. Graham, G. A. Evmenenko and P. Dutta, T. J. Marks, *J. Am. Chem. Soc.,* 2005, **127**, 3172-3183.

19.   Y. H. Kim, C. Sachse, M. L. Machala, C. May, L. M. Meskamp and K. Leo, *Adv. Func. Mat.,* 2011, **21**, 1076-1081.

20.   P. Tehrani, A. Kanciurzewska, X. Crispin, N. D. Robinson, M. Fahlman and M. Berggren, *Solid State Ionics,* 2007, **177**, 3521-3527.

21.   J. Ni, H. Yan, A. Wang, Y. Yang, C. L. Stern, A. W. Metz, S. Jin, L. Wang, T. J. Marks, J. R. Ireland and C. R. Kannewurf, *J. Am. Chem. Soc.,* 2005, **127**, 5613-5624.

22.   M. Kemerink, S. Timpanaro, M. M. De Kok, E. A. Meulenkamp and F. J. Touwslager, *J. Phys. Chem. B,* 2004, **108**, 18820-18825.

23.   I. J. Marks and W. H. Alexander, 2011, U.S. Patent No. 7,888,593. 15.

24.   M. T. Lloyd, C. H. Peters, A. Garica, I. V. Kauvar, J. J. Berry, M. O. Reese, M. D. Mcgehee, D. S. Ginley and D. C. Olson, *Sol. Energy Mater. Sol. Cells,* 2011, **95**, 1382-1388.

25.   M. T. Lloyd, D. C. Olson, P. Lu, E. Fang, D. L. Moore, M. S. White, M. O. Reese, D. S. Ginley and J. W. P. Hsu, *J. Mater. Chem.,* 2009, **19**, 7638-7642.

26.   F. C. Krebs, *Sol. Energy Mater. Sol. Cells,* 2008, **92**, 715-726.

27.   L.-M. Chen, Z. Hong, G. Li and Y. Yang, *Adv. Mater.,* 2009, **21**, 1434-1449.

28.   T. N. Ng, W. S. Wong, M. L. Chabinyc and R. A. Street, *Appl. Phys. Lett.,* 2008, **92**, 213303-213303.

29.   M. Wu, K. Pangal, J. C. Sturm and S. Wagner, *Appl. Phys. Lett.,* 1999, **75**, 2244-2246.

30.   M. Glatthaar, M. Niggemann, B. Zimmermann, P. Lewer, M. Riede, A. Hinsch and J. Luther, *Thin Solid Films,* 2005, **491**, 298-300.

31.   T. Oyamada,Y. Sugawara,Y. Terao, H. Sasabe and C. Adachi, *Jpn. J. Appl. Phys.,* 2007, **46**, 1734-1734.

32.   C. J. An, C. Cho, J. K. Choi, J.-M. Park, M. L. Jin, J.-Y. Lee and H.-T. Jung, *Small*, 2013, **1**, 1278-1283.

33.   H.-W. Lin, S.-W. Chiu, L.-Y. Lin, Z.-Y. Hung, Y.-H. Chen, F. Lin and K.-T. Wong, *Adv. Mater.,* 2012, **24**, 2269-2272.

34.   S. Schubert, M. Hermenau, J. Meiss, L. Miller-Meskamp and K. Leo, *Adv. Funct. Mater.,* 2012, **24**, 2572-2577.

35.   M. Born, E. Wolf, *Principle of Optics,* 7th Edition, Cambridge University, Cambridge, UK 1999; p48.

36.   H.-W. Lin, S.-W. Chiu, L.-Y. Lin, Z.-Y. Huang, Y.-H. Chen, F. Lin and K.-T. Wong, *Adv. Mater.,* 2012, **24**, 2269-2272.

37.   K. Yao, X. K. Xin, C. C. Chueh, K. S. Chen, Y. X. Xu and A. K. Y. Jen, *Adv. Funct. Mater.,* 2015, **25**, 567-574.

38.   F. Guo, N. Li, V. V. Radmilović, V .R. Radmilović, M. Turbiez, E. Spiecker and C. J. Brabec, *Energy Environ. Sci.,* 2015, **8**, 1690-1697.

39.   M. Bukhardt, W. Liu, C. G. Shuttle, K. Banerjee and M. L. Chabinyc, *Appl. Phys. Lett.,* 2012, **101**, 033302-033302.

40. M. Song, H. J. Kim, C. S. Kim, J. H. Jeong, C. Cho, J. Y. Lee, S. H. Jin, D. G. Choi and D. H. Kim, *J. Mater. Chem. A.,* 2015, **3**, 65-70.

41. S. I. Na, S. S. Kim, J. Jo and D. Y. Kim, *Adv. Mater.,* 2008, **20**, 4061-4067.

42. R. Betancur, P. Romero-Gomez, A. Martinez-Otero, X. Elias, M. Maymo and J. Martorell, *Nature Photon.,* 2013, **7**, 995-1000.

43. E.-C. Chen, P.-T. Tsai, C.-Y. Tsai, J.-H. Chang, Z.-Y. Huang, H.-F. Meng, H.-M. Chen, H.-W. Lin, S.-F. Horng and H.-W. Zan, *Synt. Met.,* 2014, **187**, 172-177.

44. C.-W. Chu, S.-H. Li, C.-W. Chen, V. Shrotriya and Y. Yang. *Appl Phys Lett,* 2005, **87**, 193508-193508.

45. B. Qi, Z. G. Zhang and J. Wang, *Sci. Rep.,* 2015, **5**. DOI: 10.1038/srep07803

46. S. J. Pearton, D. P. Norton, Y. W. Heo and T. J. Steiner, *J. Vac. Sci. Technol., B*, 2004, **22**, 932-948.

47. J. H. Park, G. S. Kang, S. I. Kwon, D. G. Lim, Y. J. Choi, K. J. Choi and J. G. Park, *J. Nanosci. Nanotechnol.*, 2008, **8**, 4658-4661.

48. M. S. White, D. C. Olson, S. E. Shaheen, N. Kopidakis and D. S. Ginley, *Appl. Phys. Lett*., 2006, **89**, 143517-143517.

49. X. Gong, *Polymer,* 2012, **53**, 5437-5448.

50. S. O'Brien, L. H. K. Koh and G. M. Crean, *Thin Solid Films,* 2008, **516**, 1391-1395.

51. A. K. K. Kyaw, X. W. Sun and C. Y. Jiang, *J. Sol-Gel Sci. Technol.,* 2009, **52**, 348-355.

52. A. K. K. Kyaw, X. W. Sun, C. Y. Jiang, G. Q. Lo, D. W. Zhao and D. L. Kwong, *Appl. Phys. Lett.,* 2008, **93**, 221107-221107.

53. S. K. Hau, H. L. Yip, N. S. Baek, J. Zou, K. O'Malley and A. K. Y. Jen, *Appl. Phys. Lett.,* 2008, **92**, 253301-253301.

54. F. C. Krebs, S. A. Gevorgyan and J. Alstrup, *J. Mater. Chem.,* 2009, **19**, 5442-5451.

55. B. Pradhan, S. Albrecht, B. Stiller and D. Neher, *Appl. Phys. A Mater. Sci.,* 2004, **115**, 365-369.

56. K. Zilberberg, J. Meyer and T. Riedl, *J. Mater. Chem.C,* 2013, **1**, 4796-4815.

57. S. Chen, C. E. Small, C. M. Amb, J. Subbiah, T. H. Lai, S. W. Tsang, J. R. Manders and J. R. Reynolds, *Adv. Energy Mater.,* 2012, **2**, 1333-1337.

58. J. C. Wang, W. T. Weng, M. Y. Tsai, M.-K. Lee, S.-F. Horng, T.-P. Perng, C.-C. Kei, C.-C. Yu and H.-F. Meng, *J. Mater. Chem.,* 2010, **20**, 862-866.

59. H. Cheun, C. Fuentes-Hernandez, Y. Zhou, W. J. Potscavage Jr, S. J. Kim, J. Shim, A. Dindar and B. Kippelen, *J. Phys. Chem. C,* 2010, **114**, 20713-20718.

60. C. Y. Chang and F. Y. Tsai, *J. Mater. Chem.,* 2011, **21**, 5710-5715.

61. R. L. Hoye, D. Muñoz-Rojas, D. C. Iza, K. P. Musselman and J. L. MacManus-Driscoll, *Sol. Energy Mater. Sol. Cells,* **2013**, *116*, 197-202.

62. M. Scharrer, X. Wu, A. Yamilov, H. Cao and R. P. Chang, *Appl. Phys. Lett.,* **2005**, *86*, 151113-151113.

63. M. Eita, A. E. Labban, F. Cruciani, A. Usman, P. M. Beaujuge and O. F. Mohammed, *Adv. Funct. Mater.,* 2015, **25**, 1558-1564.

64. L. Zhe, X. Chen, J. Zhou, Z. Jiang, S. Huang, F. Zhu, X. Piao and Z. Sun, *Org. Electron..,* 2015, **17**, 364-370.

65. K. Wijeratne, J. Akilavasan, A. Alamoud and J. Bandara, *Transaction on Electron Optics,* 2015, **1**, 8-13.

66. H. L. Gao, X. W. Zhang, J. H. Meng, Z. G. Yin, L. Q. Zhang, J. L. Wu and X. Liu, *J. Mater. Chem. A,* 2015, **3**, 3719-3725.

67. R. M. Pasquarelli, D. S. Ginley and R. O'Hayre, *Chem. Soc. Rev,* 2011, **40**, 5406-5441.

68. U. Diebold, S. C. Li and M. Schmid, *Annu. Rev. Phys. Chem.,* 2010, **61**, 129-148.

69. A. L. Linsebigler, G. Lu and Jr J. T. Yates, *Chem. Rev,* 1995, **95**, 735-758.

70. U. Bach, D. Lupo, P. Comte, J. E. Moser, F. Weissörtel, J. Salbeck, H. Spreitzer and M. Grätzel, *Nature,* 1998, **395**, 583-585.

71. B. O'Regan and M. Grätzel, *Nature,* 1991, **353**, 737-740.

72. B. E. Hardin, H. J. Snaith and M. D. McGehee, *Nature Photon.,* 2012, **6**, 162-169.

73. C. C. Wang and J. Y. Ying, *Chem. Mater.,* 1999, **11**, 3113-312.

74. B. E. Yoldas, *J. Mater. Sci.,* 1986, **21**, 1087-1092.

75. Y. C. Ho, P. Y. Ho, H. C. Lee, S. K. Chang, Y. R. Hong and C. F. Lin, *Sol. Energy Mater. Sol. Cells,* 2015, **132**, 570-577.

76. A. Hagfeldt and M. Graetzel, *Chem. Rev,* 1995, **95**, 49-68.

77. C. J. Barbe, F. Arendse, P. Comte, M. Jirousek, F. Lenzmann, V. Shklover and M. Grätzel, *J. Am. Ceram. Soc.,* 1997, **80**, 3157-3171.

78. B. O'Regan, J. Moser, M. Anderson and M. Graetzel, *J. Phys. Chem.*, 1990, **94**, 8720-8726.

79. J. Y. Kim, S. H. Kim, H. H. Lee, K. Lee, W. Ma, X. Gong and A. J. Heeger, *Adv. Mater.*, 2006, **18**, 572-576.

80. K. Lee, J. Y. Kim, S. H. Park, S. H. Kim, S. Cho and A. J. Heeger, *Adv. Mater.*, 2007, **19**, 2445-2449.

81. Q. Wei, T. Nishizawa, K. Tajima and K. Hashimoto, *Adv. Mater.*, 2008, **20**, 2211-2216.

82. C. Duan, K. Zhang, C. Zhong, F. Huang and Y. Cao, *Chem. Soc. Rev.*, 2013, **42**, 9071-9104.

83. J. Luo, H. Wu, C. He, A. Li, W. Yang and Y. Cao, *Appl. Phys. Lett.*, 2009, **95**, 043301-043301.

84. K. Lee, K. J. Young and A. J. Heeger, *Proc. SPIE, Organic Photonic Materials and Devices VIII*, 2006, **6117**, 61170T-61170T.

85. S. H. Park, A. Roy, S. Beaupre, S. Cho, N. Coates, J. S. Moon, D. Moses, M. Leclerc, K. Lee and A. J. Heeger, *Nature Photon.*, 2009, **3**, 297-302.

86. X. Bao, L. Sun, W. Shen, C. Yang, W. Chen and R. Yang, *J. Mater. Chem. A,* 2014, **2**, 1732-1737.

87. L. Tan, Z. He and Y. Chen, *RSC Advances*, 2015, **5**, 23213-23223.

88. T. Kuwabara, H. Sugiyama, T. Yamaguchi and K. Takahashi, *Thin Solid Films*, 2009, **517**, 3766-3769.

89. G. J. D. A. Soler-Illia, A. Louis and C. Sanchez, *Chem. Mater.,* 2002, **14**, 750-759.

90. P. C. A. Alberius, K. L. Frindell, R. C. Hayward, E. J. Kramer, G. D. Stucky and B. F. Chemlka, *Chem. Mater.*, 2002, **14**, 3284-3294.

91. K. M. Coakley, B. S. Srinivasan, J. M. Ziebarth, C. Goh, Y. Liu and M. D. McGehee, *Adv. Funct. Mater.*, 2005, **15**, 1927-1932.

92. K. M. Coakley and M. D. McGehee, *Chem. Mater.*, 2004, **16**, 4533-4542.

93. A. J. Cadby and S. H. Tolbert, *J. Phys. Chem. B,* 2005, **109**, 17879-17886.

94. P. A. Van Hal, M. M. Wienk, J. M. Kroon, W. J. H. Verhees, L. H. Slooft, W. J. H. Van Gennip, P. Jonkheijm and R. A. Janssen, *Adv. Mater.,* 2003, **15**, 118-121.

95. G. K. Mor, K. Shankar, M. Paulose, O. K. Varghese and C. A. Grimes, *Appl. Phys. Lett.,* 2007, **91**, 152111-152111.

96. B.-Y. Yu, A. Tsai, S.-P. Tsai, K.-T. Wong, Y. Yang, C.-W. Chu and J.-J. Shyue, *Nanotechnology,* 2008, **19**, 255202-255202.

97. D. C. Olson, S. E. Shaheen, R. T. Collins and D. S. Ginley, *J. Phys. Chem. C*, 2007, **111**, 16670-16678.

98. K. Takanezawa, K. Tajima and K. Hashimoto, *Jpn. J. Appl. Phys.*, 2008, **47**, 8049-8049.

99. Y. Hames, Z. Alpaslan, A. Kösemen, S. E. San and Y. Yerli, *Sol. Energy*, 2010, **84**, 426-431.

100. J. Liu, S. Shao, B. Meng, G. Fang, Z. Xie, L. Wang and X. Li, *Appl. Phys. Lett.*, 2012, **100**, 213906-213906.

101. J. Liu, J. Wu, S. Shao, Y. Deng, B. Meng, Z. Xie, Y. Geng, L. Wang and F. Zhang, *ACS Appl. Mater. Interfaces*, 2014, **6**, 8237-8245.

102. T. Hu, L. Chen, Z. Deng and Y. Chen, *J. Mater. Chem. A*, 2015, **3**, 10890-10899.

103. C. J. Brabec, S. E. Shaheen, C. Winder, N. S. Sariciftci and P. Denk, *Appl. Phys. Lett.*, 2002, **80**, 1288-1290.

104. C. Ganzorig, K. Suga and M. Fujihira, *Materials Science and Engineering: B,* 2001, **85**, 140-143.

105. T. Hasegawa, S. Miura, T. Moriyama, T. Kimura, I. Takaya, Y. Osato and H. Mizutani, *Dig. Tech. Papers-Soc. Inf. Disp. Int. Symp,* 2004, **35**, 154-157.

106. T. Hasegawa, S. Miura, T. Moriyama, T. Kimura, I. Takaya, Y. Osato and H. Muzutani, *SID Symposium Digest of Technical Papers,* 2012, **35**, 154-157.

107. H.-H. Liao, L.-M. Chen, Z. Xu, G. Li and Y. Yang, *Appl. Phys. Lett.,* 2008, **92**, 173303-173303.

108. A. H. Sommer, *J. Appl. Phys.,* 1980, **51**, 1254-1255.

109. G. Li, C.-W. Chu, V. Shrotriya, J. Huang and Y. Yang, *Appl. Phys. Lett.,* 2006, **88**, 253503-253503.

110. A. Barbot, B. Lucas, C. Di Bin, B. Ratier and M. Aldissi, *Appl. Phys. Lett.,* 2013, **102**, 193305-193305.

111. G. Cheng, W.-Y. Tong, K.-H. Low and C.-M. Che, *Sol. Energy Mater. Sol. Cells,* 2012, **103**, 164-170.

112. J. Huang, G. Li and Y. Yang, *Adv. Mater.,* 2008, **20**, 415-419.

113. D. W. Zhao, P. Liu, X. W. Sun, S. T. Tan, L. Ke and A. K. K. Kyaw, *Appl. Phys. Lett.*, 2009, **95**, 153304-153304.

114. Y. Zhou, F. Li, S. Barrau, W. Tian, O. Inganäs and F. Zhang, *Sol. Energy Mater. Sol. Cells,* 2009, **93**, 497-500.

115. Y. Zhou, C. Fuentes-Hernandez, J. Shim, J. Meyer, A. J. Giordano, H. Li, P. Winget, T. Papadopoulos, H. Cheun, J. Kim, M. Fenoll, A. Dindar, W. Haske, E. Najafabadi, T. M. Khan, H. Sojoudi, S. Barlow, S. Graham, J.-L. Brédas, S. R. Marder, A. Kahn and B. Kippelen, *Science,* 2012, **336**, 327-332.

116. H. Kang, S. Hong, J. Lee and K. Lee, *Adv. Mater.,* 2012, **24**, 3005-3009.

117. J. W. Shim, H. Cheun, J. Meyer, C. Fuentes-Hernandez, A. Dindar, Y. H. Zhou, D. K. Hwang, A. Kahn and B. Kippelen, *Appl. Phys. Lett.,* 2012, **101**, 073303-073303.

118. Z. Tang, L. M. Andersson, Z. George, K. Vandewal, K. Tvingstedt, P. Heriksson, R. Kroon, M. R. Andersson and O. Inganäs, *Adv. Mater.,* 2012, **24**, 554-558.

119. Z. He, C. Zhong, X. Huang, W.-Y. Wong, H. Wu, L. Chen, S. Su and Y. Cao, *Adv. Mater.,* 2011, **23**, 4636-4643.

120. C. He, C. Zhong, H. Wu, R. Yang, W. Yang, F. Huang, G. C. Bazan and Y. Cao, *J. Mater. Chem.,* 2010, **20**, 2617-2622.

121. A. Duarte, K. Y. Pu, B. Liu and G. C. Bazan, *Chem. Mater.,* 2011, **23**, 501-515.

122.   J. H. Seo, A. Gutacker, Y. Sun, H. Wu, F. Huang, Y. Cao, U. Scherf, A. J. Heeger and G. C. Bazan, *J. Am. Chem. Soc.*, 2011, **133**, 8416-8419.

123.   S. R. Dupont, E. Voroshazi, D. Nordlund and R. H. Dauskardt, *Sol. Energy Mater. Sol. Cells*, 2015, **132**, 443-449.

124.   S. S. Li, K. H. Tu, C. C. Lin, C. W. Chen and M. Chhowalla, *ACS nano*, 2010, **4**, 3169-3174.

125.   Y. Wang, Q. Luo, N. Wu, Q. Wang, H. Zhu, L. Chen, Y. Li, L. Luo and C. Q. Ma, *ACS Appl. Mater. Interfaces*, 2015, **7**, 7170-7179.

126.   S.-I. Na, T.-S. Kim, S.-H. Oh, J. Kim, S.-S. Kim and D.-Y. Kim, *Appl. Phys. Lett.,* 2010, **97**, 223305-223305.

127.   W. Yu, L. Shen, S. Ruan, F. Meng, J. Wang, E. Zhang and W. Chen, *Sol. Energy Mater. Sol. Cells,* 2012, **98**, 212-215.

128.   S. R. PáSilva, *J. Mater. Chem. C*, 2013, **1**, 1708-1712.

129.   J. S. Yeo, J. M. Yun, M. Kang, D. Khim, S. H. Lee, S. S. Kim, S. I. Na and D. Y.   Kim, *ACS Appl. Mater. Interfaces*, 2014, **6**, 19613-19620.

130.   J. C. Yu, J. I. Jang, B. R. Lee, G. W. Lee, J. T. Han and M. H. Song, *ACS Appl. Mater. Interfaces*, 2014, **6**, 2067-2073.

131.   J. Liu, Y. Xue and L. Dai, *J. Phys. Chem. Lett.*, 2012, **3**, 1928-1933.

132.   H. Lu, J. Lin, N. Wu, S. Nie, Q. Luo, C. Q. Ma and Z. Cui, *Appl. Phys. Lett.*, 2015, **106**, 093302-093302.

133.   S. R. Dupont, E. Voroshazi, D. Nordlund and R. H. Dauskardt, *Sol. Energy Mater. Sol. Cells*, 2015, **132**, 443-449.

134.   S. Tokito, K. Noda and Y. Taga, *J. Phys. D. Appl. Phys.,* 1996, **29**, 2750-2753.

135. J. Meyer, S. Hamwi, M. Kroger, W. Kowalsky, T. Riedl and A. Kahn, *Adv. Mater.,* 2012, **24**, 5408-5427.

136. H. Frohne, S. E. Shaheen, C. J. Brabec, D. C. Müller, N. S. Sariciftci and K. Meerholz, *Chem. Phys. Chem.,* 2002, **9**, 795-799.

137. P. Peumans and S. R. Forrest, *Appl. Phys. Lett.,* 2001, **79**, 126-128.

138. M. D. Irwin, B. Buchholz, A. W. Hains, R. P. H. Chang and T. J. Marks, *Proc. Natl. Acad. Sci. U. S. A,* 2008, **105**, 2783-2787.

139. S. Chen, J. R. Manders, S.-W. Tsang and F. So, *J. Mater. Chem.,* 2012, **22**, 24202-24212.

140. H. You, Y. F. Dai, Z. Q. Zhang and D. G. Ma, *J. Appl. Phys*., 2007, **101**, 026105-026105.

141. C. W. Chu, S. H. Li, C. W. Chen, V. Shrotriya and Y. Yang, *Appl. Phys. Lett*., 2005, **87**, 193508-193508.

142. M. Kroger, S. Hamwi, J. Meyer, T. Riedl, W. Kowalsk and A. Kahn, *Org. Electron*., 2009, **10**, 932-938.

143. K. Zilberberg, S. Trost, H. Schmidt and T. Riedl, *Adv. Energy Mater*., 2011, **1**, 377-381.

144. J. S. Park, B. R. Lee, J. M. Lee, J. S. Kim, S. O. Kim and M. H. Song, *Appl. Phys. Lett.,* 2010, **96**, 243306-243306.

145. A. Dai, A. Wan, C. Magee, Y. Zhang, S. Barlow, S. R. Marder and A. Kahn, *Org. Electron.,* 2015, **23**, 151-157.

146. J. Meyer, K. Zilberberg, T. Riedl and A. Kahn, *J. Appl. Phys.,* 2011, **110**, 033710-033710.

147. J. Subbiah, G. Sarasqueta, F. So, H. Irfan, Ding, Y. L. Gao and D. Y. Kim, *Appl. Phys. Lett.,* 2009, **95**, 093304-093304.

148. M. T. Greiner, M. G. Helander, W.-M. Tang, Z.-B. Wang, J. Qiu and Z.-H. Lu, *Nat. Mater.,* 2012, **11**, 76-81.

149. K. Kanai, K. Koizumi, S. Ouchi, Y. Tsukamoto, K. Sakanoue, Y. Ouchi and K. Seki, *Org. Electron.,* 2010, **11**, 188-194.

150. M. Irfan, Zhang, H. Ding, C. W. Tang and Y. Gao, *Org. Electron.*, 2011, **12**, 1588-1593.

151. M. Kroger, S. Hamwi, J. Meyer, T. Riedl, W. Kowalsky and A. Kahn, *Appl. Phys. Lett.*, 2009, **95**, 123301-123301.

152. T. S. Sian and G. B. Reddy, *Sol. Energy Mater. Sol. Cells,* 2004, **82**, 375-386.

153. K. Kanai, K. Koizumi, S. Ouchi, Y. Tsukamoto, K. Sakanoue, Y. Ouchi and K. Seki, *Org. Electron.,* 2010, **11**, 188-194.

154. J. Meyer, A. Shu, M. Kroger and A. Kahn, *Appl. Phys. Lett.,* 2010, **96**, 243305-243305.

155. H. J. Irfan, Ding, Y. L. Gao, C. Small, D. Y. Kim, J. Subbiah and F. So, *Appl. Phys. Lett.,* 2010, **96**, 243307-243307.

156. C. E. Small, S. Chen, J. Subbiah, C. M. Amb, S. W. Tsang, T. H. Lai and F. So, *Nature Photon.*, 2012, **6**, 115-120.

157. K. Galatsis, Y. Li, W. Wlodarski, C. Cantalini, M. Passacantando and S. Santucci, *J. Sol-Gel Sci. Technol.*, 2003, **26**, 1097-1101.

158. K. Galatsis, Y. X. Li, W. Wlodarski, E. Comini, G. Faglia and G. Sberveglieri, *Sensor Actuat B-Chem.*, 2001, **77**, 472-477.

159. K. Galatsis, Y. X. Li, W. Wlodarski, E. Comini, G. Sberveglieri, C. Cantalini, S. Santucci and M. Passacantando, *Sensor Actuat B-Chem.*, 2002, **83**, 276-280.

160. K. Galatsis, Y. X. Li, W. Wlodarski and K. Kalantar-Zadeh, *Sensor Actuat B-Chem.*, 2001, **77**, 478-483.

161. L. Boudaoud, N. Benramdane, R. Desfeux, B. Khelifa and C. Mathieu, *Catal. Today*, 2006, **113**, 230-234.

162. C. S. Hsu, C. C. Chan, H. T. Huang, C. H. Peng and W. C. Hsu, *Thin Solid Films*, 2008, **516**, 4839-4844.

163. B. Li, H. Ren, H. Yuan, A. Karim and X. Gong, *ACS Photonics*, 2014, **1**, 87-90.

164. B. Li, PhD diss., University of Akron, **2013**.

165. X. Hu, K. Wang, C. Liu, T. Meng, Y. Dong, S. Liu, F. Huang, X. Gong and Y. Cao, *J. Mater. Chem. C*, 2014, **2**, 9592-9598.

166. J. Meyer, R. Khalandovsky, P. Gorrn and A. Kahn, *Adv. Mater.,* 2011, **23**, 70-73.

167. F. M. Liu, S. Y. Shao, X. Y. Guo, Y. Zhao and Z. Y. Xie, *Sol. Energy Mater. Sol. Cells,* 2010, **94**, 842-845.

168. E. G. Voroshazi, D. Cheyns, P. Heremans and B. P. Rand, *ACS Appl. Mater. Interfaces,* 2011, **3**, 3244-3247.

169. K. Zilberberg, H. Gharbi, A. Behrendt, S. Trost and T. Riedl, *ACS Appl. Mater. Interfaces,* 2012, **4**, 1164-1168.

170. K. Zilberberg, J. Meyer and T. Riedl, *J. Mater. Chem. C*, 2013, **1**, 4796-4815.

171. K. Zilberberg, S. Trost, J. Meyer, A. Kahn, A. Behrendt, D. Lützenkirchen-Hecht, R. Frahm and T. Riedl, *Adv. Funct. Mater.*, 2011, **21**, 4776-4783.

172. W. Qiu, R. Müller, E. Voroshazi, B. Conings, R. Carleer, H. G. Boyen, M. Turbiez, L. Froyen, P. Heremans and A. Hadipour, *ACS Appl. Mater. Interfaces*, 2015, **7**, 3581-3589.

173. A. J. Bard and M. S. Wrighton, *J. Electrochem. Soc.*, 1977, **124**, 1706-1710.

174. C. Tao, S. Ruan, G. Xie, X. Kong, L. Shen, F. Meng, C. Liu, X. Zhang, W. Dong and W. Chen, *Appl. Phys. Lett.*, 2009, **94**, 043311-043311.

175. C. Tao, G. Xie, F. Meng, S. Ruan and W. Chen, *J. Phys. Chem. C*, 2011, **115**, 12611-12615.

176. S. Han, W. S. Shin, M. Seo, D. Gupta, S. J. Moon and S. Yoo, *Org. Electron.,* 2009, **10**, 791-797.

177. C. Z. Li, H. L. Yip and A. K. Y. Jen, *Progress in High-Efficient Solution Process Organic Photovoltaic Devices,* Springer Berlin Heidelberg, 2015, p273-297.

178. H. Choi, B. S. Kim, M. J. Ko, D.-W. Lee, H. Kim, S. H. Kim and K. Kim, *Org. Electron.,* 2012, **13**, 959-968.

179. C. M. Amb, S. Chen, K. R. Graham, J. Subbiah, C. E. Small, F. So and J. R. Reynolds, *J. Am. Chem. Soc.*, 2011, **133**, 10062-10065.

180. N. K. Elumalai, C. Vijila, R. Jose, A. Uddin and S. Ramakrishna, *Materials for Renewable and Sustainable Energy,* 2015, **4**, 1-25.

181. V. Shrotriya, G. Li, Y. Yao, C. W. Chu and Y. Yang, *Appl. Phys. Lett.,* 2006, **88**, 073508-073508.

182. C. Waldauf, M. Morana, P. Denk, P. Schilinsky, K. Coakley, S. A. Choulis and C. J. Brabec, *Appl. Phys. Lett.*, 2006, **89**, 233517-233517.

183. R. Steim, S. A. Choulis, P. Schilinsky and C. J. Brabec, *Appl. Phys. Lett.,* 2008, **92**, 093303-093303.

184. G. Li, C. W. Chu, V. Shrotriya, J. Huang and Y. Yang, *Appl. Phys. Lett.,* 2006, **88**, 253503-253503.

185. J. S. Huang, C. Y. Chou and C. F. Lin, *IEEE Electr. Dev. Lett.,* 2010, **31**, 332-334.

186. J. S. Huang, C. Y. Chou, M. Y. Liu, K. H. Tsai, W. H. Lin and C. F. Lin, *Org. Electron.,* 2009, **10**, 1060-1065.

187. J. Meyer, R. Khalandovsky, P. Görrn and A. Kahn, *Adv. Mater.,* **2011**, *23*, 70-73.

188. Y. M. Chang and J. M. Ding, *Thin Solid Films*, 2012, **520**, 5400-5404.

189. C. P. Chen, Y. D. Chen and S. C. Chuang, *Adv. Mater.*, 2011, **23**, 3859-3863.

190. T. Kololuoma, J. Lu, S. Alem, N. Graddage, R. Movileanu, S. Moisa and Y. Tao, *In SPIE OPTO International Society for Optics and Photonics*, **2015**, *93640K*, DOI:10.1117/12.2079270.

191. D. Adler and J. Feinleib, *Phys. Rev. B: Solid State,* 1970, **2**, 3112-3134.

192. F. A. Kroger, *J. Phys. Chem. Solids 1968*, **29**, 1889-1899.

193. S. Mrowec and Z. Grzesik, *J. Phys. Chem. Solids,* 2004, **65**, 1651-1657.

194. M. A. Langell, C. L. Berrie, M. H. Nassir and K. W. Wulser, *Surf. Sci.*, 1994, **320**, 25-38.

195. M. A. Langell and M. H. Nassir, *J. Phys. Chem.,* 1995, **99**, 4162-4169.

196. M. W. Roberts and R. S. C. Smart, *Surf. Sci.,* 1980, **100**, 590-604.

197. E. L. Ratcliff, J. Meyer, K. X. Steirer, A. Garcia, J. J. Berry, D. S. Ginley, D. C. Olson, A. Kahn and N. R. Armstrong, *Chem. Mater.,* 2011, **23**, 4988-5000.

198. E. L. Ratcliff, J. Meyer, K. X. Sterier, N. R. Armstrong, D. Olson and A. Kahm, *Org. Electron.,* 2012, **13**, 744-749.

199. K. X. Steirer, J. P. Chesin, N. E. Widjonarko, J. J. Berry, A. Miedaner, D. S. Ginley and D. C. Olson, *Org. Electron.*, 2010, **11**, 1414-1418.

200. K. X. Steirer, P. F. Ndione, N. E. Widjonarko, M. T. Lloyd, J. Meyer, E. L. Ratcliff, A. Kahn, N. R. Armstrong, C. J. Curtis, D. S. Ginley, J. J. Berry and D. C. Olson, *Adv. Energy. Mater.,* 2011, **1**, 813-820.

201. J. G. Aiken and A. G. Jordan, *J. Phys. Chem. Solids,* 1968, **29**, 2153-2167.

202. L. Wu, F. Li, Y. Xu, J. W. Zhang, D. Zhang, G. Li and H. Li, *Applied Catalysis B: Environmental*, 2015, **164**, 217-224.

203. T. Stubhan, N. Li, N. A. Luechinger, S. C. Halim, G. J. Matt and C. J. Brabec, *Adv. Energy Mater.*, 2012, **2**, 1433-1438.

204. B.-Y. Yu, A. Tsai, S.-P. Tsai, K.-T. Wong, Y. Yang, C.-W. Chu and J.-J. Shyue, *Nanotechnology,* 2008, **19**, 255202-255202.

205. R. Steim, S. A. Choulis, P. Schilinsky and C. J. Brabec, *Appl. Phys. Lett.*, 2008, **92**, 093303-093303.

206. L. L. Chua, J. Zaumseil, J. F. Chang, E. C. W. Ou, P. K. H. Ho, H. Sirringhaus and R. H. Friend, *Nature*, 2005, **434**, 194-199.

207. D. Credgington, F. Jamieson, B. Walker, T. Nguyen and J. R. Durrant, *Adv. Mater.,* 2012, **24**, 2135-2141.

208. S. Albrecht, S. Janietz, W. Schindler, J. Frisc, J. Kurpiers, J. Kniepert, S. Inal, P. Pingel, K. Fostiropoulos, N. Koc and D. Neher, *J. Am. Chem. Soc.,* 2012, **134**, 14932- 14944.

209. C. G. Shuttle, R. Hamilton, B. C. O'Regan, J. Nelso and J. R. Durrant, *Proc. Natl. Acad. Sci. U. S. A.*, 2010, **107**, 16448-16452.

210. M. Gluecker, A. Foertig, V. Dyakonov and C. Deibel, *Phys. Status Solidi RRL.,* 2012, **8**, 337-339.

211. H.-L. Yip, S. K. Hau, N. S. Baek, H. Ma and A. K.-Y. Jen, *Adv. Mater.,* 2008, **20**, 2376-2382.

212. S. K. Hau, H.-L. Yip, H. Ma and A. K.-Y. Jen, *Appl. Phys. Lett., 2008*, **93**, 233304-233304.

213. S. K. Hau, H.-L. Yip, O. Acton, N. S. Baek, H. Ma and A. K.-Y. Jen, *J. Mater. Chem.,* 2008, **18**, 5113-5119.

214. S. Khodabakhsh, B. M. Sanderson, J. Nelson and T. S. Jones, *Adv. Func. Mater.*, 2006, **16**, 95-100.

215. N. R. Armstrong, C. Carter, C. Donley, A. Simmonds, P. Lee, M. Brumbach, B. Kippelen, B. Domercq and S. Yoo, *Thin Solid Films,* 2003, **445**, 342-352.

216. J. S. Kim, J. H. Park, J. H. Lee, J. Jo, D.-Y. Kim and K. Cho, *Appl. Phys. Lett.*, 2007, **91**, 112111-112111.

217. C. Cabanetos, A. El Labban, J. A. Bartelt, J. D. Douglas, W. R. Mateker, J. M. Fréchet, M. D. McGehee and P. M. Beaujuge, *J. Am. Chem. Soc.*, 2013, **135**, 4656-4659.

218. J. C. Love, L. A. Estroff, J. K. Kriebel, R. G. Nuzzo and G. M. Whitesides, *Chem. Rev.,* 2005*,* **105**, 1103-1170.

219. N. S. Sariciftci, L. Smilowitz, A. J. Heeger and F. Wudl, *Science,* 1992, **258**, 1474-1476.

220. S. K. Hau, Y. J. Cheng, H. L. Yip, Y. Zhang, H. Ma and A. K. Y. Jen, *ACS Appl. Mater. Interfaces*, 2010, **2**, 1892-1902.

221. T. Stubhan, M. Salinas, A. Ebel, F. C. Krebs, A. Hirsch, M. Halik and C. J. Brabec, *Adv. Energy Mater.*, 2012, **2**, 532-535.

222. C. Duan, C. Zhong, C. Liu, F. Huang and Y. Cao, *Chemistry of Materials*, 2012, **24**, 1682-1689.

223. K. M. O'Malley, C. Z. Li, H. L. Yip and A. K. Y. Jen, *Adv. Energy Mater.*, 2012, **2**, 82-86.

224. K. M. ÁO'Malley, *J. Mater. Chem.*, 2012, **22**, 8574-8578.

225. Z. G. Zhang, H. Li, B. Qi, D. Chi, Z. Jin, Z. Qi, J. Hou, Y. Li and J. Wang, *J. Mater. Chem. A*, 2013, **1**, 9624-9629.

226. C. Yi, K. Yue, W. B. Zhang, X. Lu, J. Hou, Y. Li, L. Huang, G. R. Newkome, S. ZD. Cheng and X. Gong, *ACS Appl. Mater. Interfaces*, 2014, **6**, 14189-14195.

227. C. Chen, H. He, Y. Lu, K. Wu and Z. Ye, *ACS Appl. Mater. Interfaces,* 2013, **5**, 6354-6359.

228. H. L. Yip, S. K. Hau, N. S. Baek and A. K.-Y. Jen, *Appl. Phys. Lett.*, 2008, **92**, 193313-193313.

229. C. Goh, S. R. Scully and M. D. McGehee, *J. Appl. Phys.*, 2007, **101**, 114503-114503.

230. J. Yu, M. Guan, F. Li, Z. Zhang, C. Wang, C. Shu, H. Wei and X.-E. Zhang, *Chem. Commun.*, 2012, **48**, 11011-11013.

231. J. Moser, S. Punchihewa, P. P. Infelta and M. Grätzel, *Langmuir,* 1991, **7**, 3012-3018.

232. C. C. Chueh, C. Z. Li and A. K. Y. Jen, *Energy Environ. Sci.*, 2015, **8**, 1160-1189.

233. G. Ramakrishna, H. N. Ghosh, A. K. Singh, D. K. Palit and J. P. Mittal, *J. Phys. Chem. B,* 2001, **105**, 12786-12796.

234. E. L. Tae, S. H. Lee, J. K. Lee, S. S. Yoo, E. J. Kang and K. B. Yoon, *J. Phys. Chem. B*, 2005,**109**, 22513-22522.

235. P. Kar, S. Verma, A. Das and H. N. Ghosh, *J. Phys. Chem. C,* 2009, **113**, 7970-7977.

236. P. Persson, R. Bergstrom and S. Lunell, *J. Phys. Chem. B,* 2000, **114**, 10348-10351.

237. R. Ernstorfer, L. Gundlach, S. Felber, W. Storck, R. Eichberger and F. Willig, *J. Phys. Chem. B,* 2006, **110**, 25383-25391.

238. J. Li, M. Nilsing, I. Kondov, H. Wang, P. Persson, S. Lunell and M. Thoss, *J. Phys. Chem. C,* 2008, **112**, 12326-12333.

239. Y. Shi, L. Tan, L. Chen and Y. Chen, *Phys. Chem. Chem. Phys.*, 2015, **17**, 3637-3646.

240. Y. E. Ha, M. Y. Jo, J. Park, Y. C. Kang, S. I. Yoo and J. H. Kim, *J. Phys. Chem. C*, 2013, **117**, 2646-2652.

241. C. H. Hsieh, Y. J. Cheng, P. J. Li, C. H. Chen, M. Dubosc, R. M. Liang and C. S. Hsu, *J. Am. Chem. Soc.*, 2010, **132**, 4887-4893.

242. Y.-J. Cheng, M. S. Liu, Y. Zhang, Y. Niu, F. Huang, J.-W. Ka, H.-L. Yip, Y. Tian and A. K.-Y. Jen, *Chem. Mater.,* 2008, **20**, 413-422.

243. F. Huang, Y.-J. Cheng, Y. Zhang, M. S. Liu and A. K.-Y. Jen, *J. Mater. Chem.,* 2008, **18**, 4495-4509.

244. W. J. E. Beek, M. M. Wienk, R and A. J. Janssen, *Adv. Funct. Mater.,* 2006, **16**, 1112-1116.

245. P. A. Van Hal, M. P. T. Christiaans, M. M. Wienk, J. M. Kroon and R. A. J. Janssen, *J. Phys. Chem. B,* 1999, **103**, 4352-4359.

246. Y.-H. Niu, M. S. Liu, J. W. Ka and A. K.-Y. Jen, *Appl. Phys. Lett.,* 2006, **88**, 093505-093505.

247. Y. J. Cheng, C. H. Hsieh, Y. He, C. S. Hsu and Y. Li, *J. Am. Chem. Soc.,* 2010, **132**, 17381-17383.

248. R. Steim, S. A. Choulis, P. Schilinsky, U. Lemmer and C. Brabec, *J. Appl. Phys. Lett.,* 2009, **94**, 043304-043304.

249. J. Jean, P. R. Brown, R. L. Jaffe, T. Buonassisi and V. Bulović, *Energy Environ. Sci.,* 2015, **8**, 1200-1219.

250. W. He and C. Ye, *Journal of Materials Science & Technology*, 2015, **31**, 581-588.

251. T. Sagawa, S. Yoshikawa and H. Imahori, *J. Phys. Chem. Lett.,* 2010, **1**, 1020-1025.

252. C. Y. Kuo, W. C. Tang, C. Gau, T. F. Guo and D. Z. Jeng, *Appl. Phys. Lett.,* 2008, **93**, 033307-033307.

253. H. H. Wang, C. Y. Liu, S. B. Wu, N. W. Liu, C. Y. Peng, T. H. Chan, C. F. Hsu, J. K. Wang and Y. L. Wang, *Adv. Mater.,* 2006, **18**, 491-495.

254. N. W. Liu, C. Y. Liu, H. H. Wang, C. F. Hsu, M. Y. Lai, T. H. Chuang and Y. L. Wang, *Adv. Mater.,* 2008, **20**, 2547-2551.

255. K. T. Tsai, Y. R. Huang, M. Y. Lai, C. Y. Liu, H. H. Wang, J. H. He and Y. L. Wang, *J. Nanosci. Nanotechnol.*, 2010, **10**, 8293-8297.

256. C.-Y. Chang, C.-E. Wu, S.-Y. Chen, C. Cui, Y.-J. Cheng, C.-S. Hsu, Y.-L. Wang and Y. Li, *Angew. Chem. Int. Ed.*, 2011, **50**, 9386-9390.

257. Y. J. Cheng, F. Y. Cao, W. C. Lin, C. H. Chen and C. H. Hsieh, *Chem. Mater.*, 2011, **23**, 1512-1518.

258. F. S. Kim, G. Ren and S. A. Jenekhe, *Chem. Mater.*, 2010, **23**, 682-732.

259. A. Santos, P. Formentín, J. Pallarés, J. Ferré-Borrull and L. F. Marsal, *Sol. Energy Mater. Sol. Cells*, 2010, **94**, 1247-1253.

260. Y. C. Lin, B. Y. Yu, W. C. Lin, S. H. Lee, C. H. Kuo and J. J. Shyue, *J. Colloid Interface Sci.*, 2009, **340**, 126-130.

261. D. C. Müller, A. Falcou, N. Reckefuss, M. Rojahn, V. Wiederhirn, P. Rudati, H. Frohne, O. Nuyken, H. Becker and K. Meerholz, *Nature,* 2003, **421**, 829-833.

262. E. Bacher, M. Bayerl, P. Rudati, N. Reckefuss, C. D. Müller, K. Meerholz and O. Nuyken, *Macromolecules,* 2005, **38**, 1640-1647.

263. M. C. Gather, A. Koehnen, A. Falcou, H. Becker and K. Meerholz, *Adv. Funct. Mater.*, 2007, **17**, 191-200.

264. P. Zacharias, M. C. Gather, M. Rojahn, O. Nuyken and K. Meerholz, *Angew. Chem., Int. Ed.,* 2007, **46**, 4388-4392.

265. P. M. Beaujuge and J. M. Fréchet, *J. Am. Chem. Soc.*, 2011, **133**, 20009-20029.

266. A. Köhnen, N. Riegel, J. H. W. Kremer, H. Lademann, D. C. Müller and K. Meerholz, *Adv. Mater.*, 2009, **21**, 879-884.

267. H. Yan, B. J. Scott, Q. Huang and T. J. Marks, *Adv. Mater.*, 2004, **16**, 1948-1953.

268. M. Shtein, J. Mapel, J. B. Benziger and S. R. Forrest, *Appl. Phys. Lett.,* 2002, **81**, 268-270.

269. R. O. P. Ortiz, A. Facchetti and T. J. Marks, *Chem. Rev*., 2009, **110**, 205-239.

270. Q. Huang, G. A. Evmenenko, P. Dutta, P. Lee, N. R. Armstrong and T. J. Marks, *J. Am. Chem. Soc.,* 2005, **127**, 10227-10242.

271. C. Kim, Z. Wang, H.-J. Choi, Y.-G. Ha, A. Facchetti and T. J. Marks, *J. Am. Chem. Soc*., 2008, **130**, 6867-6878.

272. R. T. Weitz, U. Zschieschang, F. Effenberger, H. Klauk, M. Burghard and K. Kern, *Nano Lett*., 2006, **7**, 22-27.

273. V. N. Novikov and A. P. Sokolov, *Nature,* 2004, **431**, 961-963.

274. W. W. Liang, C. Y. Chang, Y. Y. Lai, S. W. Cheng, H. H. Chang, Y. Y. Lai, Y. J. Cheng, C. L. Wang and C. S. Hsu, *Macromolecules,* 2013, **46**, 4781-4789.

275. Y. Y. Lai, Y. J. Cheng and C. S. Hsu, *Energy & Environmental Science*, 2014, **7**, 1866-1883.

276. Z. C. He, C. M. Zhong, S. J. Su, M. Xu, H. B. Wu and Y. Cao, *Nat. Photon*., 2012, **6**, 591-595.

277. L. Wang, B. Liang, F. Huang, J. Peng and Y. Cao, *Appl. Phys. Lett.,* 2006, **89**, 151115-151115.

278. S. Fabiano, S. Himmelberger, M. Drees, Z. Chen, R. M. Altamimi, A. Salleo, M. A. Loi and A. Facchetti, *Adv. Energy Mater.,* 2014, **4**, 1301409-1-7.

279. A. Hayakawa, O. Yoshikawa, T. Fujieda, K. Uehara and S. Yoshikawa, *Appl. Phys. Lett.,* 2007, **90**, 163517-163900..

280. S. I. Na, T. S. Kim, S. H. Oh, J. Kim, S. S. Kim and D. Y. Kim, *Appl. Phys. Lett.*, 2010, **97**, 223305.

281. S.-H. Oh, S.-I. Na, J. Jo, B. Lim, D. Vak and D.-Y. Kim, *Adv. Funct. Mater.*, 2010, **20**, 1977-1983.

282. H. Ma, H.-L. Yip, F. Huang and A. K.-Y. Jen, *Adv. Funct. Mater.*, 2010, **20**, 1371-1388.

283. J. Kötz, S. Kosmella and T. Beitz, *Prog. Polym. Sci.*, 2001, **26**, 1199-1232.

284. W. Shi, X. Jiang, W. Zen, F. Huang, W. Yang, R. Liu and Y. Cao, *Macromol. Chem. Phys.*, 2009, **210**, 150-160.

285. X. Xu, Y. Zhu, L. Zhang, J. Sun, J. Huang, J. Chen and Y. Cao, *J. Mater. Chem.*, 2012, **22**, 4329-4336.

286. X. Xu, B. Han, J. Chen, J. Peng, H. Wu and Y. Cao, *Macromolecules,* 2011, **44**, 4204-4212.

287. Y. Zhu, X. Xu, L. Zhang, J. Chen and Y. Cao, *Sol. Energ. Mat. Sol.,* 2012, **97**, 83-88.

288. N. Blouin, A. Michaud and M. Leclerc, *Adv. Mater.,* 2007, **19**, 2295-2300.

289. J. Sun, Y. Zhu, X. Xu, L. Lan, L. Zhang, P. Cai, J. Chen, J. Peng and Y. Cao, *J. Phys. Chem. C,* 2012, **116**, 14188-14198.

290. X. Xu, W. Cai, J. Chen and Y. Cao, *J. Polym. Sci. A Polym. Chem.,* 2011, **49**, 1263 -1272.

291. K. Yao, L. Chen, Y. Chen,F. Li and P. Wang, *J. Mater. Chem.,* 2011, **21**, 13780-13784.

292. C. Xie, L. Chen and Y. Chen, *J. Phys. Chem. C.,* 2013, **117**, 24804-24814.

293. J. H. Seo, A. Gutacker, Y. Sun, H. Wu, F. Huang, Y. Cao, U. Scherf, A. J. Heeger and G. C. Bazan, *J. Am. Chem. Soc.*, 2011, **133**, 8416-8419.

294. J. Kesters, T. Ghoos, H. Penxten, J. Drijkoningen, T. Vangerven, D. M. Lyons, B. Verreet, T. Aernouts, L. Lutsen, D. Vanderzande, J. Manca and W. Maes, *Adv. Energy Mater.,* 2013, **3**, 1180-1185.

295. K. Zilberberga, A. Behrendt, M. Kraft, U. Scherf and T. Riedl, *Org. Electron.*, 2013, **14**, 951-957.

296. C. S. Kim, S. S. Lee, E. D. Gomez, J. B. Kim and Y.-L. Loo, *Appl. Phys. Lett.,* 2009, **94**, 113302-113302.

297. S. Sista, M.-H. Park, Z. Hong, Y. Wu, J. Hou, W. L. Kwan, G. Li and Y. Yang. *Adv. Mater.,* 2010, **22**, 380-383.

298. J. Kim, G. Kim, Y. Choi, J. Lee, S. H. Park and K. Lee, *J. Appl. Phys.,* 2012, **111**, 114511-114511.

299. B. J. Worfolk, T. C. Hauger, K. D. Harris, D. A. Rider, J. A. M. Fordyce, S. Beaupré, M. Leclerc and J. M. Buriak, *Adv. Energy Mater.,* 2012, **2**, 361-368.

300. M. Carrara, J. J. Kakkassery, J.-P. Abid and D. J. Fermín, *Chem. Phys. Chem.,* 2004, **5**, 571-575.

301. N. Blouin, A. Michaud, D. Gendron, S. Wakim, E. Blair, R. Neagu-Plesu, M. Belletête, G. Durocher, Y. Tao and M. Leclerc, *J. Am. Chem. Soc.,* 2008, **130**, 732-742.

302. C. H. Peters, I. T. Sachs-Quitana, J. P. Kastrop, S. Beaupré, M. Leclerc and M. D. McGehee, *Adv. Energy Mater.,* 2011, **1**, 491-494.

303. Y. Sun, J. H. Seo, C. J. Takacs, J. Seifter and A. J. Heeger, *Adv. Mater.,* 2011, **23**, 1679-1683.

304. S. Cho, J. H. Seo, S. H. Park, S. Beaupré, M. Leclerc and A. J. Heeger, *Adv. Mater*., 2010, **22**, 1253-1257.

305. Y. Sun, C. J. Takacs, S. R. Cowan, J. H. Seo, X. Gong, A. Roy and A. J. Heeger, *Adv. Mater.,* 2011, **23**, 2226-2230.

306. H. Wu, F. Huang, Y. Mo, W. Yang, D. Wang, J. Peng and Y. Cao, *Adv. Mater.,* 2004, **16**, 1826-1830.

307. F. Huang, H. Wu, D. Wang, W. Yang and Cao, Y. *Chem. Mater.,* 2004, **16**, 708-716.

308. X. Hu, Y. Dong, F. Huang, X. Gong and Y. Cao, *J. Phys. Chem. C.,* 2013, **117**, 6537-6543.

309. R. Xia, D.-S. Leem, T. Kirchartz, S. Spencer, C. Murphy, Z. He, H. Wu, S. Su, Y. Cao, J. S. Kim, J. C. DeMello, D. D. C. Bradly and J. Nelson, *Adv. Energy Mater.*, 2013, **3**, 718-723.

310. S. Liu, K. Zhang, J. Lu, J. Zhang, H.-L. Yip, F. Huang and Y. Cao, *J. Am. Chem. Soc.,* 2013, **135**, 15326-15329.

311. Y. Liang, Z. Xu, J. Xia, S.-T. Tsai, Y. Wu, G. Li, C. Ray and L. Yu, *Adv. Mater.,* 2010, **22**, E135-E138.

312. H. Wu, F. Huang, J. Peng and Y. Cao, *Org. Electron.,* 2005, **6**, 118-128.

313. H. Ishii, K. Sugiyama, E. Ito and K. Seki, *Adv. Mater.,* 1999, **11**, 605-625.

314. W. Y. Wong, K. H. Choi, G. L. Lu and Z. Y. Lin, *Organometallics,* 2002, **21**, 4475-4481.

315. T. Yang, M. Wang, C. Duan, X. Hu, L. Huang, J. Peng, F. Huang and X. Gong, *Energy Environ. Sci.,* 2012, **5**, 8208-8214.

316. M. C. Scharber, D. Mühlbacher, M. Koppe, P. Denk, C. Waldauf, A. J. Heeger and C. J. Brabec, *Adv. Mater.,* 2006, **18**, 789-794.

317. Y.-M. Chang and C.-Y. Leu, *J. Mater. Chem. A,* 2013, **1**, 6446-6451.

318. H. Choi, J. S. Park, E. Jeong, G.-H. Kim, B. R. Lee, S. O. Kim, M. H. Song, H. Y. Wo and J. Y. Kim, *Adv. Mater.,* 2011, **23**, 2759-2763.

319. X. Hu, C. Yi, M. Wang, C.-H. Hsu, S. Liu, K. Zhang, C. Zhong, F. Huang, X. Gong and Y. Cao, *Adv. Energy Mater.,* 2014, **4**, 1400378-1400378.

320. Y. Wang and A. Suna, *J. Phys. Chem. B*, 1997, **101**, 5627-5638.

321. C. Xie, L. Chen and Y. Chen, *J. Phys. Chem. C,* 2013, **117**, 24804-24814.

322. G. Yu, J. Ga and J. C. Hummelen, *Science-AAAS-Weekly Paper Edition,* 1995, **270**, 1789-1790.

323. G. Yu and A. J. Heeger, *J. Appl. Phys.,* 1995, **78**, 4510-4515.

324. F. Padinger, R. S. Rittberger and N. S. Sariciftci, *Adv. Funct. Mater.,* 2003, **13**, 85-88.

325. L. Bao, Y. Yao, A. Kumar, Y. Yang and V. Ozolins, *J. Appl. Phys.,* 2008, **104**, 024504-024504.

326. P. K. Watkins, A. B. Walker and G. L. Verschoor, *Nano letters,* 2005, **5**, 1814-1818.

327. S. Goffri, C. Müller, N. Stingelin-Stutzmann, D. W. Breiby, C. P. Radano, J. W. Andreasen, R. Thompson, R. A. J. Janssen, M. M. Nielsen, P. Smith and H. Sirringhaus, *Nat. Mater.,* 2006, **5**, 950-956.

328. C. M. Björström, A. Bernasik, J. Rysz, A. Budkowski, S. Nilsson, M. Svensson, M. R. Andersson, K. O. Magnusson and E. Moons, *J. Phys. Condens. Matter,* 2005, **17**, L529-L534.

329. R. A. Jones, L. J. Norton, E. J. Kramer, F. S. Bates and P. Wiltzius, *Phys. Rev. Lett.,* 1991, **66**, 1326-1329.

330. A. M. Higgins, S. J. Martin, R. L. Thompson, J. Chappell, M. Voigt, D. G. Lidzey, R. AL Jones and M. Geoghegan, *J. Phys.: Condens. Matter.,* 2005, **17**, 1319-1328.

331. M. Reyes-Reyes, K. Kim, J. Dewald, R. López-Sandoval, A. Avadhanula, S. Curran and D. L. Carroll, *Org. Lett.,* 2005, **7** , 5749-5752.

332. C. Waldauf, M. Morana, P. Denk, P. Schilinsky, K. Coakley, S. A. Choulis and C. J. Brabec, *Appl. Phys. Lett.,* 2006, **89**, 233517-233517.

333. M. Campoy-Quiles, T. Ferenczi, T. Agostinelli, P. G. Etchegoin, Y. Kim, T. D. Anthopoulos, P. N. Stavrinou, D. D. C. Bradley and J. Nelson, *Nat. Mater.,* 2008, **7**, 158-164.

334. Z. Xu, L. M. Chen, G. Yang, C. H. Huang, J. Hou, Y. Wu, G. Li, C. S. Hsu and Y. Yang, *Adv. Funct. Mater.,* 2009, **19**, 1227-1234.

335. A. Kumar, G. Li, Z. Hong and Y. Yang, *Nanotechnology,* 2009, **20**, 165202-165202.

336.   K. Ohno and Y. Kawazoe, *Scr. Mater.,* 2001, **44**, 1579-1582.

337.   A. Orimo, K. Masuda, S. Honda, H. Benten, S. Ito, H. Ohkita and H. Tsuji, *Appl. Phys. Lett.,* 2010*,* **96***,* 043305-043305.

338.   W. Ma, C. Yang, X. Gong, K. Lee and A. J. Heeger, *Adv. Funct. Mater.,* 2006, **15**, 1617-1622.

339.   R. Kang, S. H. Oh, S. Na, T. S. Kim and D. Y. Kim, *Sol. Energ. Mat. Sol. Cells,* 2014, **120**, 131-135.

340.   J. S. Moon, C. J. Takacs, S. R. Cho, C. Coffin, H. Kim and G. C. Bazan, *Nano Lett.,* 2010**, 10**, 4005-4008.

341.   Y. Yao, J. Hou, Z. Xu, G. Li and Y. Yang, *Adv. Funct. Mater.,* 2008, **18**, 1783-1789.

342.   J. T. Rogers, K. Schmidt, M. F. Toney, E. J. Kramer and G. C. Bazan, *Adv. Mater.,* 2011, **23***,* 2284-2288.

343.   R. Lin, M. Wright and A. Uddin, *Phys. Status Solidi A,* 2013**, 210***,* 1785-1790.

344.   J. Peet, J. Y. Kim, N. E. Coates, W. L. Ma, D. Moses, A. J. Heeger and G. C. Bazan, *Nat. Mater.,* 2007, **6***,* 497-500.

345.   H. Y. Chen, S. H. Lin, J. Y. Sun, C. H. Hsu, S. Lan and C. F. Lin, *Nanotechnology,* 2013, **24***,* 484009-484009.

346.   C. Yi, X. Hu, H. C. Liu, R. Hu, C.-H. Hsu, J. Zheng and X. Gong, *J. Mater. Chem. C*, 2014, **3**, 26-32.

347.   C. Liu, X. Hu, C. Zhong, M. Huang, K. Wang, Z. Zhang, X. Gong, Y. Cao and A. J. Heeger, *Nanoscale*, 2014, **6**, 14297-14304.

348.   G. D. Sharma, V. S. Choudhary and M. S. Roy, *Sol. Energy Mater. Sol. Cells,* 2007, **91**, 275-284.

349. Y. Li, Y. Hou, Y. Wang, Z. Feng, B. Feng, L. Qin and F. Teng, *Synt. Met.,* 2008**, 158***,* 190-193.

350. K. Pandey, J.-M. Nunzi, H. Wang, C. C. Oey, A. B. Djurišić, M. H. Xie, Y. H. Leung, K. K. Y. Man and W. K. Chan, *Org. Electron.,* 2007, **8**, 396-400.

351. S. Y. Ma, Y. M. Shen, P. C. Yang, C. S. Chen and C. F. Lin, *Org. Electron.,* 2012, **13**, 297-301.

352. K. Wang, C. Yi, C. Liu, X. Hu, S. Chuang and X. Gong, *Sci. Rep.,* 2015, **5**, 9265-1-9.

353. K. Wang, C. Yi, X. Hu, C. Liu, Y. Sun, J. Hou, Y. Li, J. Zheng, S. Chuang, A. Karim and X. Gong, *ACS Appl. Mater. Interfaces,* 2014, **6**, 13201-13208.

354. V. D. Mihailetchi, P. W. M. Blom, J. C. Hummelen and M. T. Rispens*, J. Appl. Phys*., 2003, **94**, 6849-6854.

355. K.-C. Liao, C. M. Bowers, H. J. Yoon and G. M. Whitesides, *J. Am. Chem. Soc.,* 2015, **137**, 3852-3858.

356. S. K. Hau, K. M. O'Malley, Y.-J. Cheng, H.-L. Yip, H. Ma and A. K.-Y. Jen, *IEEE J. Sel. Top. Quant. Electron.,* 2010, **16**, 1665-1675.

357. C. J. Brabec, A. Cravino, D. Meissner, N. S. Sariciftci, T. Fromherz, M. T. Rispens, L. Sanchez and J. C. Hummelen, *Adv. Funct. Mater.,* 2001, **11** ,374-380.

358. H. Guo, N. Lin, Y. Chen, Z. Wang, Q. Xie, T. Zheng, N. Gao, S. Li, J. Kang, D. Cai and D.-L. Peng, *Sci. Rep.,* 2013, **3**, 2323-1-8.

359. H.-G. Im, J. Jin, J.-H. Ko, J. Lee, J.-Y. Lee and B.-S. Bae, *Nanoscale,* 2014**, 6**, 711-715.

360. S. Jung, S. Lee, M. Song, D.-G. Kim, D. S. You, J.-K. Kim, C. S. Kim, T.-M. Kim, K.-H. Kim, J.-J. Kim and J.-W. Kang, *Adv. Energy Mater.,* 2014, **4**, 1300474-1-8.

361. J.-Y. Lee, S. T. Connor, Y. Cui and P. Peumans, *Nano Lett.,* 2008, **8**, 689-692.

362. T. Tokuno, M. Nogi, J. Jiu and K. Suganuma, *Nanoscale Res. Lett.,* 2012, **7**, 1-7.

363. C.-H. Liu and X. Yu, *Nanoscale Res. Lett.*, 2011, **6**, 75-1-8.

364. D.-S. Leem, A. Edwards, M. Faist, J. Nelson, D. D. C. Bradley and J. C. De Mello, *Adv. Mater.,* 2011, **23***, 4371-4375.

365. M. Reinhard, R. Eckstein, A. Slobodskyy, U. Lemmer and A. Colsmann, *Org. Electron.,* 2013, **14**, 273-277.

366. T. M. Barnes, J. D. Bergeson, R. C. Tenent, B. A. Larsen, G. Teeter, K. M. Jones, J. L. Blackburn and J. V. D.Lagemaat, *Appl. Phys. Lett.,* 2010, **96**, 243309-243309.

367. J. Wu, H. A. Becerril, Z. Bao, Z. Liu, Y. Chen and P. Peumans, *Appl. Phys. Lett.,* 2008, **92**, 263302-263302.

368. H. Do, M. Reinhard, H. Vogeler, A. Puetz, M. F. G. Klein, W. Schabel, A. Colsmann and U. Lemmer, *Thin Solid Films*, 2009, **517**, 5900-5902.

369. A. Colsmann, M. Reinhard, T.-H. Kwon, C. Kayser, F. Nickel, J. Czolk, U. Lemmer, N. Clark, J. Jasieniak, A. B. Holmes and D. Jones, *Sol. Energy Mater. Sol. Cells,* 2012, **98**, 118-123.

370. Y. Xia, K. Sun and J. Ouyang, *Adv. Mater*., 2012, **24**, 2436-2440.

371. H. Do, M. Reinhard, H. Vogeler, A. Puetz, M. F. G. Klein, W. Schabel, A. Colsmann and U. Lemmer, *Thin Solid Films,* 2009, **517**, 5900-5902.

372. H. H. Klein, J. Steinberger and W. Knake, *PACE,* 1990, **13**, 134-137.

373. Y. Shi, L. J. Pan, B. Liu, Y. Wang, Y. Cui, Z. Bao and G. Yu, *J. Mater. Chem. A,* 2014, **2**, 6086-6091.

374. S.-B. Kang and H.-K. Kim, *Thin Solid Films,* 2014, **559**, 31-35.

375. S. Günes, H. Neugebauer and N. S. Sariciftci, *Chem. Rev*., 2007, **107**, 1324-1338.

376. M. Jorgensen, K. Normann and F. C. Krebs, *Sol. Energy Mater. Sol. Cells.,* 2008, **92**, 686-714.

377. W. Gaynor, G. F. Burkhard, M. D. McGehee and P. Peumans, *Adv. Mater.,* 2011, **23**, 2905-2910.

378. S. Coskun, E. S. Ates and H. E. Unalan, *Nanotechnology,* 2013, **24**, 125202-125202.

379. L. Li, Z. Yu, W. Hu, C.-H. Chang, Q. Chen and Q. Pei, *Adv. Mater.,* 2011, **23**, 5563-5567.

380. C.-C. Chen, L. Dou, R. Zhu, C.-H. Chung, T.-B. Song, Y. B. Zheng, S. G. Hawks, P. S. Weiss, G. Li and Y. Yang, *ACS Nano*, 2012, **6**, 7185-7190.

381. R. Zhu, C.-H. Chung, K. C. Cha, W. Yang, Y. B. Zheng, H. Zhou, T.-B. Song, C.-C. Chen, P. S. Weiss, G. Li and Y. Yang, *ACS Nano,* 2011, **5**, 9877-9882.

382. L. T. Dou, J. B. You, J. Yang, C. C. Chen, Y. J. He, S. Murase, T. Moriarty, K. Emery, G. Li and Y. Yang, *Nat. Photonics*, 2012, **6**, 180-185.

383. Y. Zhou, F. Li, S. Barrau, W. Tian, O. Inganäs and F. Zhang, *Sol. Energ. Mat. Sol.,* 2009, **93**, 497-500.

384. S. K. Hau, H.-L. Yip, J. Zou and A. K.-Y. Jen, *Org. Electron.,* 2009, **10**, 1401-1407.

385. J. Ouyang, Q. Xua, C.-W. Chua, Y. Yang, G. Li and J. Shinar, *Polymer,* 2004, **45**, 8443-8450.

386. Y. Zhou, H. Cheun, S. Choi, C. Fuentes-Hernandez and B. Kippelen, *Org. Electron.,* 2011, **12**, 827-831.

387. Q. Dong, Y. Zhou, J. Pei, Z. Liu, Y. Li, S. Yao, J. Zhang and W. Tian, *Org. Electron.,* 2010, **11**, 1327-1331.

388. Y. Zhou, H. Cheun, S. Choi, Jr. W. J. Potscavage, C. F. Hernandez and B. Kippelen, *Appl. Phys. Lett.,* 2010, **97**, 153304-153304.

389. D. Gupta, M. M. Wienk and R. A. J. Janssen, *Adv. Energy Mater.,* 2013, **3**, 782-787.

390. A. Cheknane, *Prog. Photovolt: Res. Appl.,* 2011, **19**, 155-159.

391. Y. Galagan, B. Zimmermann, E. W. C. Coenen, M. Jørgensen, D. M. Tanenbaum, F. C. Krebs, H. Gorter, S. Sabik, L. H. Slooff, S. C. Veenstra, J. M. Kroon and R. Andriessen, *Adv. Energy Mater.,* 2012, **2**, 103-110.

392. H. Peng, J. Sun, X. Zhu, X. Yu, M. Wong and H.-S. Kwok*, Appl. Phys. Lett.,* 2006, **88**, 073517-073517.

393. A. Colsmann; J. Junge, C. Kyser and U. Lemmer, *Appl. Phys. Lett.,* 2006, **89**, 203506-203506.

394. C. Tao, G. Xie, C. Liu, X. Zhang, W. Dong, F. Meng, X. Kong, L. Shen and S. Ruan, W. Chen, *Appl. Phys. Lett.,* 2009, **95**, 053303-053303.

395. L. S. Hung, C. W. Tang, M. G. Mason, P. Raychaudhuri and J. Madathil, *Appl. Phys. Lett.,* 2001, **78**, 544-546.

396. L. Boudaoud, N. Benramdane, R. Desfeux, B. Khelifa and C. Mathieu, *Catal. Today,* 2006, **113**, 230-234.

397. V. Shrotriya, G. Li, Y. Yao, C.-W. Chu and Y. Yang, *Appl. Phys. Lett.,* 2006, **88**, 073508-073508.

398. T. Matsushima, Y. Kinoshita and H. Murata, *Appl. Phys. Lett.,* 2007, **91**, 253504-253504.

399. N.-K. Persson, H. Arwin and O. Inganäs, *J. Appl. Phys.,* 2005, **97**, 034503-034503.

400. L. A. A. Pettersson, L. S. Roman and O. Inganäs, *J. Appl. Phys.,* 1999, **86**, 487-496.

401. C. Tao, G. Xie, F. Meng, S. Ruan and W. Chen, *J. Phys. Chem. C,* 2011, **115**, 12611-12615.

402. H. Jin, C. Tao, M. Velusamy, M. Aljada, Y. Zhang, M. Hambsch, P. L. Burn and P. Meredith, *Adv. Mater.,* 2012, **24**, 2572-2577.

403. D. Han, S. Lee, H. Kim, S. Jeong and S. Yoo, *Org. Electron.,* 2013, **14**, 1477-1482.

404. H. W. Choi, N. D. Theodore and T. L. Alford, *Sol. Energ. Mat. Sol.,* 2013, **117**, 446-450.

405. G. H. Jung, K. Hong, W. J. Dong, S. Kim and J.-L. Lee, *Adv. Energy Mater.*, 2011, **1**, 1023-1028.

406. S. K. Hau, H. L. Yip, N. S. Baek, J. Zhou, K. O'Malley and A. K. Y. Jen, *Appl. Phys. Lett.,* 2008, **92**, 253301-253301.

407. M. Jorgensen, K. Norrman and F. C. Krebs, *Sol. Energy Mater. Sol. Cells,* 2008, **92**, 686-714.

408. M. Jørgensen, K. Norrman, S. A. Gevorgyan, T. Tromholt, B. Andreasen and F. C. Krebs, *Adv. Mater.,* 2012, **24**, 580-612.

409. D. Zhao, D. A. Mourey and T. N. Jackson, *IEEE Electron Device Lett.,* 2010, **31**, 323-325.

410. K. Kawano, R. Pacios, D. Poplavskyy, J. Nelson, D. D. Bradley and J. R. Durrant, *Sol. Energy Mater. Sol. Cells,* 2006, **90**, 3520-3530.

411. K. Kawano, N. Ito, T. Nishimori and J. Sakai, *App. Phys. Lett.,* 2007, **88**, 073514-073514.

412. K. Kawano and C. Adachi, *Adv. Funct. Mater.,* 2009, **19**, 3934-3940.

413. E. Voroshazi, B. Verreet, A. Buri, R. Müller, D. Di Nuzzo and P. Heremans, *Org. Electron.,* 2011, **12**, 736-744.

414. E. Voroshazi, B. Verreet, T. Aernouts and P. Heremans, *Sol. Energy Mater. Sol. Cells,* 2011, **95**, 1303-1307.

415. N. Li, T. Stubhan, N. A. Luechinger, S. C. Halim, G. J. Matt, T. Ameri and C. J. Brabec, *Org. Electron.,* 2012, **13**, 2479-2484.

416. L. Chen, C. Xie and Y. Chen, *Adv. Funct. Mater.,* 2014, **24**, 3986-3995.

417. L. Motiei, Y. Yao, J. Choudhury, H. Yan, T. J. Marks, M. E. V. D. Boom and A. Facchetti, *J. Am. Chem. Soc.,* 2010, **132**, 12528-12530.

418. K. Norrman, M. V. Madsen, S. A. Gevorgyan and F. C. Krebs, *J. Am. Chem. Soc.,* 2010, **132**, 16883-16892.

419. T. Salim, H.−W. Lee, L. H. Wong, J. H. Oh, Z. Bao and Y. M. Lam, *Adv. Funct. Mater.,* 2016, **26**, 51-65.

420. A. Jeziorny, *Polymer,* 1978, **19**, 1142-1144.

421.   J. U. Lee, J. W. Jung, T. Emrick, T. P. Russell and W. H. Jo, *J. Mater. Chem.* 2010, **20**, 3287-3294.

422. Z. Sun, K. Xiao, J. K. Keum, X. Yu, K. Hong, J. Browning, I. N. Ivanov, J. Chen , J. Alonzo, D. Li, B. G. Sumpter, E. A. Payzant, C. M. Rouleau and D. B. Geohegan, *Adv. Mater.*, 2011, **23**, 5529-5535.

423. S. Bertho, B. Campo, F. Piersimoni, D. Spoltore, J. D'Haen, L. Lutsen, W. Maes, D. Vanderzande and J. Manca, *Sol. Energy Mater. Sol. Cells,* 2013, **110**, 69-76.

424. C. Yang, J. K. Lee, A. J. Heeger and F. Wudl, *J. Mater. Chem.* 2009, **19**, 5416-5423.

425. J. U. Lee, J. W. Jung, T. Emrick, T. P. Russell and W. H. Jo, *Nanotechnology* 2010, **21**, 105201-105201.

426. B. J. Kim, Y. Miyamoto, B. Ma and J. M. J. Fréchet, Adv. Funct. Mater. 2009, **19**, 2273-2281.

427. M. Drees, H. Hoppe, C. Winder, H. Neugebauer, N. S. Sariciftci, W. Schwinger, F. Schaffler, C. Topf, M. C. Scharber, Z. Zhu and R. Gaudiana, *J. Mater. Chem.,* 2005, **15**, 5158-5163

428. Y.-J. Cheng C.-H. Hsieh, P.-J. Li and C.-S. Hsu, *Adv. Funct. Mater.*, 2011, **21**, 1723-1732.

429. H. J. Kim, A. R. Han, C.-H. Cho, H. Kang, H.-H. Cho, M. Y. Lee, J. M. J. Fréchet, J. H. Oh and B. J. Kim, *Chem. Mater.*, 2011, **24**, 215-221.

430. S. Khiev, L. Derue, G. Ayenew, H. Medlej, R. Brown, L. Rubatat, R. C. Hiorns, G. Wantz and C. Dagron-Lartigau, *Polym. Chem.*, 2013, **4**, 4145-4150.

431. S.-O. Kim, D. Sung Chung, H. Cha, J. Wan Jang, Y.-H. Kim, J.-W. Kang, Y.-S. Jeong, C. E. Park and S.-K. Kwon, *Sol. Energy Mater. Sol. Cells,* 2011, **95**, 432-439.

432. H.-W. Liu, D.-Y. Chang, W.-Y. Chiu, S.-P. Rwei and L. Wang, *J. Mater. Chem.,* 2012, **22**, 15586-15591.

433. C.-Y. Chen, C.-S. Tsao, Y.-C. Huang, H.-W. Liu, W.-Y. Chiu, C.-M. Chuang, U. S. Jeng, C.-J. Su, W.-R. Wu, W.-F. Su and L. Wang, Nanoscale 2013, **5**, 7629-7638.

434. C. H. Woo, B. C. Thompson, B. J. Kim, M. F. Toney and J. M. J. Fréchet, *J. Am. Chem. Soc.,* 2008, **130**, 16324-16329.

435. Z. Zhou, X. Chen and S. Holdcroft, *J. Am. Chem. Soc*., 2008, **130**, 11711-11718.

436. S. Bertho, G. Janssen, T. J. Cleij, B. Conings, W. Moons, A. Gadisa, J. D'Haen, E. Goovaerts, L. Lutsen, J. Manca and D. Vanderzande, *Sol. Energy Mater. Sol. Cells* 2008, **92**, 753-760.

437. J. Vandenbergh, B. Conings, S. Bertho, J. Kesters, D. Spoltore, S. Esiner, J. Zhao, G. Van Assche, M. M. Wienk, W. Maes, L. Lutsen, B. Van Mele, R. A. J. Janssen, J. Manca and D. J. M. Vanderzande, Macromolecules 2011, **44**, 8470-8478.

438. B. Zimmermann, U. Würfel and M. Niggemann, *Sol. Energ. Mat. Sol.,* 2009, **93**, 491-496.

439. R. Roesch, K. R. Eberhardt, S. Engmann, G. Gobsch and H. Hoppe, *Sol. Energ. Mat. Sol.,* 2013, **117**, 59-66.

440. S. Brittman, G. W. P. Adhyaksa and E. C. Garnett, *MRS Communications*, 2015, **5**, 7-26.

Table 1. The examples of the inverted OPVs with ZnO EEL.

Process methods	Device configuration	V_{OC} (V)	J_{SC} (mA/cm^2)	FF (%)	PCE (%)	Ref
Solution -process	ITO/ZnO/P3HT:PC$_{61}$BM/Ag	0.55	11.22	47.50	2.97	48
	ITO/ZnO/PSiF-DBT:PC$_{61}$BM/MoO$_3$/Au	0.90	5.03	60.00	3.80	49
	FTO/ZnO/P3HT:PC$_{61}$BM/Au	0.56	8.19	43.00	2.01	51
	FTO/ZnO/P3HT:PC$_{71}$BM/MoO$_3$/Ag	0.62	8.86	57.00	3.09	52
	ITO/ZnO NPs/P3HT:PC$_{71}$BM/PEDOT:PSS/Au	0.62	11.17	54.30	3.78	53
	ITO/ZnO/P3HT:PC$_{71}$BM/PEDOT:PSS/Au	0.62	11.53	51.70	3.68	
	ITO/ZnO/P3HT:PC$_{61}$BM/PEDOT:PSS/Ag	0.54	8.85	56.00	2.67	54
	ITO/diethylzinc-ZnO/P3HT:PC$_{61}$BM/MoO$_3$/Ag	0.57	11.26	52.50	4.03	55
ALD -process	ITO/PEN/ZnO/P3HT:PC$_{61}$BM/MoO$_3$/Ag	0.59	11.90	60.00	4.14	58
	ITO/ZnO/P3HT:PC$_{61}$BM/PEDOT:PSS/Ag	0.59	8.70	64.00	3.23	59
	ITO/ZnO/P3HT:PC$_{61}$BM/PEDOT:PSS/Au	0.59	11.14	61.80	4.10	60
	ITO/ZnO/HfO$_2$/P3HT:PC$_{61}$BM/PEDOT:PSS/Au	0.59	11.89	64.10	4.50	
	ITO/AALD ZnO/P3HT:PC$_{61}$BM/MoO$_3$/Ag	0.60	9.70	54.00	3.30	61
	ITO/ZnO/P3HT:PC$_{61}$BM/MoO$_3$/Au	0.47	12.60	51.00	3.62	62
	ITO/ZnO/PBDTTPD: PC$_{71}$BM/MoO$_3$/Ag	0.86	12.10	54.00	6.00	63

Table 2. The examples of the inverted OPVs with TiO_2 or TiO_x TMOs EEL

Device configuration	V_{OC} (V)	J_{SC} (mA/cm^2)	FF (%)	PCE (%)	Ref.
ITO/TiO_2/P3HT:PC_{61}BM/PEDOT:PSS/Ag	0.61	9.80	46.90	2.80	
ITO/TiO_2/C_{60}/P3HT:PC_{61}BM/PEDOT:PSS/Ag	0.62	10.60	57.20	3.80	
ITO/TiO_2/Terthiophene (TT)/P3HT:PC_{61}BM/PEDOT:PSS/Ag	0.60	10.00	56.20	3.40	158
ITO/TiO_2/Benzoic acid (BA)/P3HT:PC_{61}BM/PEDOT:PSS/Ag	0.60	10.50	50.20	3.20	
ITO/TiO_2/Lauric acid (LA)/P3HT:PC_{61}BM/PEDOT:PSS/Ag	0.61	9.92	49.50	3.00	
ITO/TiO_x/P3HT:PC_{61}BM/MoO_3/Ag	0.58	10.65	57.76	3.57	
ITO/TiO_x/SA-PCBO/P3HT:PC_{61}BM/MoO_3/Ag	0.60	11.14	60.73	4.06	81
ITO/TiO_x/C-PCBOD/P3HT:PC_{61}BM/MoO_3/Ag	0.61	11.25	61.26	4.50	
ITO/TiO_x/PTBT:PC_{61}BM/MoO_3/Au	0.86	6.77	56.00	3.28	
ITO/TiO_x/mono-FSAMs/PTBT:PC_{61}BM/MoO_3/Au	0.86	8.36	60.00	4.32	82
ITO/TiO_x/bis-FSAMs/PTBT:PC_{61}BM/MoO_3/Au	0.86	9.43	64.00	5.13	
ITO/TiO_x/BA-SAMs/PTBT:PC_{61}BM/MoO_3/Au	0.87	7.00	59.00	3.60	
ITO/TiO_2(nanorod)/PTB7:PC_{71}BM/MoO_3/Al	0.75	13.66	67.60	6.92	
ITO/TiO_2(nanorod):phen/PTB7:PC_{71}BM/MoO_3/Al	0.74	15.37	71.40	8.12	83
ITO/TiO_2(nanorod)/P3HT:PC_{61}BM/MoO_3/Al	0.53	10.55	62.50	3.51	
ITO/TiO_2(nanorod):phen/P3HT:PC_{61}BM/MoO_3/Al	0.53	12.13	62.20	4.02	

Table 3. The examples of the inverted OPVs with TMOs HEL

TMOs	Device configuration	V_{OC} (V)	J_{SC} (mA/cm^2)	FF (%)	PCE (%)	ref
MoO$_x$	ITO/TiO$_x$/P3HT:PC$_{61}$BM/MoO$_3$/Au	0.57	7.23	64.00	2.65	318
	ITO/TiO$_x$/FPQ-Br/P3HT:PC$_{61}$BM/MoO$_3$/Au	0.58	8.85	70.00	3.55	
	ITO/ZnO/PDTG-TPD:PC$_{71}$BM/MoO$_3$/Ag	0.86	14.10	67.30	8.10	57
	ITO/ZnO/PDTS-TPD:PC$_{71}$BM/MoO$_3$/Ag	0.90	13.10	56.50	7.80	
	ITO/TiO$_x$/P3HT:PC$_{61}$BM/MoO$_3$/Ag	0.59	10.17	58.78	3.52	172
	ITO/TiO$_x$/P3HT:PC$_{61}$BM/MoO$_3$/Ag	0.60	9.65	60.34	3.49	
	ITO/TiO$_x$/PDPP5T:PC$_{71}$BM/MoO$_3$/Ag	0.55	18.98	64.31	6.71	
	ITO/TiO$_x$/PDPP5T:PC$_{71}$BM/MoO$_3$/Ag	0.56	18.66	63.16	6.60	
	ITO/ZnO/PDTGTPD:PC$_{71}$BM/MoO$_3$/Ag	0.85	12.60	68.00	7.30	179
	ITO/ZnO/PCDTBT:PC$_{71}$BM/MoO$_3$/Ag	0.88	10.40	69.00	6.30	303
WO$_3$	ITO/AZO/P3HT:PC$_{61}$BM/WO$_3$/Ag	0.54	8.50	51.30	2.40	203
	ITO/TiO$_2$/P3HT:PC$_{61}$BM/WO$_3$/Ag	0.60	7.20	60.00	2.58	174
	ITO/ZnO/P3HT:PC$_{61}$BM/WO$_3$/Ag	0.55	11.57	58.77	3.74	409
	ITO/AZO/P3HT:PC$_{61}$BM/WO$_3$/Ag	0.53	8.56	59.10	2.68	415
	ITO/AZO/P3HT:Si-PCPDTBT:PC$_{61}$BM /WO$_3$/Ag	0.52	10.53	59.30	3.26	
	ITO/PFN-CbpSO/PDBTTT-C-T:PC$_{71}$BM/ WO$_3$/Ag	0.75	14.20	60.50	6.44	416
	ITO/PFN-CbpSO/PDBTTT-C-T:PC$_{71}$BM/ WO$_3$/Ag	0.75	14.90	64.20	7.17	
V$_2$O$_5$	TiO$_x$/P3HT:PC$_{61}$BM/s-VO$_x$/Al/Ag	0.52	9.50	60.00	3.00	171
	TiO$_x$/P3HT:PC$_{61}$BM/e-V$_2$O$_5$/Al/Ag	0.53	10.70	51.00	2.90	
	ZnO/P3HT:PC$_{61}$BM/NP-V$_2$O$_5$/Ag	0.55	10.80	60.00	3.60	186
	ZnO/P3HT:PC$_{61}$BM/s-VO$_x$/Ag	0.51	10.10	67.00	3.90	189
	ZnO/P3HT:PC$_{61}$BM/NP-V$_2$O$_5$/Ag	0.56	10.40	66.00	3.80	
	ZnO/a-PTPTBT:PC$_{71}$BM/VO$_x$/Ag	0.82	11.60	53.00	5.00	
	ZnO/OPV3/PC$_{61}$BM/VO$_x$/Ag	0.72	12.80	70.00	6.10	188
	ITO/ZnO/a-PTPTBT:PC$_{71}$BM/VO$_x$/Ag	0.82	11.60	53.00	5.00	189.
	ITO/SPMA/P3HT:PC$_{61}$BM/ V$_2$O$_5$/Al	0.60	10.50	57.00	3.60	417

Scheme 1. Critical pentagram showing five restrictions for evaluation of commercialization for organic photovoltaics.
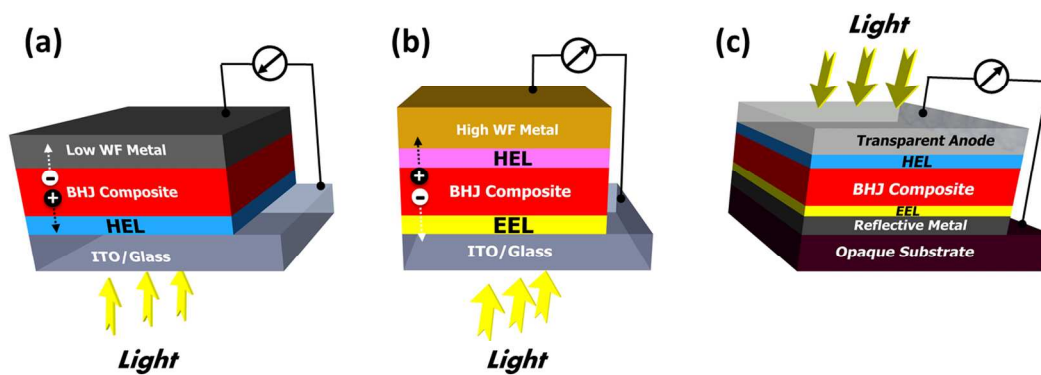
Scheme 2 Bottom-illuminated OPVs with **(a)** conventional device structure and **(b)** inverted structure and (**c**) top-illuminated OPVs with an inverted device architecture.

(a)

Sol gel process

Zinc Acetate
(Zn(C₂H₃O₂)₂)
+
Isopropanol
((CH₃)₂CHOH)

Monoethanolamine
(H₂NCH₂CH₂OH)

Stirring (50°C, 1 hr)

Sol

Filtered & Aged (24 hrs)

Thin Film Process

Spin Coating
(1000, 2000, 3000, 4000) rpm
30 secs

Hotplate Drying
(60°C, 1 hr)

Air cooled

Furnace Annealing
(650 °C/min, 1 hr)

Furnace cooled

ZnO Films

(b)

Sol Gel Process

Method A

Zinc Acetate Dihydrate
[Zn(CH₃COO).2H₂O]
+
2-methoxyethanol
(CH₃OCH₂-CH₂OH)
+
Ethanolamine
[NH₂CH₂CH₂OH]

Stirring (RT, 12 hr)

Sol

Method B

Zinc Acetate Dihydrate
[Zn(CH₃COO).2H₂O]
+
ethanol
(CH₃CH₂OH)

Ethanolamine
[NH₂CH₂CH₂OH]

Stirring (80°C, 2 - 3 hr)

Stirring (60°C, 12 – 15 hr)

Sol

Thin Film Process

Spin Coating
(3000 rpm, 1min)

Repeat coating until desired thickness is obtained

Drying at 150°C
For 15 min

Annealing at
350°C for 1 hr

Air Cooled

ZnO thin film

(c) precursors   ink-formation   thin film deposition   post processing

| Metal-
halides
nitrates
carboxylates
(oxo)alkoxides
alkamides
β-diketonates | precursor
+ solvent
+ additives
colloidal NPs
+ capping agent
+ solvent | spin/dip coating
chemical bath dep.
spray coating
meyer rod / Dr.-blade
slot die
gravure
ink-jet | condensation
decomposition
drying
thermal annealing
gas exposure
(UV)-light exposure
plasma treatment |

(d) (1)   (2)

M   I   O   M   I   O

substrate   substrate   oxide

Scheme 3. **(a-c)** flow chart for different preparation methods of the ZnO EEL via solution-process: **(a)** Reproduced from ref 50, Copyright (2008), with permission from Elsevier. **(b)** Reproduced from ref 51, Copyright (2009), with permission from Springer. **(c)** Reproduced from ref 56, Copyright (2013), with permission from The Royal Society of Chemistry. **(d)** Reproduced from ref 61, Copyright (2013), with permission from Elsevier.
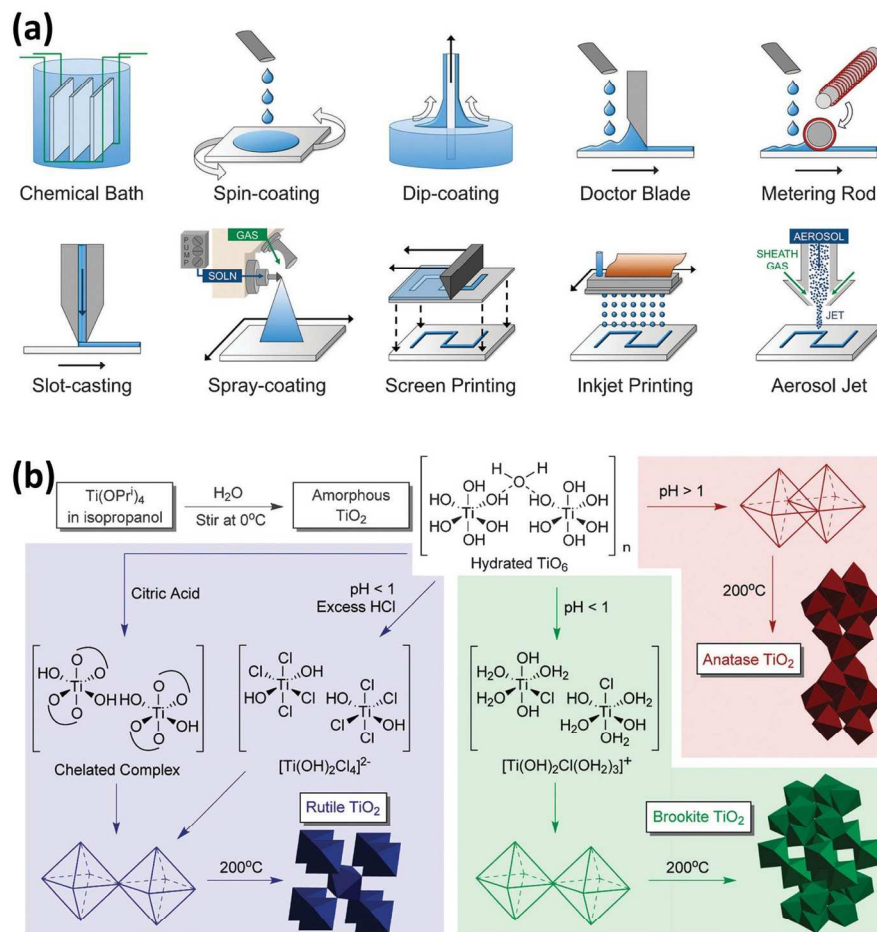
Scheme 4. (a) Depiction of various solution deposition methods, **(b)** TiO_2 polymorphs and reaction Schemes for the formation of phase-pure TiO_2 materials. Reproduced from ref 67, Copyright (2011), with permission from The Royal Society of Chemistry.
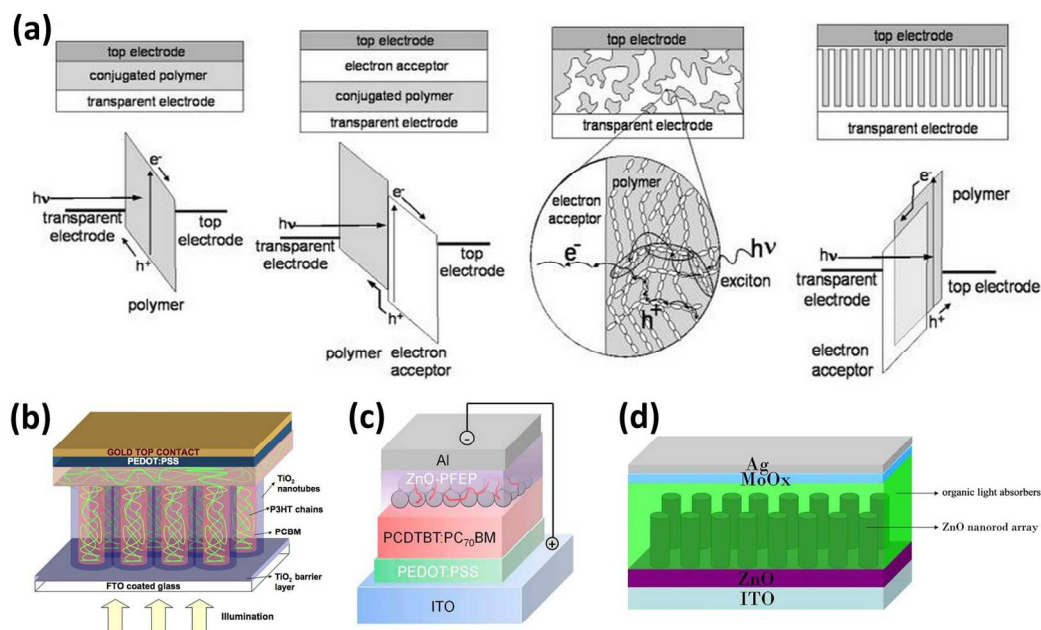
Scheme 5. (a) Four device architectures of conjugated polymer-based photovoltaic cells: single-layer photovoltaic cell; bilayer photovoltaic cell; disordered bulk heterojunction; ordered bulk heterojunction. Reprinted from ref 92, Copyright (2004) with permission from American Chemical Society. **(b-d)** OPVs devices using nanostructured TiO_x or ZnO layer. **(b)** Reproduced from ref 95, Copyright (2007), with permission from American Institute of Physics. **(c)** Reproduced from ref 101, Copyright (2014), with permission from American Chemical Society. **(d)** Reproduced from ref 75, Copyright (2014), with permission from Elsevier.

a

Cs⁺ Cs⁺ Cs⁺ H⁺ Cs⁺Cs⁺ Cs⁺ Cs⁺

b
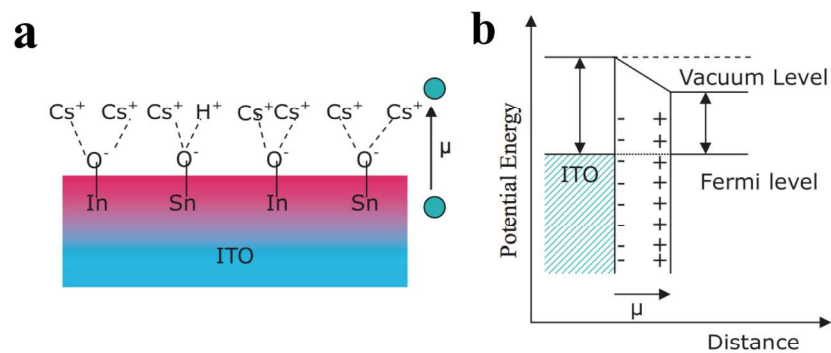
Scheme 6. (a) Evolution of secondary electron edge with different buffer layers on ITO, **(b)** Scheme for the formation of dipole layer on ITO and its effect on reducing the WF of ITO. Reproduced from ref 112, Copyright (2008), with permission from John Wiley & Sons.
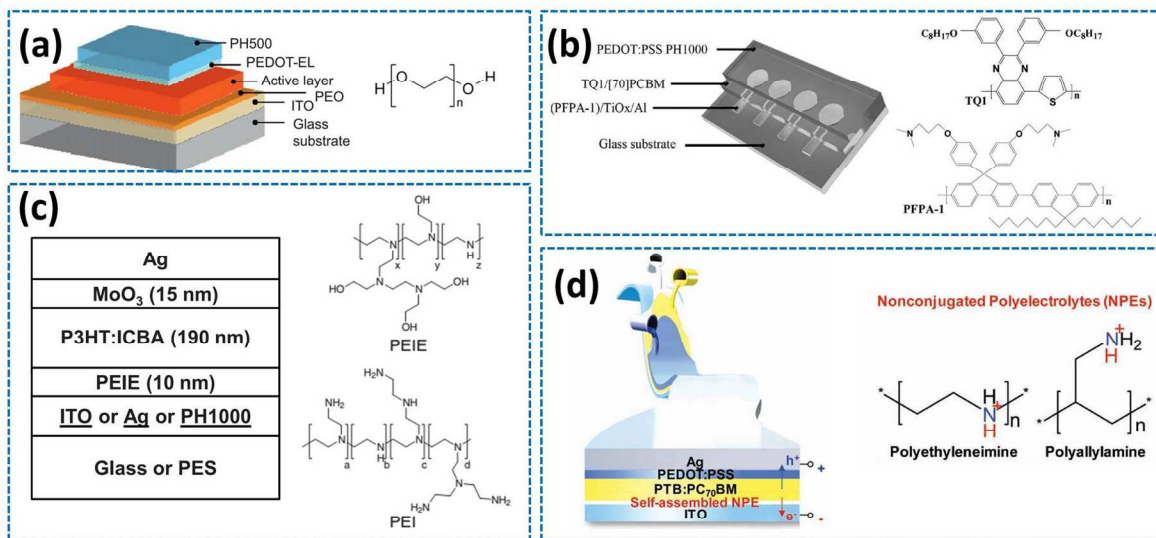
Scheme 7. OPVs device structures and the corresponding polymer EEL. **(a)** Adapted from ref 114, Copyright (2008), with permission from Elsevier. **(b)** Adapted from ref 118, Copyright (2012), with permission from John Wiley & Sons. **(c)** Adapted from ref 115, Copyright (2012), with permission from The American Association for the Advancement of Science. **(d)** Adapted from ref 116, Copyright (2012), with permission from John Wiley & Sons.
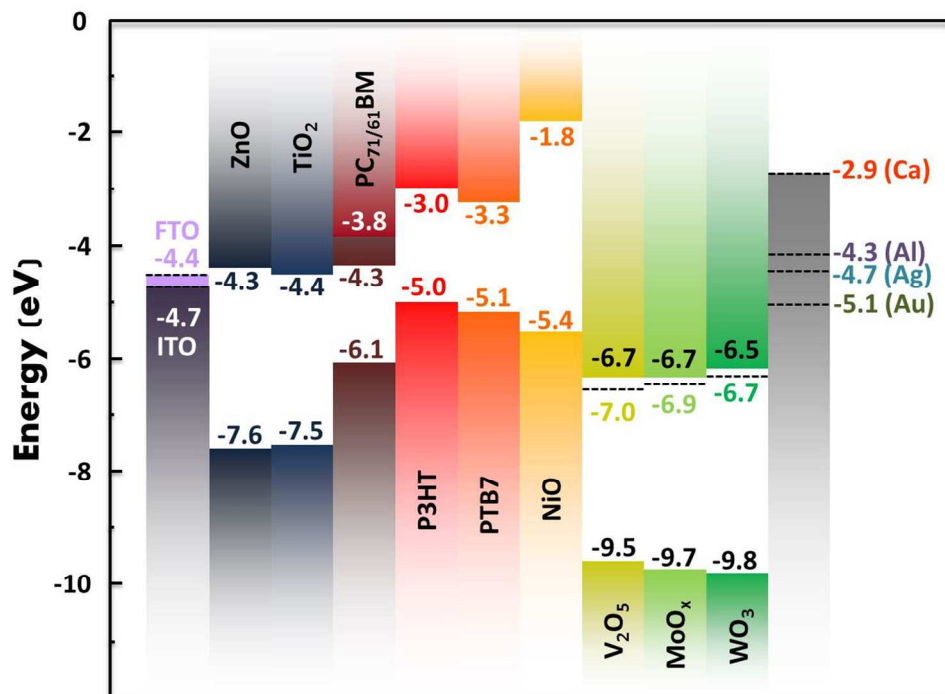
Scheme 8. The energy level diagram of state-of-art photovoltaic polymers, electron accepting fullerene derivatives and transition metal oxides.
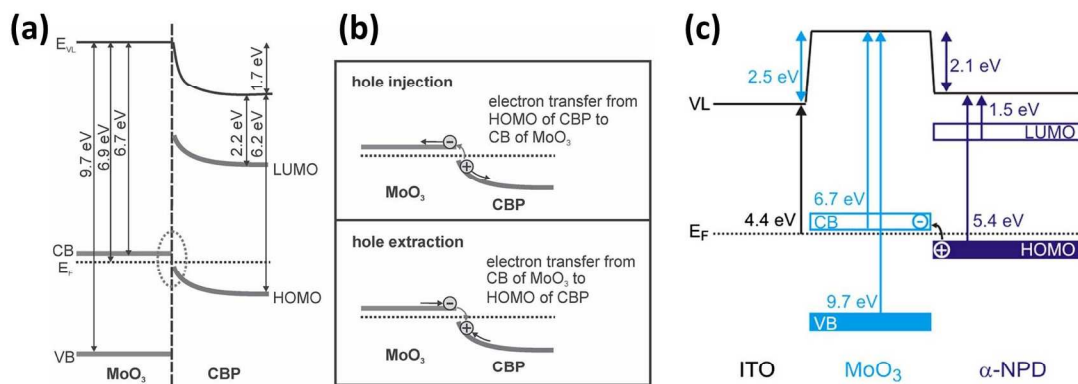
Scheme 9. (a) Energy level alignment and band bending at the MoO$_x$/CBP interface, as deduced from the UPS, and **(b)** proposed hole-injection and hole-extraction mechanisms. Adapted from ref 135, Copyright (2012), with permission from John Wiley & Sons. **(c)** Energy level alignment and band bending at the ITO/MoO$_3$/NPD interfaces. Reproduced from ref 151, Copyright (2009), with permission from American Institute of Physics.

C$_{60}$-SAM   **SAM [1]**   **SAM [2]**   **SAM [3]**   **SAM [4]**

SAM [5]   **SAM(C6-C60)**   **SAM(C18-C60)**   **PCBM-G2**

TT-SAM

LA-SAM   **BA-SAM**   **DPP-COOH**

N719   **SAM(C6)**   **FBA**   **BBA**   **MBA**
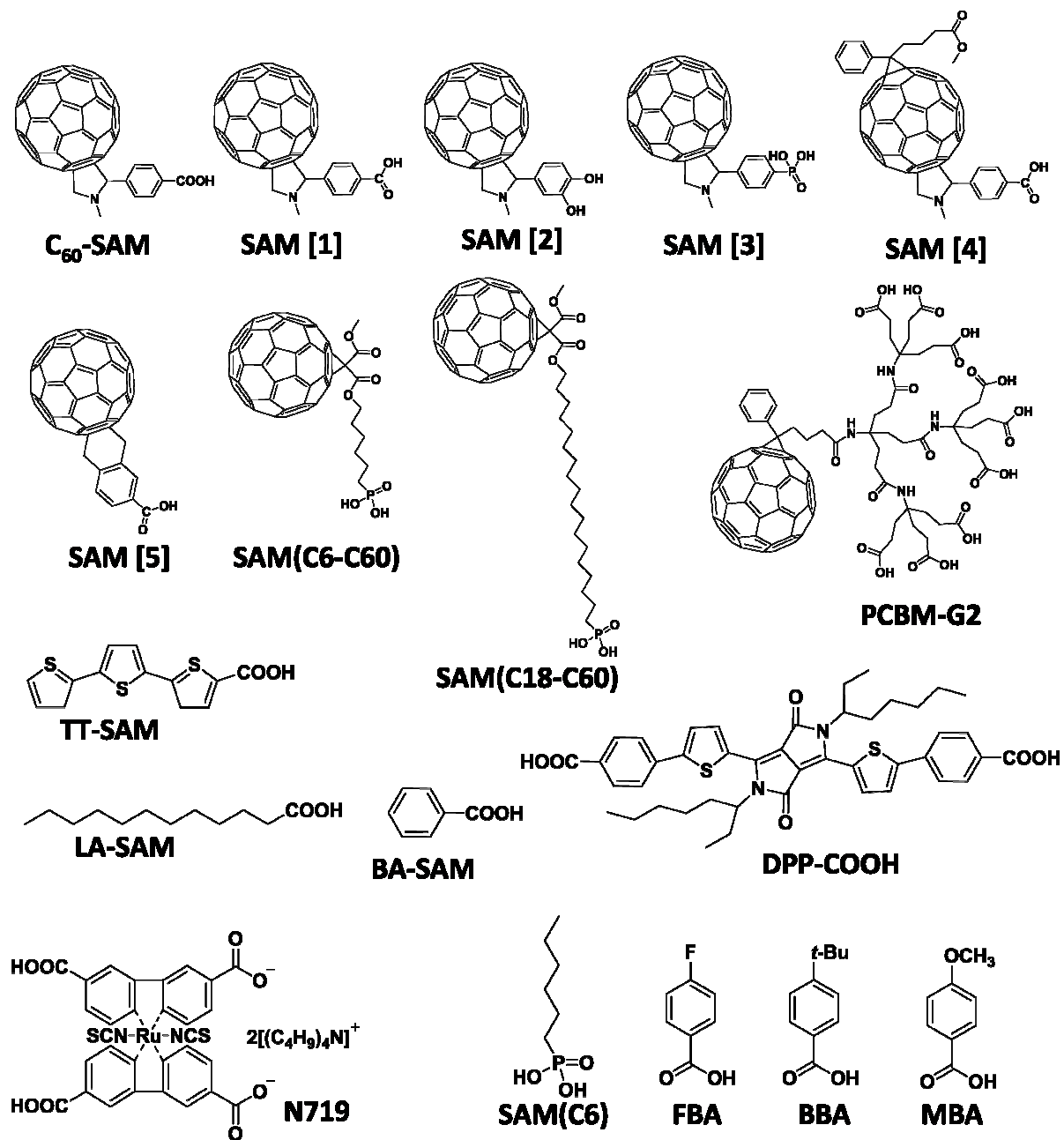
Scheme 10. Molecular structures of non-cross-linkable self-assembled monolayers (SAMs).
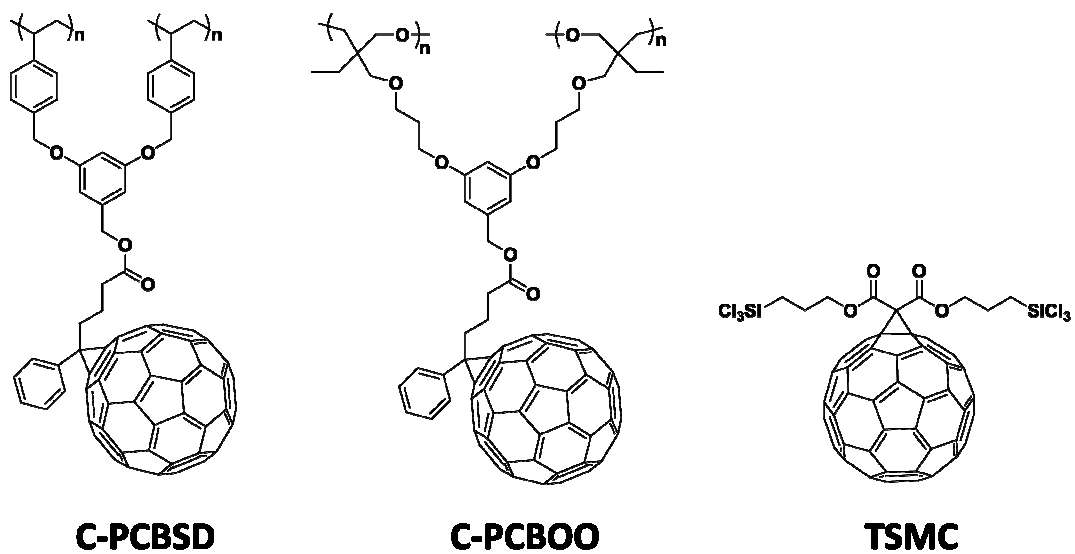
Scheme 11. Molecular structures of fullerene derivatives.
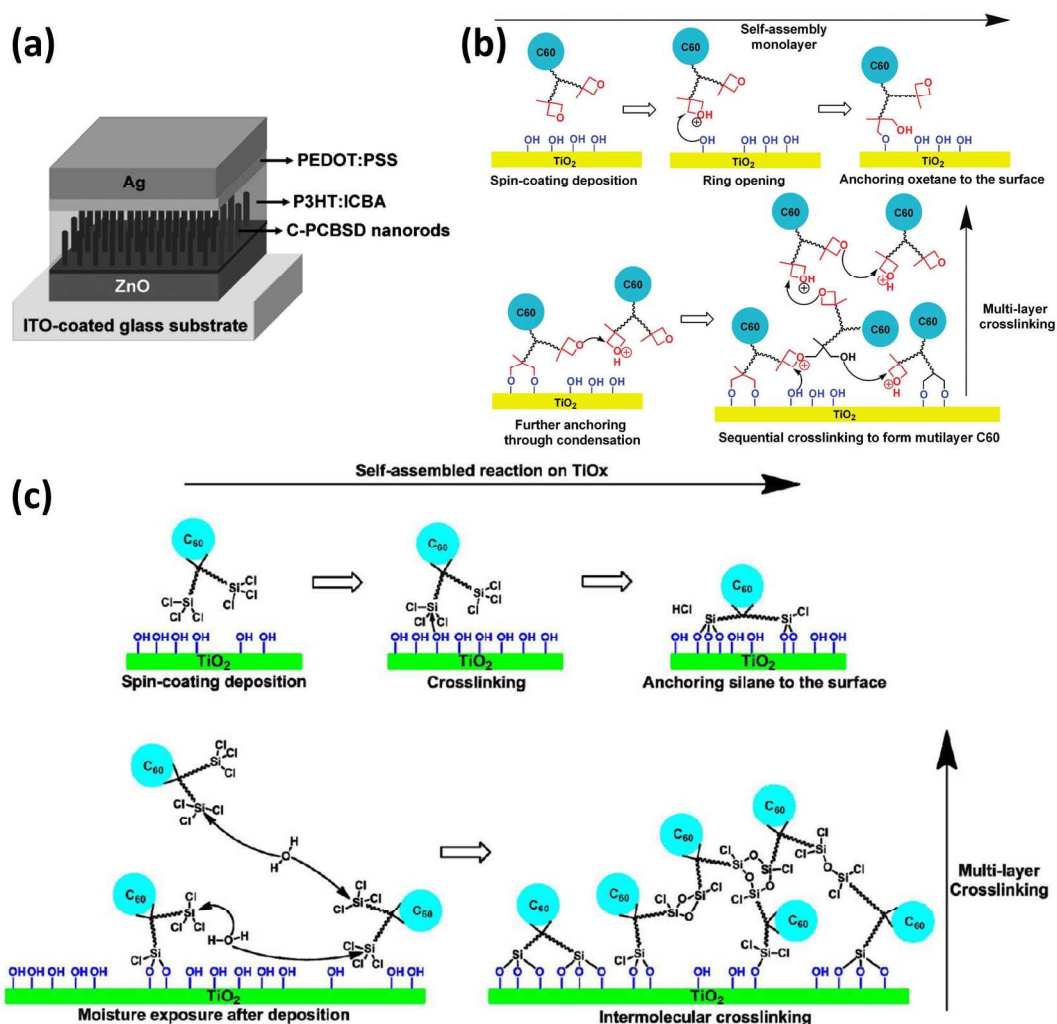
Scheme 12. (a) Device structure of ITO/ZnO/C-PCBSD nanorods/P3HT:ICBA/PEDOT:PSS/Ag. Reproduced from ref 256, Copyright (2011), with permission from John Wiley & Sons. **(b)** proposed mechanism for self-assembly and multi-molecular cross-linking of PCBOD on the TiO_x surface. Reprinted from ref 257, Copyright (2011), with permission from American Chemical Society. **(c)** hydrolysis of the trichlorosilane groups of TSMC: (top) self-assembled reaction on TiO_x, (bottom) intermolecular cross-linking to form multilayer network. Reprinted from ref 274, Copyright (2013), with permission from American Chemical Society.
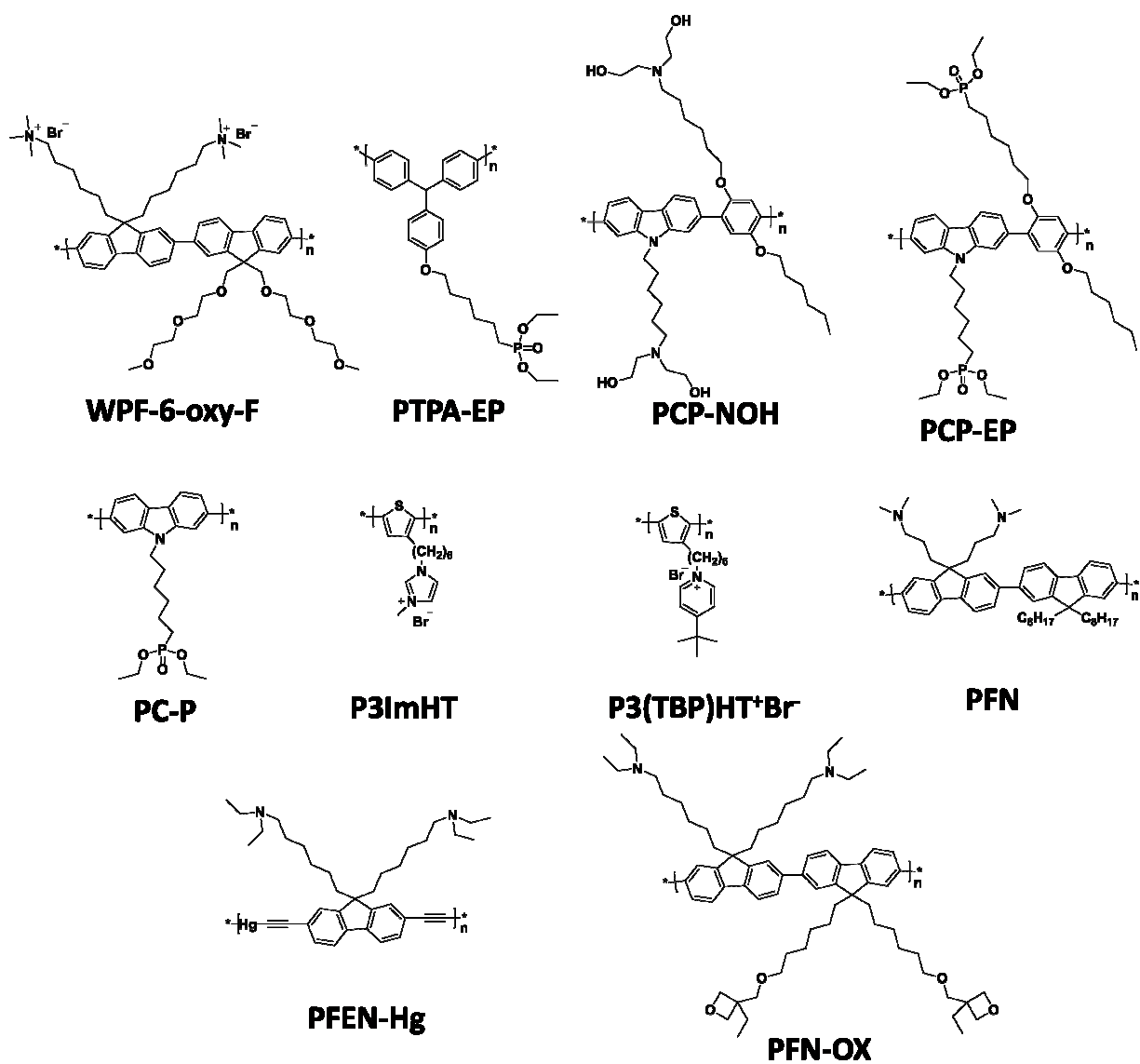
Scheme 13. Molecular structure of WPF-6-oxy-F, PTPA-EP, PCP-NOH, PCP-EP, PC-P, P3ImHT, P3(TBP)HT⁺Br⁻, PFN, PFEN-Hg and PFN-OX.
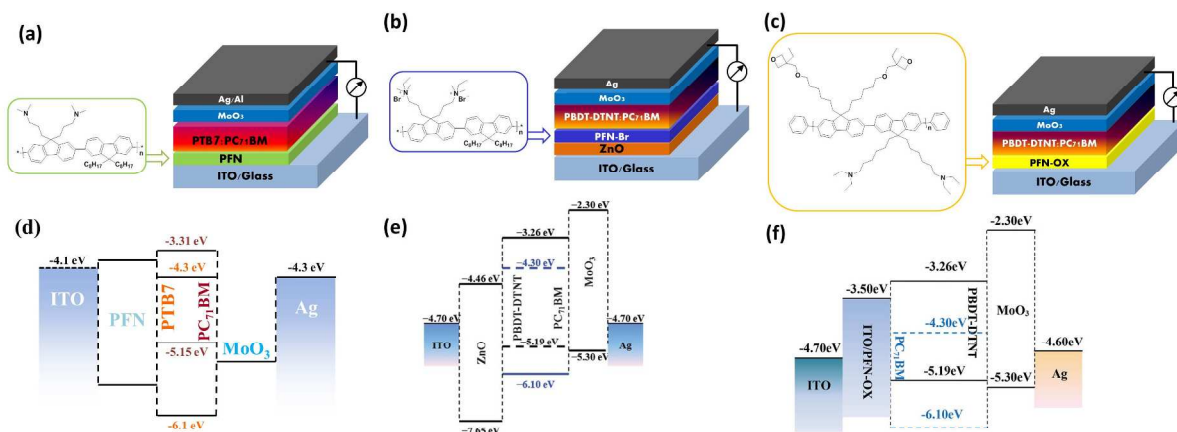
Scheme 14. An inverted device structure of polymer solar cells and the corresponding energy levels. (The energy levels of MoO$_3$ are in accordance with ref 276, ref 315 and ref 319) **(a) & (d)** Adapted from ref 276, Copyright (2012), with permission from Nature Publishing Group; **(b) & (e)** Adapted from ref 315, Copyright (2012), with permission from The Royal Society of Chemistry; **(c) & (f)** Adapted from ref 319, Copyright (2014), with permission from John Wiley & Sons.

Without OT   With OT
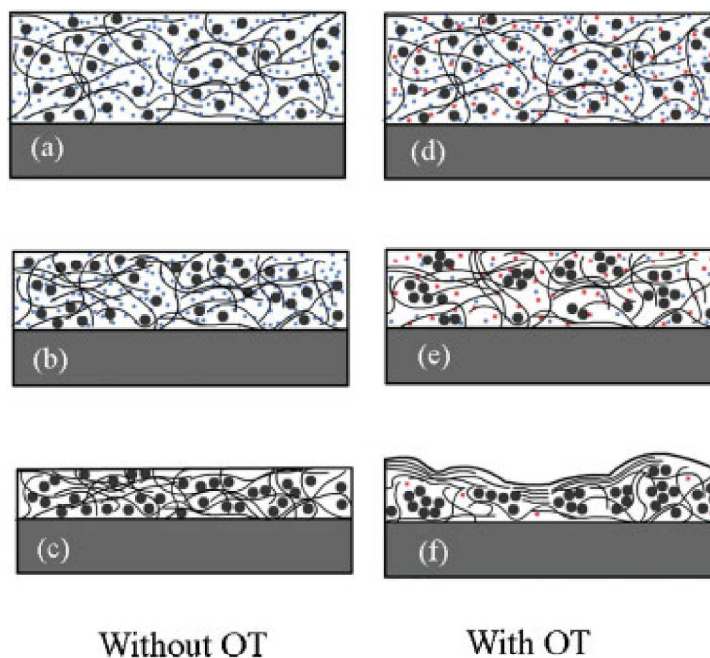
Scheme 15. Process of phase separation during spin-coating. Black lines: P3HT polymer chains; big black dots: PCBM molecules; blue dots: DCB molecules; red dots: OT. **(a)** to **(c)** represent the period of spin-coating when DCB as the sole solvent; **(d)** to **(f)** refer the stages of spin-coating when DCB as the solvent and OT as the additives. Reproduced from ref 341, Copyright (2014), with permission from John Wiley & Sons.
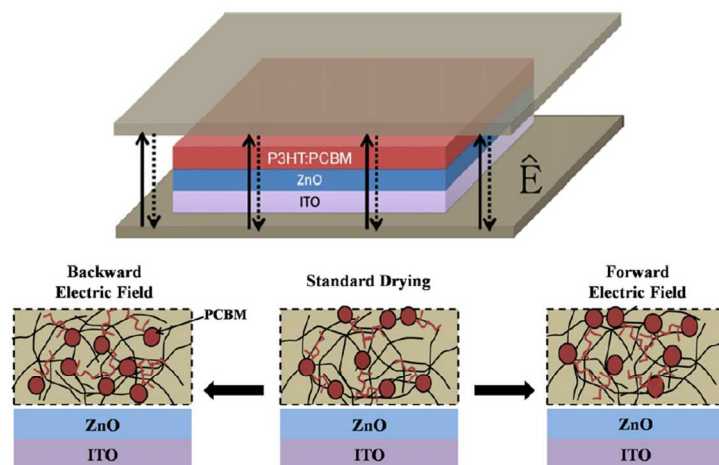
Scheme 16. (a) Vertical electric field. Solid lines: forward direction; dashed lines: backward direction. **(b)** Vertical phase separation with different electric field treatment. Long lines: P3HT polymer chains; dots: PCBM molecules. Reproduced from ref 351, Copyright (2011), with permission from Elsevier.
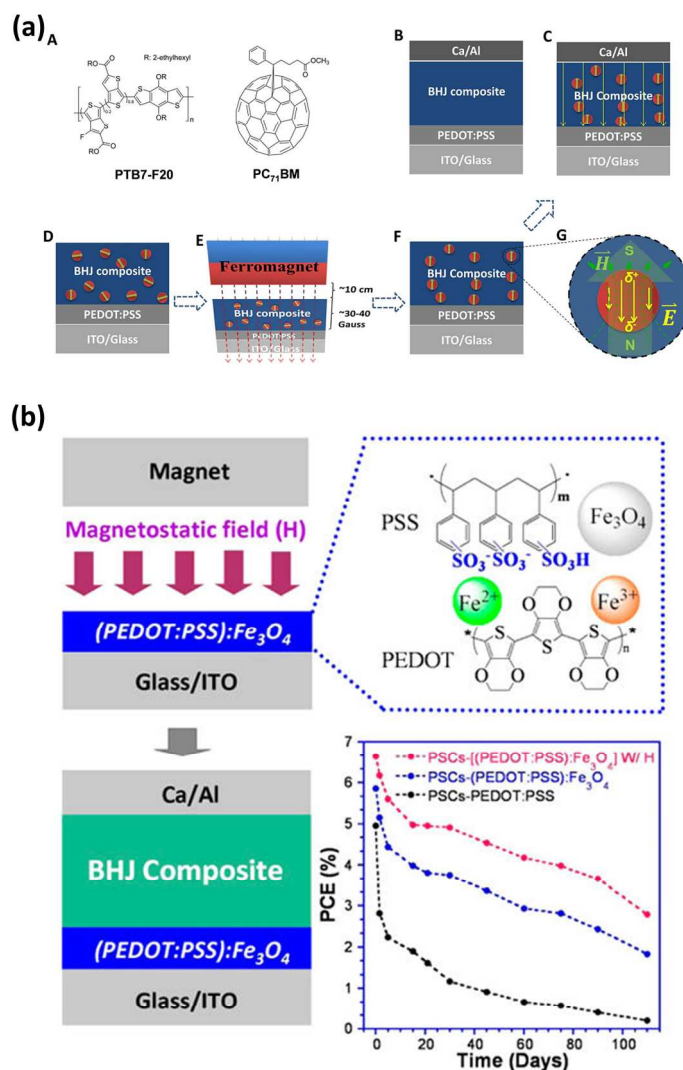
Scheme 17. Procedures of using MNPs and external magnetic field in **(a)** active layer. Reproduced from ref 352, Copyright (2015), with permission from Nature Publishing Group. Procedures of using MNPs and external magnetic field in **(b)** HEL for OPVs. Reproduced from ref 353, Copyright (2013), with permission from American Chemical Society.
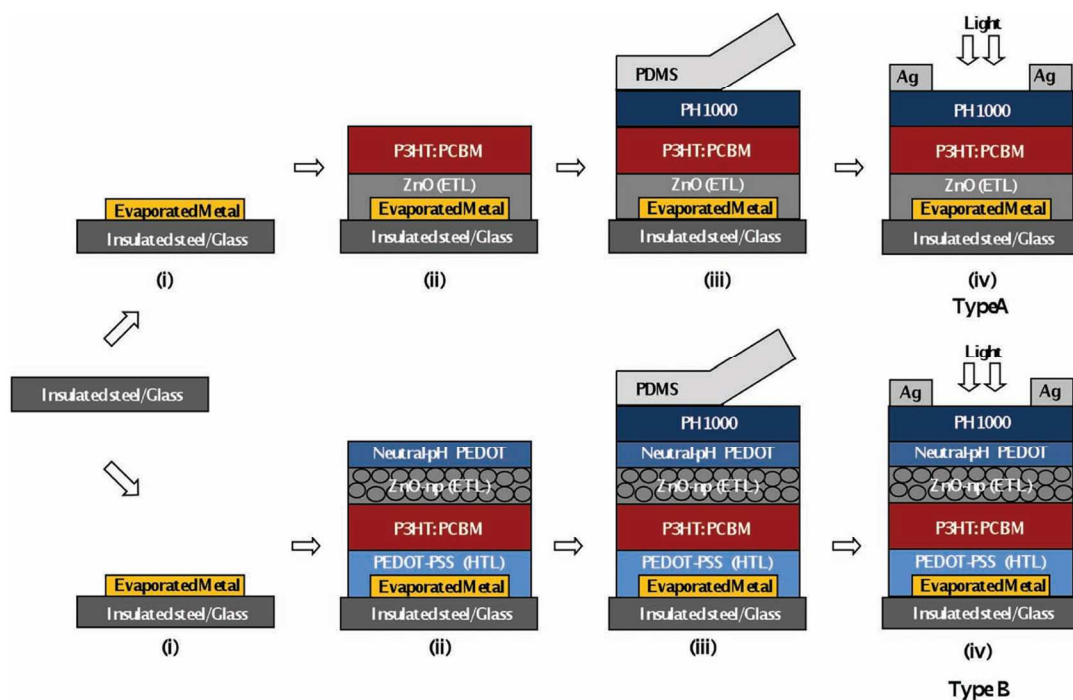
Scheme 18. Schematic depiction of device fabrication steps. (i) Thermally evaporated Cr/Au on glass, and Ag on the insulated steel substrates is used as the optically reflecting back-contact and current collection electrode. (ii) ZnO electron extraction layer (EEL), PEDOT-PSS hole extraction layer (HEL), P3HT:PCBM blend photoactive layer (PAL) are deposited by spin-coating. (iii) High-conductivity PEDOT-PSS (PH1000) is laminated on top of spin coated stack by stamp-transfer lamination technique. (iv) Ag is thermally evaporated through a shadow mask. Reproduced from ref 389, Copyright (2013), with permission from John Wiley & Sons.
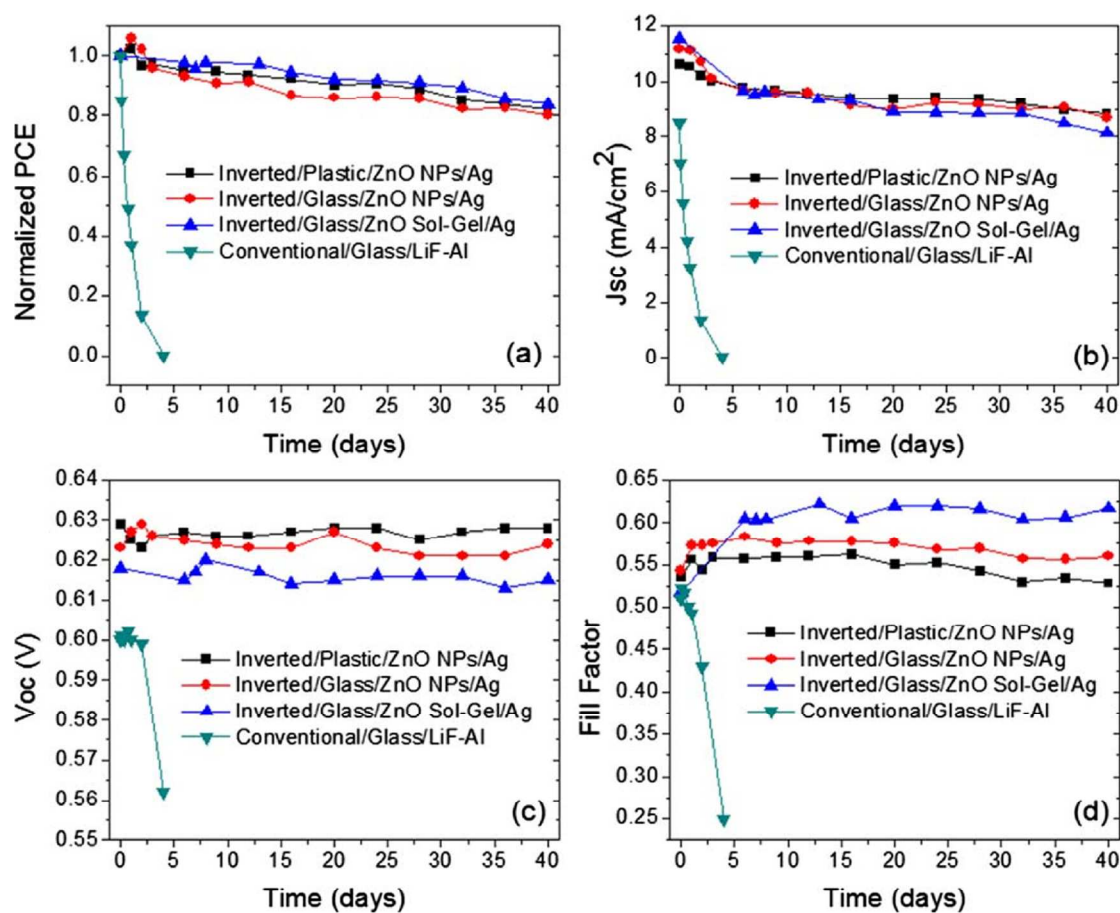
Figure 1. Device performance of un-encapsulated conventional and inverted solar cells stored 40 days in air under ambient conditions. **(a)** Normalized power conversion efficiency (PCE), **(b)** short-circuit current density (J_{SC}), **(c)** open-circuit voltage (V_{OC}), **(d)** fill factor. Reproduced from ref 53, Copyright (2008), with permission from American Institute of Physics.
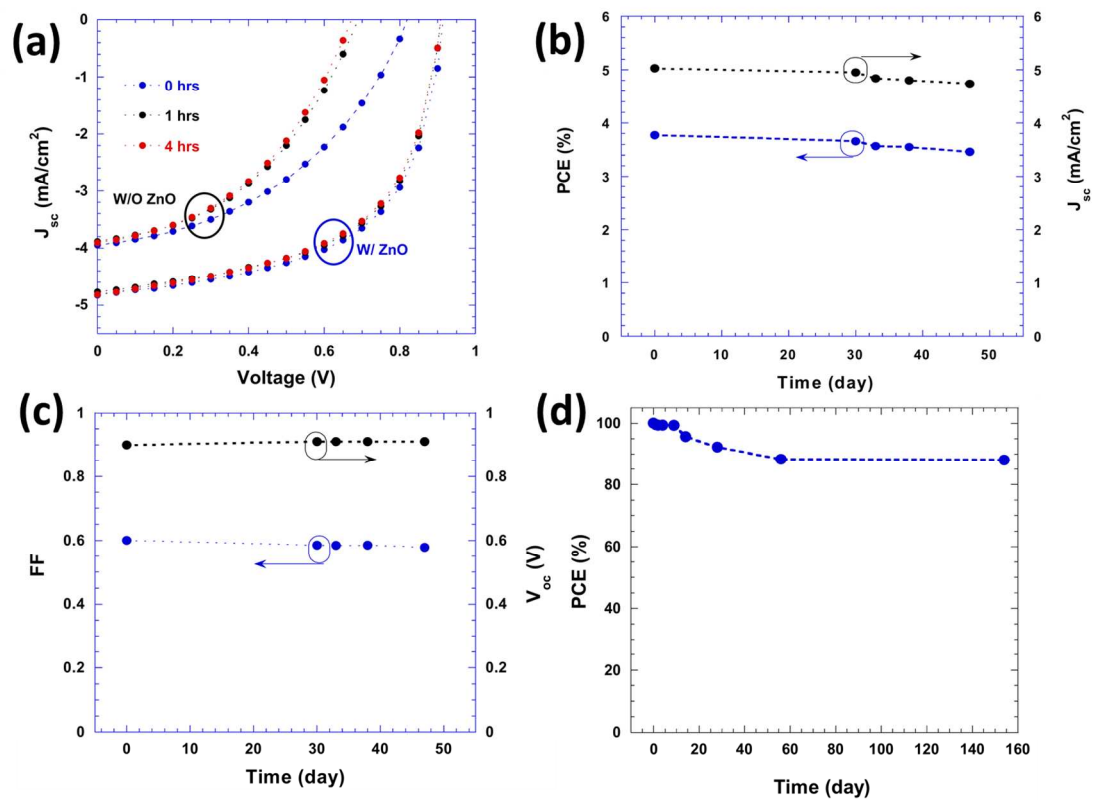
Figure 2. Stability of OPVs with and without ZnO layer, **(a)** operation lifetime; **(b-d)** shelf lifetimes. Reproduced from ref 49, Copyright (2012), with permission from Elsevier Ltd.